Engineering human hepatic organoids for *in vitro* liver modeling and implantable cell therapies

Sarah H. Saxton

A dissertation

submitted in partial fulfillment of the

requirements for the degree of

Doctor of Philosophy

University of Washington

2022

Reading committee:

Kelly R. Stevens, Chair

Jennifer Davis

Cole DeForest

Program Authorized to Offer Degree:

Bioengineering

University of Washington

Abstract

Engineering human hepatic organoids for *in vitro* liver modeling
and implantable cell therapies

Sarah H. Saxton

Chair of the Supervisory Committee:
Kelly R. Stevens
Department of Bioengineering

The adult liver performs hundreds of life-sustaining functions while also exhibiting a miraculous capacity to regenerate, but methods to expand primary hepatic cells *in vitro* while supporting their phenotype and function remain elusive. Organoid culture has successfully grown dozens of otherwise difficult-to-culture primary cells in 3D, generating valuable biological models and offering a new source of healthy cells for regenerative medicine. Here, we describe establishment of organoid culture systems for human hepatic cells and demonstrate their utility for in vitro modeling and liver tissue engineering. We demonstrate the robustness of our adult human hepatocyte organoid culture conditions by generating organoids from eight different adult donors. Mature organoids accurately model the phenotype and morphology of hepatocytes in the adult liver, express a mature liver transcriptome distinct from fetal hepatocytes, and exhibit adult

functions such as inducible cytochrome activity. To demonstrate their translational potential, we implanted human hepatocyte organoids *in vivo* and found that they exhibited up to 25-fold greater functionality after engraftment compared to previous adult hepatocyte models. Furthermore, organoids negate the need for inclusion of exogenous non-parenchymal cells in engineered tissues to support engraftment, an important translational milestone. Finally, we established a strategy for rapid vascularization and scale-up of engineered liver tissues to move this therapeutic idea closer to clinical reality. These results demonstrate the potential of adult human hepatocyte organoids for basic and translational applications such as pharmaceutical screening and hepatic regenerative medicine.

TABLE OF CONTENTS

LIST OF FIGURES

LIST OF TABLES

ACKNOWLEDGEMENTS

First, I would like to thank my advisor, Dr. Kelly Stevens for supporting me through the highs and lows of grad school. Kelly's warmth, enthusiasm, and kindness ensured that I was never afraid to approach her with a mistake. Kelly fostered a lab environment that was full of fun colleagues and creativity, and she urged me to tinker and explore so that I could find a fulfilling project that we were both excited about. I'm so appreciative of all the time and encouragement she has given me over the years and am so excited to see all of the exciting research sure to come out of the lab in the future!

I am also so thankful to my incredible lab mates who have made coming to work so much more fun over the last 5 years. The obvious comradery and support between all of the lab members were the reason I joined the lab and I am so thankful to have worked alongside my close friends through the trials of grad school. I've learned so much from each and every one of you and cannot wait to see what you all accomplish!

To my incredible parents, your endless love and support means the world to me. You've been the greatest role models throughout my life, as parents, as adventure-seekers, and as scientists. You've always made family the number one priority and exemplified what work-life balance can be. I've been so lucky to have you just a phone call away throughout my PhD and could always count on you for advice as the #1 parents with a unique understanding of grad school. And to Dan, thank you for always paving the way and letting me follow the trail you've blazed. I'm endlessly impressed by your humility, patience, and intelligence and so thankful to have had your example to follow for my whole life.

And finally, to Joe – I can't find words to describe how much I've appreciated your love and support over the last 5 years. Whether its sympathy, encouragement, or honesty, you always know what I need and how to cheer me up, even at a distance. I'm so excited to take on life together!

Chapter 1. INTRODUCTION

1.1 LIVER DEVELOPMENT AND MORPHOGENESIS

The process of hepatic organogenesis is orchestrated by a series of temporally and spatially localized signals that collectively drive the differentiation and morphogenesis that forms the mature liver. Between weeks 3 and 8 of human gestation, the early liver buds from the foregut endoderm, driven by mesodermal signals such as fibroblast growth factor (FGF) (*1*), bone morphogenic protein (BMP) (*2*), and Wnt (*3*, *4*). During this hepatic fate specification, the endodermal cells in the liver bud give rise to liver progenitor cells called hepatoblasts that form a monolayer surrounded by a ring of stromal cells (Figure 1.1A) (*5–7*). Signals from the neighboring stroma, in particular Wnt (*8–10*), FGF (*11*), and hepatocyte growth factor (HGF) (*12*) initiate hepatoblast proliferation and subsequent migration into the surrounding mesenchyme (Figure 1.1B) (*13*). After a period of continued proliferation and tremendous growth of the liver bud (*7*), hepatoblasts directly adjacent to the portal vein differentiate into fetal cholangiocytes or biliary epithelial cells. This process is mediated primarily by Notch (*14*, *15*) and a gradient of transforming growth factor beta (TGFβ) (*16*, *17*) produced by the portal mesenchyme, with possible contributions from FGF, BMP, and Wnt (*18*). The single layer of differentiated cholangiocytes, known as the ductal plate, then undergoes significant remodeling to form tubules, or bile ducts, that establish the intrahepatic biliary tree (Figure 1.1C) (*14–17*, *19*, *20*).

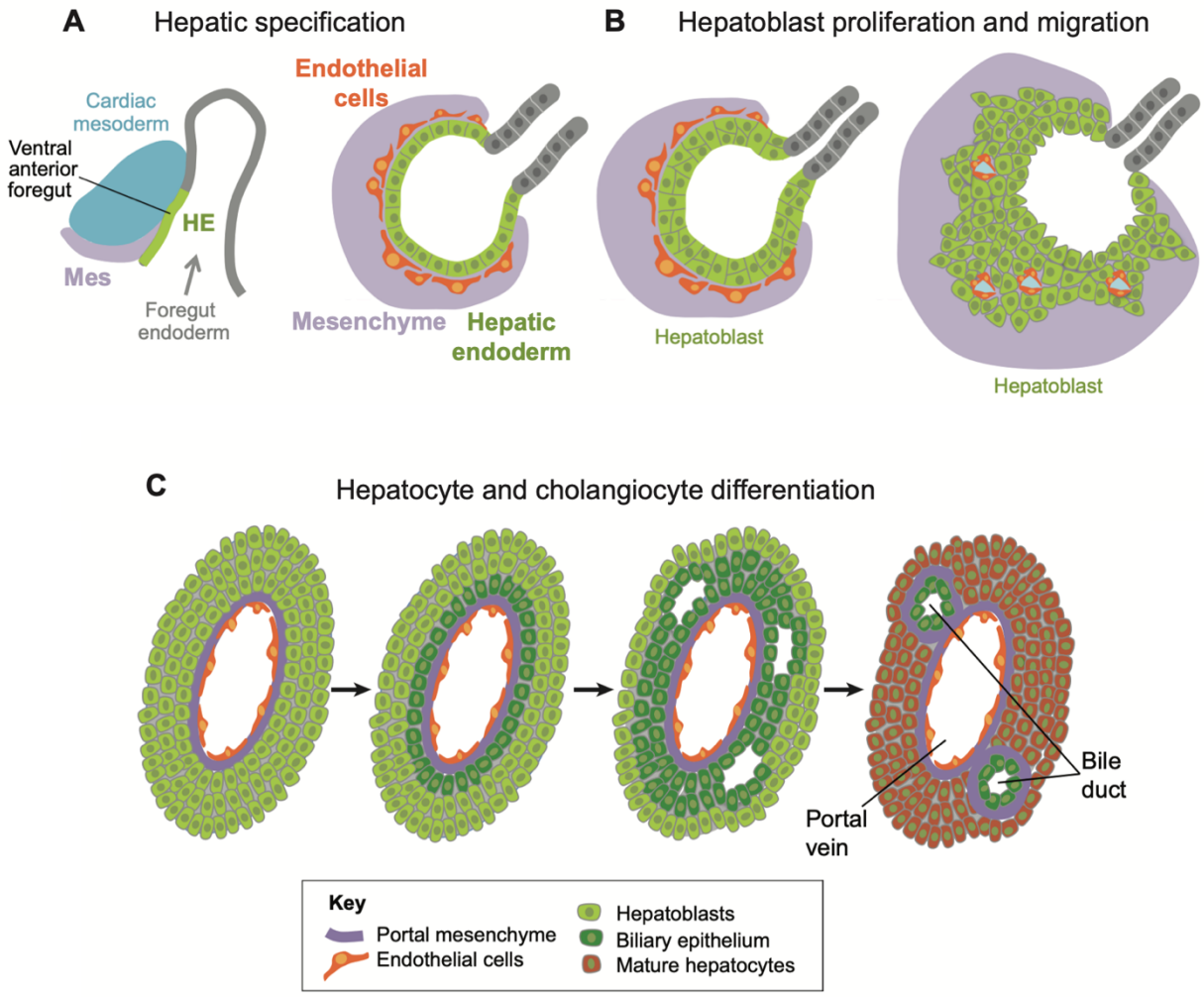

Figure 1.1: Liver development

(A) Liver specification as the hepatic endoderm buds from the foregut endoderm.
(B) Hepatoblast proliferation and migration into the surrounding mesenchyme.
(C) Hepatoblast differentiation into cholangiocytes (around the portal vein) and hepatocyte maturation. Adapted from reference (*6*).

Hepatoblasts away from the ductal plate differentiate into fetal hepatocytes and eventually mature hepatocytes, mediated in part by the opposing forces of tumor nuclear factor alpha (TNFα) and oncostatin M (OSM) (*21*), as well as HGF and Wnt (Figure 1.1C) (*10*, *22–24*). Hepatocyte maturation is evidenced by a gradual drop in expression of fetal proteins such as alpha fetoprotein

(AFP) (*25*), and acquisition of mature hepatic functions such xenobiotic metabolism (*26–28*). Throughout this differentiation process, mature liver structure is also established. The basic functional unit of the mature liver, the liver lobule, is highly conserved and repeats throughout the entire liver parenchyma (*6*). The lobule is organized into a roughly hexagonal shape, with strips of hepatocytes known as cords radiating between the central vein and portal triads in the outer six(ish) corners (Figure 1.2). Each portal triad is composed of one portal vein, supplying nutrient-rich blood from the intestine, one hepatic artery, supplying oxygen-rich blood from the heart, and a bile duct (*7*). Portal blood enters the liver and flows between hepatocyte cords through specialized hepatic capillaries known as sinusoids, lined by fenestrated sinusoidal endothelial cells (*19*, *29*). Additional specialized hepatic cell types also reside within the sinusoidal area, including the liver macrophage, or Kupffer cell, and the liver fibroblast, or stellate cell (*19*). Collectively, the non-parenchymal cells make up ~15% of the liver, with cholangiocytes accounting for ~3% of cells and the remaining ~80% composed of hepatocytes (*19*).

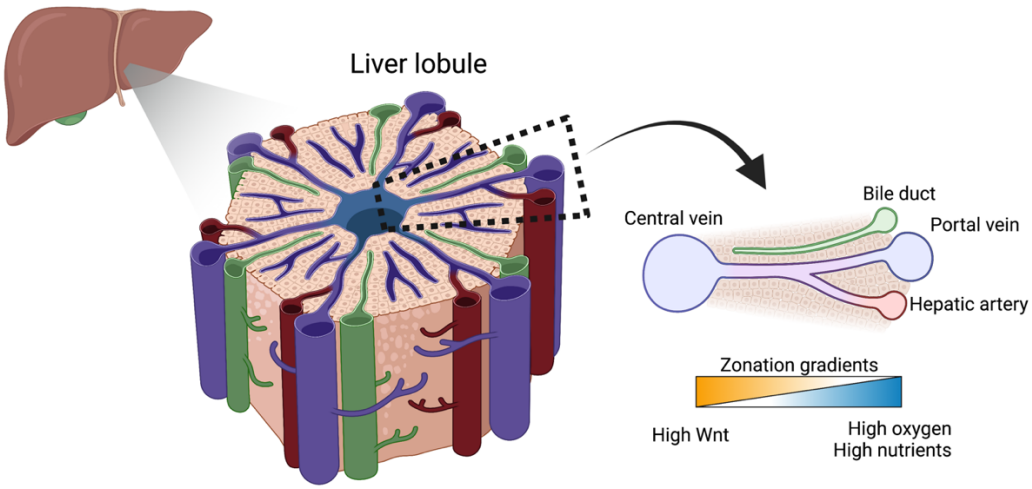

Figure 1.2: Adult liver physiology

1.2 LIVER PHYSIOLOGY AND FUNCTION

The mature human liver performs over 500 critical functions that are primarily executed by hepatocytes. Individual hepatocytes exhibit major metabolic variability in order to efficiently share the heavy functional workload of the liver. This spatial division of labor is known as zonation and is established along the portal-to-central axis in each lobule (*7*).

Blood enters the liver through the hepatic artery and portal vein, which collectively supply high concentrations of oxygen, nutrients, and hormones to nearby periportal hepatocytes. These signals, as well as an opposing gradient of Wnt, originating from central vein endothelial cells, act as the regulators of zonation (Figure 1.2) (*30*, *31*). With a greater supply of oxygen and nutrients (*32*), portal hepatocytes preferentially carry out more energy-demanding tasks such as protein production and ureagenesis, while central zone hepatocytes execute functions such as bile acid production and xenobiotic metabolism (*33*, *34*). Processes in glucose and fatty acid metabolism are also zonally distributed, with gluconeogenesis → glycolysis and β-oxidation → lipogenesis occurring along the portal to central axis (*35*).

In addition to lobular zonation, hepatocytes are also polarized with apical and basal domains (*5*). Hepatocyte cord morphology exposes each hepatocyte to a basal sinusoidal capillary, allowing for easy transfer of proteins and molecules between blood serum and hepatocytes (*36*, *37*). On the apical domain of hepatocytes, transmembrane drug transporters then pump bile, metabolized xenobiotics, and other waste out of hepatocytes into narrow canals called bile canaliculi (*36*, *37*). Bile canaliculi organize into a complex and delicate network throughout the liver lobule that eventually converges and drains into bile ducts (*7*, *20*). This polarization enables protein and nutrient transfer, as well as isolated waste removal, allowing for the liver's hundreds of functions to proceed efficiently and maintain homeostasis throughout the body.

1.3 LIVER DISEASE

Due to the liver's numerous and critical roles in metabolism, detoxification, and storage, liver disease can be devastating to human health. Liver disease can be caused by genetic mutations (tyrosinemia, alpha-1 antitrypsin deficiency), viral infection (hepatitis), or physical damage caused by alcohol, drugs, or diet (*38*). Though some causes, such as drug overdose, can lead to acute liver failure, the most common progression of liver disease is caused by gradual destruction of liver tissue over months to years (*39*). Chronic liver disease can be initiated by any of the causes mentioned previously, but over time repeated damage to the tissue leads to a condition called cirrhosis, which is characterized by severe scarring and impaired liver function (*39*). Cirrhosis can lead to liver failure and significantly increases the risk of developing liver cancer (*40*).

Unfortunately, treatments for late-stage liver disease are currently quite limited, leading to significant morbidity and mortality globally. Cirrhosis and liver cancer are respectively the 11th and 16th most common causes of death in the world, accounting for a combined 3.5% of global deaths (*41*). Chronic liver disease has a high economic burden and significantly reduces the quality of life for patients (*42*). The only curative treatment for late-stage liver disease is liver transplant, but the number of patients waiting for transplants far outnumbers the availability of donor organs, with the gap in supply and demand widening each year (*41*, *43*, *44*). Additionally, patients in the United States have unequal access to liver transplant, with Black and Latine/Hispanic patients less likely to be referred for transplant, leading to more advanced disease and worse outcomes after surgery (*45–47*). Women also have lower transplant rates when on the waitlist (*46*). Collectively, 10-20% of patients die while waiting for a liver transplant (*48*). Alternative treatment options are critical for reducing the morbidity and mortality of liver disease.

1.4 LIVER REGENERATION

The inability of the liver to recover from many forms of damage and disease is somewhat surprising given the fact that the liver is a highly regenerative organ. Up to two-thirds of a liver can be removed, known as partial hepatectomy, and the remaining mass will grow over a matter of weeks to recover the organ's original size (*49*). This procedure is used clinically, where surgeons can remove tumor-laden liver tissue from patients and allow the surrounding healthy tissue to regrow the lost mass. However, we have a limited understanding of the exact cellular and molecular mechanisms driving the complex process of liver regeneration, especially in humans, as most of our knowledge comes from rodent models of regeneration (*50*). The limitations that we face in modeling human liver will be addressed in a later section titled "*In vitro* liver models".

In rodents, partial hepatectomy is characterized by three phases: priming, proliferation, and termination (*51*). The priming phase is initiated within the first hour of injury, but the exact stimulus is unknown. One potential initiator is hemodynamic overload, as the full blood volume is restricted to ~30% of the original vascular network (*52*). Studies have suggested that this rapid shift in blood volume/pressure may trigger upregulation of stretch- or shear-induced angiocrine signals in LSECs, particularly HGF, interleukin 6 (IL-6), and TNFα, cytokines known to also be involved in liver regeneration (*52–54*). Vascular changes may also stimulate activation of matrix metalloproteinase 9 (MMP9) and urokinase plasminogen activator (uPA) which initiate remodeling of the liver's extracellular matrix and release matrix-bound growth factors such as HGF and TGFβ (*49*, *55*, *56*). Additionally, the increased portal blood flow relative to the remaining liver mass increases availability of portal factors such as epidermal growth factor (EGF) (*57*), norepinephrine (*58*), insulin, bile acids (*59*), and serotonin (*60*). These factors can either sensitize hepatocytes to other mitogens or act directly to stimulate cell cycle entry.

After the priming phase of regeneration, remaining hepatocytes undergo one or two rounds of cell division to recover the lost cell mass (*51*). Hepatocyte metabolism shifts during this growth phase to allow for mass cell division (e.g., lipogenesis genes upregulate (*61*) and drug metabolic genes downregulate (*62–64*)) but remarkably the liver maintains its functions and bodily homeostasis throughout (*65*). Then, upon reaching the original liver size, hepatocyte proliferation suddenly ceases. This unique phenomenon of almost perfect recovery of liver mass is known as the "hepatostat" (*66*) and is thought to be regulated by a combination of Hippo/Yap (*67*, *68*), TGFβ (*49*, *66*), and/or glypican-3 signaling (*69*), but the mechanisms stimulating those pathways are unclear. One hypothesis suggests that normalization of bile acid secretion in a fully regenerated liver stimulates FGF19 secretion from the intestine which acts in a negative feedback loop to arrest liver growth (*70*). Another possibility is that return to homeostatic stretch and shear forces on liver endothelial cells acts as the trigger of termination signaling (*52*).

The cellular repopulation that occurs during liver regeneration is unique, in that normally quiescent hepatocytes demonstrate "stem-ness" through cell division en masse (*51*) while in other regenerative organs such the intestines and the skin, proliferation is restricted to an adult stem cell niche (*71*). Whether a liver stem cell exists that is capable of unlimited proliferation beyond a few cell divisions is a point of contention in the liver field. As evidenced by serial transplantation of allogeneic hepatocytes in mouse livers, some hepatocytes have the capacity to double at least 69 times (*72*). Various groups have published conflicting discoveries identifying *the* liver stem cells as rare periportal hepatocytes (*73*), pericentral hepatocytes (*74*), and dispersed TERT+ hepatocytes (*75*). However, it is still up for debate whether one rare stem cell populations exists or whether the majority of hepatocytes have the capacity to extensively proliferate.

1.5 *IN VITRO* LIVER MODELS

As is clear from the previous sections on hepatic development, disease, and regeneration, the liver is a dynamic and complex organ – and we have a limited understanding of the molecular mechanisms regulating its health and disease. Most of our knowledge is derived from rodent models and while many developmental signals are conserved between vertebrates, there is still much to discover specifically about the human liver. *In vitro* human hepatic models are thus critical to further our understanding of liver biology and pathophysiology, and drive progress in drug discovery, as hepatotoxicity is a major reason for attrition in the pharmaceutical development pipeline (*76*, *77*).

Unfortunately, despite the liver's incredible regenerative capacity, harnessing growth *ex vivo* remains difficult. In basic 2D culture formats, isolated hepatocytes tend to rapidly dedifferentiate and lose function (*78*). More complex culture formats can stabilize hepatocytes, but no strategy exists yet that can sustain function and phenotype while also inducing cell division to expand the hepatocyte population. Alternative cell types and culture methods are described and illustrated below (Figure 1.3), along with the advantages and disadvantages of each.

1.5.1 *Cell types*

1.5.1.1 Primary human hepatocytes

The gold standard cell type for liver modelling is the primary human hepatocyte, which is isolated directly from human liver tissue. These cells retain their hepatic phenotype and functions for a short period of time (days) in a 2D monolayer but then progressively dedifferentiate (*78*). Primary hepatocyte morphology and functional stability can be prolonged in 2D by incorporating elements that mimic the hepatic microenvironment, such as culturing hepatocytes at high-density to increase

cellular interactions, and/or growing cells on a collagen-coated surface or between two layers of extracellular matrix, known as sandwich culture (*79*). However, even in these formats, hepatic function declines within a few days in culture, limiting use to short-term studies of function and acute toxicity. Furthermore, research is limited by cell sourcing, as long-term expansion of functional adult primary human hepatocytes *in vitro* has not yet been achieved.

An additional complication of using primary hepatocytes is significant donor-to-donor differences in cell viability, 2D adhesion, and *in vitro* function (*80–82*). Such variability leads to inconsistency between experiments and between labs and often necessitates selection of a single "ideal" lot, which removes important biological variability (*83*, *84*). Lot screening also requires hepatocyte banking through cryopreservation, where cells are frozen under controlled conditions and can be thawed years later for use. Unfortunately, the stress of cell isolation followed by the shock of cryopreservation can induce structural damage to hepatocytes, and therefore often leads to low viability, transcriptional changes, and functional abnormalities after thaw (*82*, *85–87*).

1.5.1.2 Induced pluripotent stem cell-derived hepatic cells

Induced pluripotent stem cells (iPSC) can be differentiated into hepatocyte-like cells by recapitulating developmental signaling networks *in vitro*. While iPSC-derived hepatocytes offer a potentially unlimited cell source, current differentiation protocols attain only a fetal-like hepatocyte state (*88*). Drug metabolizing enzymes and other functional proteins exhibit reduced expression, which precludes pharmacologic studies and research into adult hepatic function (*89*). However, if maturity and functionality can be improved, the patient-specificity afforded by iPSC-derived hepatocytes will allow for important future applications in cell therapy and precision medicine (*90–92*).

1.5.1.3 Hepatic cell lines

Various cell lines have been developed from liver tumors and immortalized hepatocytes, including HepaRG, HepG2, Huh7, and others. These cell lines are expandable and affordable, making them especially useful for studies that require large numbers of cells. However, most cell lines exhibit misregulated liver-specific functions (e.g., drug metabolism), are genetically abnormal, and imperfectly replicate all aspects of hepatocyte biology (*79*, *93*). Their uncontrolled growth and malignant origin also preclude them from *in vivo* applications (*90*, *91*). As maturation of iPSC-derived hepatic cells improves and methods are refined for consistent culture of primary human hepatocytes, researchers should move away from hepatic cell lines.

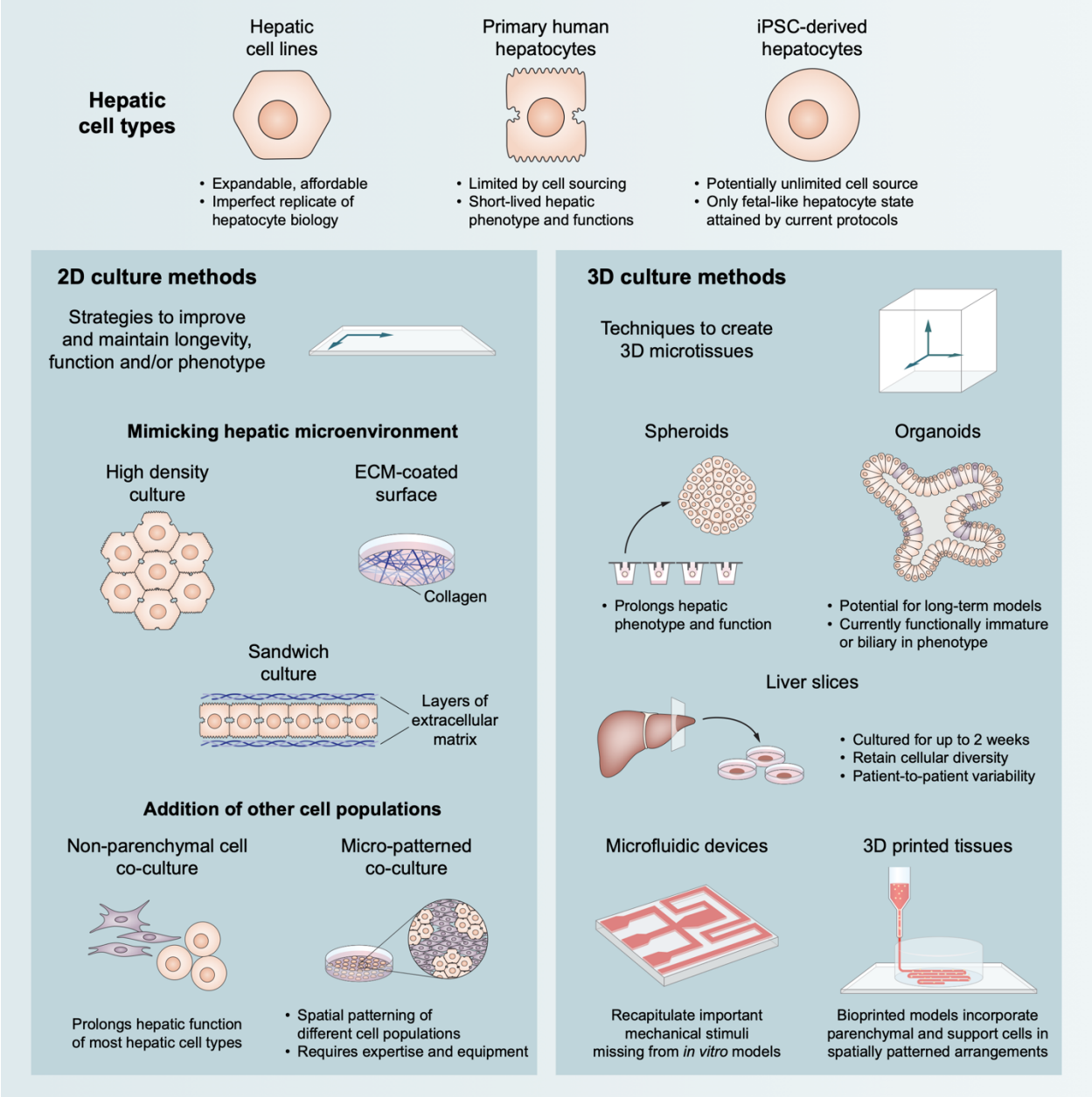

Figure 1.3: Illustration of 2D and 3D human liver models

1.5.2 *2D culture*

In traditional 2D culture, cells from the various sources mentioned above are plated onto a cell culture dish as a monolayer. The simplicity of 2D approaches makes it particularly amenable for high-throughput studies, such as pharmaceutical screening. However, as mentioned previously,

hepatic cells tend to rapidly lose function in 2D culture (*78*, *94*). Plating hepatocytes at high density helps to establish cell-cell contacts, mimicking *in situ* cord morphology and thereby increasing longevity (*95*). Additionally, inclusion of a variety of stromal or non-parenchymal liver cell populations to hepatic cultures prolongs hepatic function in most of the hepatic cell types above (*96–98*). Further spatially patterning these different cell populations in 2D culture (e.g., micropatterned co-culture (*78*, *99*)) stabilizes hepatic morphology and function for weeks, enabling chronic toxicity and metabolism studies not possible with other 2D models. However, this method requires expertise and equipment not easily accessible to all laboratories (*79*).

1.5.3 *Spheroids*

Primary hepatocytes can form spheroids through culture in hanging drops, microwells, non-adherent plates, or other aggregation strategies. Spheroid culture prolongs maintenance of hepatic phenotype and function by reestablishment of cell-cell junctions, which is further improved by co-aggregation with stromal or non-parenchymal cells (*99–101*). Spheroid culture has been shown to enhance hepatocyte engraftment in engineered liver tissues (*100*, *102*), and hepatic:stromal cell stoichiometry within spheroids plays a major role in liver function both *in vitro* and *in vivo* (*100*). However, forced aggregation through spheroid culture drives all plated hepatocytes together, including dead and dying cells which may negatively impact neighboring, healthy cells. Hepatocytes also remain quiescent in spheroids, limiting cell numbers.

1.5.4 *Organoids*

Organoids, or “mini-organs”, offer a culture method that can mimic the structure and function of a cell or organ of interest when cultured under specific media and matrix conditions. An early reference to liver organoids isolated heterogenous cells from rat liver and cultured them in roller

bottles where they formed “tissues” with layers of hepatic cells, ductal structures, and non-parenchymal cells. However, the organoid field as we know it today was based around a seminal paper establishing human intestinal organoids from Lgr5+ intestinal stem cells (*104*). This discovery inspired organoids to be established from dozens of cells and organs throughout the body, including a number of hepatic organoid models have been developed from assorted liver cell types across development that vary in their similarity to human hepatocytes.

1.5.4.1 Stem cell-derived organoid models of liver development

In one of the earliest demonstrations of a developmental-stage hepatic organoid, Takebe et. al. targeted early hepatic specification by establishing an *in vitro* “liver bud” (*106*). Hepatic endodermal cells were differentiated from iPSCs (iPSC-HE) and co-cultured with endothelial and mesenchymal stem cells to recapitulate the early stromal/hepatoblast signaling of hepatic organogenesis. Over 48 hours the cells self-organized into 3-dimensional masses that demonstrated increased transcription of hepatic functional genes compared to iPSC-HEs alone. Though liver buds remained immature *in vitro*, when transplanted in a mouse model of liver failure, the implanted tissues matured and rescued function. Subsequent papers differentiated stromal cell components from iPSCs to improve implant immunogenicity, established techniques to generate liver buds in high throughput for scaled generation, and used single cell RNA sequencing to better understand multilineage signaling in liver bud maturation (*107*, *108*).

Another paper from the same group modeled multi-organ lineage specification and organogenesis from slightly earlier in development. To do this, they generated pluripotent stem cell-derived anterior and posterior gut spheroids, which, when fused, differentiated into hepato-biliary-pancreatic domains at the anterior-posterior boundary. The midzone cells then undergo early morphogenesis to generate primitive structures of all three organ lineages (*109*). Others have

also generated multi-lineage hepatic organoids focusing on the later hepatoblast differentiation stage, where biliary and hepatic cells co-arise within a single organoid (*110*, *111*).

1.5.4.2 Primary fetal hepatic organoids

While all aforementioned developmental organoids have been generated from stem cell-derived hepatic progenitors, organoids have also been established from primary fetal liver cells that serve as better models of later stages of development. These include hepatoblast organoids, derived from the fetal liver bud between gestational weeks 3-7 (*112*) and fetal hepatocyte organoids, derived from the differentiated fetal liver between gestational weeks 7-20 (*113*). Fetal cells at both stages form relatively homogenous, dense organoids that are expandable through many passages, maintain expression of fetal markers such as AFP, and demonstrate early hepatic functions such as albumin secretion. Alongside hepatic proteins, hepatoblast organoids also exhibit low expression of some biliary/stem markers such as CK19 and retain bipotentiality, with the ability to differentiate into either fetal hepatocyte or cholangiocyte cells. Further maturation of both hepatocyte and biliary lineages can be achieved after *in vivo* implant, described in detail in Chapter 2.

1.5.4.3 Post-natal organoid models of human liver

Though many organoids exist that recapitulate various stages of human liver development, a major gap remains as there is no model of mature, post-natal human hepatocytes. Organoids have been established from ductal cells in the adult liver that can be induced to express some hepatic markers but overall remain biliary in phenotype and function (*114*). These cells were originally referred to as liver stem cells but are now generally recognized as ductal organoids (*115*). Other ductal organoids have been established from primary intrahepatic cholangiocytes (*116*), primary

extrahepatic cholangiocytes (*117*), and iPSC-derived cholangiocytes (*118*) that have the capacity to repair or reconstruct a damaged biliary tree *in vivo*. However, the closest the field has come to engineering mature hepatocyte organoids that maintain adult liver functions have been either mouse-derived (*113*, *119*) or from pediatric donors (*113*). Recent progress towards developing reliable and functional adult human hepatocyte organoids will be detailed in Chapter 3 -Chapter 5.

1.5.5 *Liver slice culture*

Resected liver biopsies can be sliced into thin tissue sections and cultured *ex vivo* for up to 2 weeks. Liver slices retain the cellular diversity of the liver and maintain *in vivo* cellular architecture but are subject to major patient-to-patient variability and cell death after resection and culture (*120*).

1.5.6 *Organ-on-a-chip and microfluidic models*

Using fabrication methods such as soft lithography, hepatocytes with or without non-parenchymal cells can be spatially patterned in 3D. Fluid flow can be introduced to recapitulate important mechanical stimuli that are missing from most other *in vitro* models. Liver-on-a-chip devices can also be integrated with microfluidic models of other organs to study systems-level biology and function. While such models offer physiologic improvements, they can be labor-intensive to make and maintain, limiting their throughput (*79*, *99*).

1.5.7 *Bioprinted liver models*

By marrying 3D printing technologies with cytocompatible biological “inks”, engineers can bioprint tissue models that incorporate parenchymal and support cells in spatially patterned arrangements (*121*, *122*). Traditional extrusion printing techniques can introduce destructive shear forces on fragile hepatocytes, but newer printing techniques such as stereolithography (*123*) have enabled more liver-compatible cellular assembly. Stereolithography uses spatial control of light to

precisely crosslink polymers, allowing cells to rest in a bath of unpolymerized hydrogel instead of being forced through a narrow nozzle. However, light-based printing requires photocrosslinkable bioinks, which limits materials options and thus may not afford the flexibility to optimize hepatocyte/matrix interactions. Another printing option that is also gentle on cells while remaining materials agnostic is sacrificial scaffolding, where a dissolvable material is 3D printed into negative mold around which a cellularized material is polymerized, followed by removal or "sacrifice" of the printed scaffold (*124*). This strategy is compatible with any polymerizable material and has the advantage of rapid fabrication time at potentially massive scales, as cells are only involved in the casting and curing steps. 3D integrity and resolution were initially issues for sacrificial scaffolding (*125*), but recent progress in scaffold fabrication using laser sintering has eliminated that limitation (*126*), elaborated on in Chapter 7.

Currently, options are limited for studying long term liver function, metabolism, and toxicity *in vitro*, slowing biological research and drug discovery. Future strategies that can recover primary hepatocytes from cryopreservation and sustain function in high throughput-compatible formats will be integral for screening experiments. Additionally, methods to expand hepatocytes will be critical to provide a reliable and reproducible cell source for basic and translational studies. Researchers can target regenerative stimuli, microenvironmental changes, and cytokine signaling to induce cell division in primary hepatocytes or can recapitulate developmental processes to produce more mature iPSC-derived hepatocytes.

1.6 LIVER CELL THERAPY AND ENGINEERED TISSUES

In addition to *in vitro* liver modeling, human hepatocytes are also critical for clinical translation of liver transplant alternatives. As mentioned previously, the number of patients requiring liver transplants vastly outnumbers available donor organs. Two promising alternatives to whole organ transplant are liver cell therapy, where healthy hepatocytes are reseeded in a patient's liver, and engineered liver tissues, which can be implanted in patients to compensate for the lacking native liver function. In this section we will detail the progress that has been made in animal models and clinical trials, as well as the hurdles that must be overcome to translate research accomplishments from bench to bedside.

1.6.1 *Orthotopic cell therapy*

For decades orthotopic liver transplant has been a promising clinical possibility for treatment of certain acute and genetic liver diseases. First explored in mouse and rat models, researchers observed partial engraftment and sustained function of primary human hepatocytes implanted in host livers (*127–129*). Since these early rodent studies, hepatocyte transplant has been tested in a number of human patients with acute liver failure (*130–133*) or inborn metabolic disorders (*134–151*). In general, transplant has been found to be safe for patients, but poor cell engraftment usually leads to failure and is influenced significantly by the quality of implanted hepatocytes (*152*). Additionally, each transplant requires more than 100 million hepatocytes (*90*), which, as discussed previously, are difficult to source. These limitations have prevented broad adoption of hepatocyte transplant for clinical treatment of liver disease, but an abundant and reliable hepatic cell source could renew the potential to treat patients with liver cell therapy.

Alternative cell sources have been explored for their engraftment potential as a cell-based therapeutic. Fetal hepatocytes have been tested clinically and demonstrated some success in

treating acute liver failure (*131*, *133*). However, fetal liver tissue is even more scarce than adult, so culture methods to expand fetal cells would be critical for cell sourcing. Stem cell-derived hepatic cells have huge potential due to their scalability, but current protocols still fail to produce mature hepatocytes with broad hepatic functionality (*88*). Though some rodent studies have shown that iPSC-derived, immature hepatic cells can mature after implant (*106*), other research shows that more mature cells have more rapid and efficient engraftment after implant (*113*, *153*, *154*). Thus, cell maturity will be important for transplant success.

1.6.2 *Engineered liver tissues*

Notably, hepatocyte transplant has only successfully treated patients with acute liver failure and metabolic disorders, as these diseases are generally cellular and leave the hepatic microenvironment healthy and intact. Unfortunately, the majority of patients needing liver transplants suffer from chronic liver disease with advanced cirrhosis or liver cancer (*39*, *41*). Such diseases are usually accompanied by severe fibrosis and pathological remodeling of the liver which would not be fixed by simply reseeding healthy cells. Until treatments are developed to reverse chronic liver disease, new organs are the only therapeutic option for these patients. Thus, tissue engineers are working to build implantable liver tissues *de novo* as an alternative to complete liver transplant.

Though engineered liver tissues are further from clinical adoption than cell transplant therapies, huge progress has been made in the last decade to propel the field forward. The original demonstration of ectopic liver tissue survival was performed using rat hepatocytes implanted in the dorsal fat of hepatectomized rats (*155*). Since then, multiple other implant sites have been explored including the lymph node (*156*), gonadal fat pad (*102*), kidney capsule (*106*), mesentery (*106*), cranium (*106*), subcutaneous space (*157*), and liver itself (*158*). Some studies rely on self-

organization, allowing developmental and regenerative multi-cellular signaling to direct appropriate morphogenesis in engineered tissues (*102*, *106*). Others have taken advantage of native liver structure by reseeding decellularized liver tissue with human cells (*158*) and more highly engineered models have used biofabrication techniques such as bioprinting to exogenously control tissue architecture (*123*). However, all strategies are still hampered by cell sourcing, with stem cell-derived hepatic cells raising concerns of tumorigenicity and functional maturity, and primary hepatocytes facing the recurrent issues of limited cell expansion and low viability after isolation and cryopreservation. To address some of these limitations, a new strategy to culture and expand primary hepatocytes that primes them for implantation in engineered liver tissues will be explored in Chapter 6.

1.7 CONCLUSION

To alleviate the burden of liver disease around the world, alternative treatments must be developed to prevent or reverse disease progression. This will require a reliable and expandable population of hepatocytes to generate human liver models and drive progress on cell-based therapies. By harnessing developmental and regenerative signaling, in this work we explore organoid culture as a method to grow hepatic cells for *in vitro* modeling and as a source for engineered liver tissues.

Chapter 2. HEPATOBLAST ORGANOIDS HAVE BIPOTENTIAL FATE IN ENGINEERED LIVER TISSUES

2.1 INTRODUCTION

Studies in mice and humans have clearly established that hepatocytes and cholangiocytes originate from bipotential progenitors called hepatoblasts (*159*, *160*), which represent a proliferative population that plays a crucial role in liver organogenesis. Hepatoblasts are mainly characterized by the expression of markers specific for both hepatocytes and cholangiocytes such as albumin and cytokeratin-19 (CK19) and markers of hepatic immaturity such as AFP (*161*). Of note, transplantation of isolated human hepatoblasts has established the capacity of these cells to colonize the adult rat liver in hepatic failure models thereby demonstrating their interest for regenerative medicine applications (*162*). Thus, culture of human hepatoblasts could provide a unique platform not only to study human liver development but also to produce cells for clinical applications. However, the development of robust protocols to grow human hepatoblast *in vitro* has remained elusive.

To culture and expand human hepatoblasts, we applied organoid technology to the human fetal liver for the first time with an aim at investigating human liver development and generating an abundant cell source for tissue engineering. We developed protocols to isolate hepatoblasts from fetal livers and grow them as organoids that were expandable for more than 20 passages and retained transcriptional, morphological, and functional characteristics of their tissue of origin (Figure 2.1A and B). We then used hepatoblast organoids to probe human liver development by exploring the signaling pathways driving hepatoblast differentiation into hepatocytes and cholangiocytes. We uncovered that maturation signals including OSM could direct hepatoblasts

towards a hepatocyte fate and that absence of Wnt signaling combined with the presence of TGFβ could direct hepatoblast organoids to adopt cholangiocytes signatures (Figure 2.1C and D). However, both resulting cell types were not fully differentiated, suggesting that additional signals are necessary for complete maturation. This problem has long plagued the hepatic stem cell field, which has struggled to develop protocols to differentiate fully mature hepatocytes. However, research has found that implantation of immature, iPSC-derived hepatic cells in mice can induce maturation, leading us to hypothesize that the *in vivo* environment could drive hepatoblast organoids to fully differentiate.

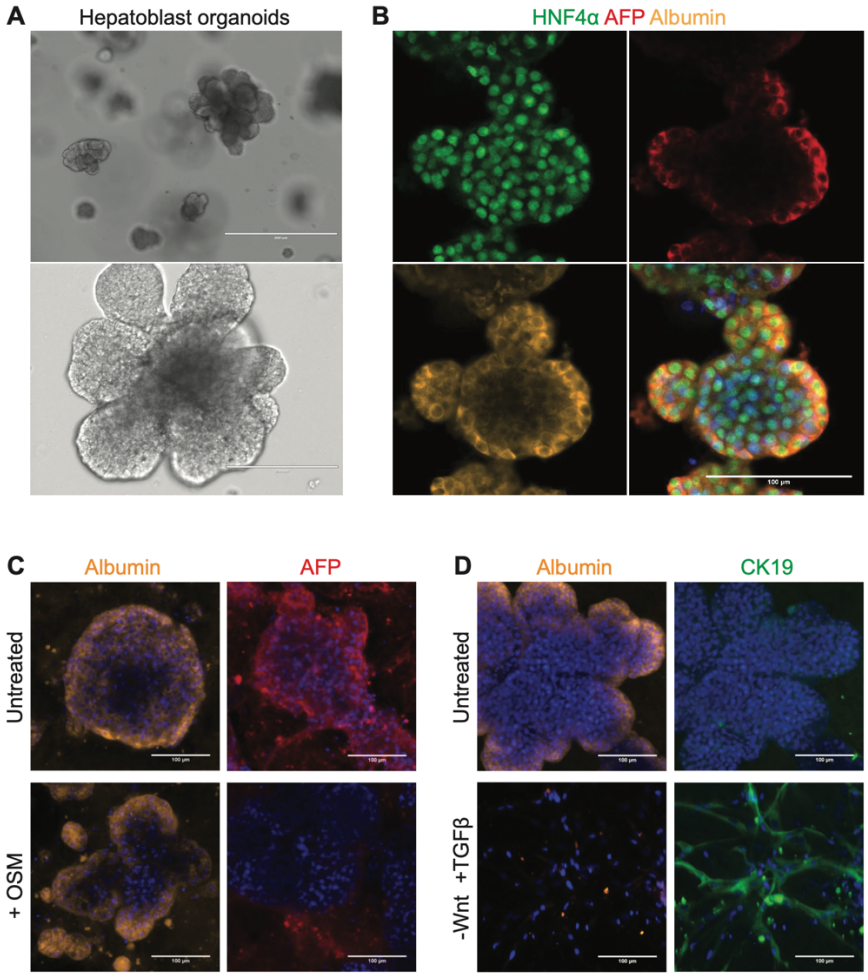

Figure 2.1: Establishment and *in vitro* differentiation of hepatoblast organoids

(A) Representative brightfield images of hepatoblast organoids. Top scale bar = 400 μm, bottom scale bar = 200 μm.
(B) Immunofluorescent staining of hepatoblast organoids for HNF4a (green), AFP (red), Albumin (yellow), and overlay image. Nuclear staining (blue) using Hoechst dye. Scale bar = 100 μm.
(C) Immunostaining for Albumin (left, yellow) and AFP (right, red) in untreated hepatoblast organoids (top) and organoids treated with +OSM (bottom). Scale bars = 100 μm.
(D) Immunostaining for Albumin (left, yellow) and CK19 (right, green) in untreated hepatoblast organoids (top) and organoids treated with -Wnt and +TGFβ (bottom). Scale bars = 100 μm.

Here, we demonstrate that hepatoblast organoids transplanted in a mouse model of chronic liver injury not only survive but also differentiate into both hepatocytes and cholangiocytes without exogenous signaling. Implants produce human albumin, demonstrating hepatic function and connection to host vasculature. This not only provides a model to investigate human liver development but could also open the current bottleneck in liver cell therapy of limited access to high quality, transplantable hepatic cells.

2.2 RESULTS

Upon establishment of hepatoblast organoids, we sought to test whether human hepatoblasts could survive and differentiate into hepatocyte- and cholangiocyte-like cells upon implantation *in vivo*. We were inspired by previous work which demonstrated that endothelial cells could support ectopic engraftment of hepatocytes in engineered tissue formats (*102*, *106*, *163*). To create tissues suitable for ectopic implantation, we thus constructed “human organoid tissues” containing hepatoblast organoids and human umbilical vein endothelial cells (HUVECs) embedded in fibrin-matrigel hydrogel (20:1 fibrin:matrigel mixture). For these studies, we used TdTomato-labeled hepatoblast organoids from two hepatoblast donors. Organoid tissues were sutured onto the inguinal fat pad of Fah-/-, Rag2-/-, Il2rg-/-, NOD (FRGN) mice. These mice experience

progressive liver failure unless administered nitisinone (NTBC) (*164*). We cycled transplanted mice on and off of NTBC over the course of the experiment to induce chronic liver disease, which has been shown previously to support hepatic engraftment and growth (*102*, *165*). After 27 days, implants were identified using the suture as a landmark and retrieved along with surrounding fat. Imaging of explanted tissues identified fluorescent cells along the suture and within the fat in all engrafted mice (Figure 2.2A), indicating that TdTomato-expressing organoids had engrafted.

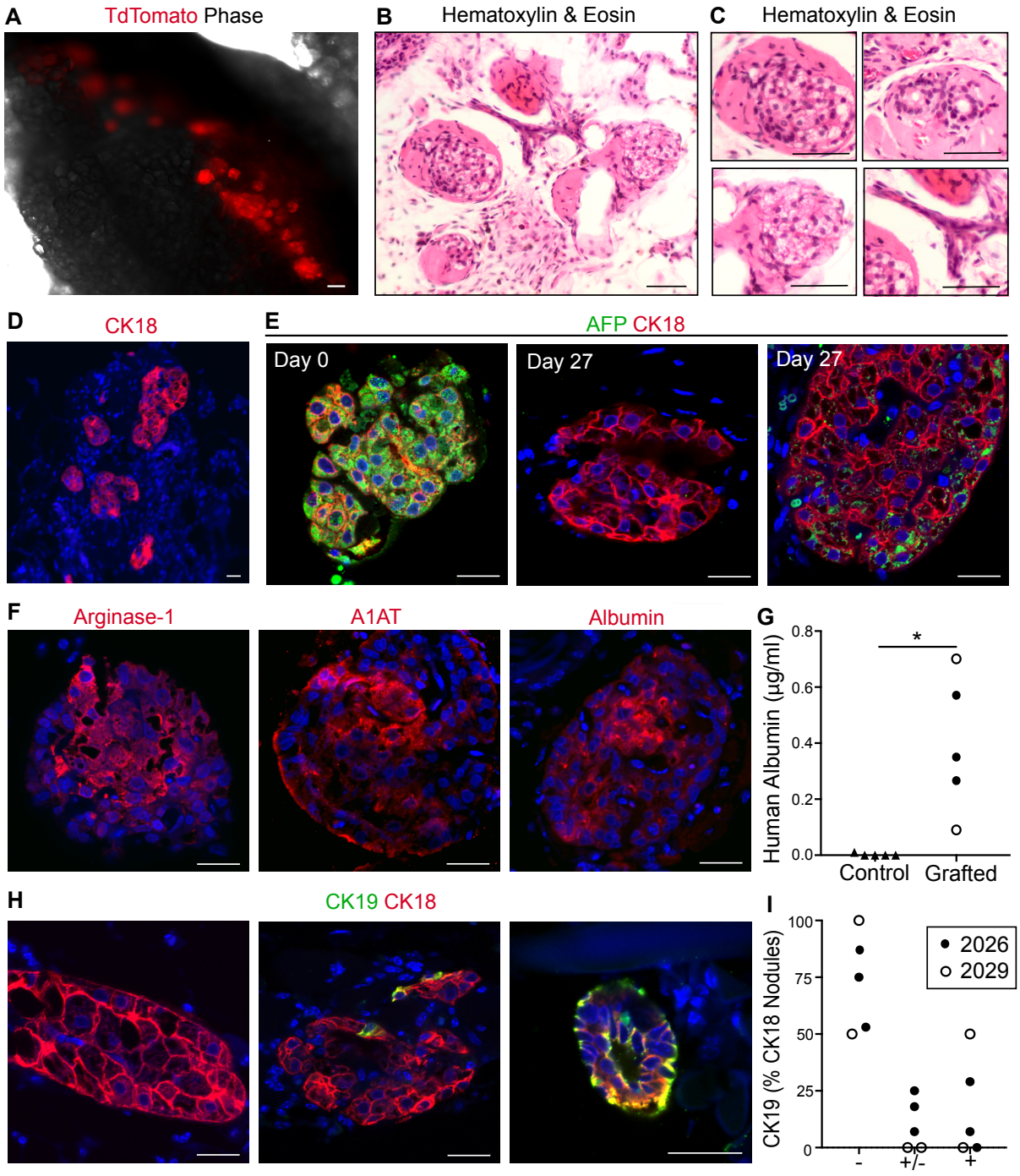

Figure 2.2: Hepatoblast organoids survive and differentiate upon implantation

(A) TdTomato-positive cell grafts (red) were identified in mouse fat (black, phase) upon explant of organoid tissues after 27 days of engraftment.

(B, C) Hematoxylin & eosin staining of explanted grafts identified numerous nodules with cells that morphologically resembled either densely packed hepatocytes (C, left) or biliary ductal-like structures (C, transverse section, right top; longitudinal section, right bottom).

(D) Nodules stained positively for human CK18 (red), suggesting they arose from grafted organoids.

(E) Despite high levels of AFP (green) expression in organoid tissues immediately prior to implant (Day 0, left), AFP expression was either not identified (center) or markedly decreased (right) in CK18-positive (red) nodules after 27 days of engraftment.

(F) Nodules with "hepatic" morphology contained cells that stained positively for hepatocyte markers Arginase-1 (left, red), A1AT (center, red), and albumin (right, red).

(G) Human albumin was detected in the blood serum of mice with organoid tissues at the time of sacrifice (closed circles, Donor 2026; open circles, Donor 2029; control is mouse serum without grafts, $p = 0.0223$).

(H, I) Immunostaining for cholangiocyte marker CK19 (green) and CK18 (red) identified nodules with no CK19 expression (left, "-"), nodules that contained some CK19-positive cells (center, "+/-"), and nodules in which cells self-assembled to resemble bile ducts and were nearly entirely positive for CK19 (right, "+"; closed circles, Donor 2026; open circles, Donor 2029).

Scale bars, 100 μm (A-C) or 20 μm (D-H). *$p < 0.05$, unpaired t-test with unequal variance.

We reasoned that hepatoblast organoids may have differentiated into cells characterized by hepatocyte or biliary signatures after engraftment. Interestingly, hematoxylin & eosin staining of explanted tissue sections revealed the presence of numerous nodules (Figure 2.2B) that contained cells morphologically resembling densely packed hepatocytes (Figure 2.2C, left), as well as cells resembling cholangiocytes that had self-assembled into structures reminiscent of bile ducts (Figure 2.2C, right top, transverse orientation; right bottom, longitudinal orientation). Nodules stained positively for human CK18, an intermediate filament expressed by both hepatocytes and biliary cells, suggesting that they indeed arose from grafted organoids. To assess the maturation state of grafted organoids, we stained tissue sections with alpha fetoprotein (AFP) and CK18. Organoids in engineered tissues stained positively for AFP at the time of implant, but AFP was either not identified (Figure 2.2E, center) or markedly decreased (Figure 2.2E, right) in CK18-positive

grafted organoids after engraftment. When present, AFP was typically localized to cells at the periphery of nodules (Figure 2.2E, right). CK18 also became more concentrated at the plasma membrane after implantation, assuming a morphology resembling mature hepatocytes (Figure 2.2D). To further assess whether any grafted cells expressed hepatocyte markers, we immunostained sections with arginase-1, an enzyme that catalyzes the hydrolysis of arginine to ornithine and urea (*166*), alpha-1-antitrypsin (A1AT), and albumin. Numerous cells stained positively for the three proteins in explanted grafts, often having greater levels of expression in the center of the graft in contrast to AFP localization (Figure 2.2F). Furthermore, human albumin was identified in mouse blood serum, suggesting that grafted organoid tissues synthesize human protein and had integrated with host vasculature (Figure 2.2G). Finally, to assess whether any grafted cells express markers associated with biliary phenotype, we immunostained tissue sections with CK19 (stem/biliary marker) and CK18. We found that most CK18-positive nodules (71%) had no cells that expressed CK19, 11% had some cells that expressed CK19, and 18% had cells which were nearly entirely positive for CK19 and had self-assembled to form smaller structures with characteristic ductal morphology (Figure 2.2H and I). Together, our results suggest that cells in organoid tissues have the capacity to progressively differentiate into cells characterized by hepatocyte and cholangiocyte markers upon engraftment.

2.3 DISCUSSION

Here, we describe the first use of human hepatoblast organoids as the parenchymal cell source in engineered liver tissues. Organoids not only can survive transplant, but also demonstrate function through human albumin secretion. Excitingly, in the *in vivo* environment hepatoblasts differentiate into both hepatocyte and cholangiocyte-like cells, a step that was not achievable *in vitro*.

Though the exact stimuli that drive maturation after implant is not yet known, multiple microenvironmental factors are likely at play. Paracrine signals and direct cell-cell contact between hepatoblasts and the neighboring endothelial and mesenchymal cells are thought to drive hepatoblast proliferation, migration, and eventual differentiation in the developing liver (*6*). While individual factors such as Wnt, TGFβ, and OSM are known to be critical in these processes (*7*), they are not the only pathways involved and thus simple media substitutions are unlikely to drive similar morphogenesis. After implantation, hepatoblasts are once again neighbors with stromal cells, exposing them to more complex angiocrine and paracrine signals that likely better mimic the hepatic developmental niche.

Additionally, bathing organoids in a homogenous media bath, as is done in basic *in vitro* culture, eliminates gradients of signaling factors known to drive differentiation and establish liver zonation (*16*, *30*). Signals that originate from stroma are more likely to be spatially restricted and thus establish gradients, which can direct differentiation of both hepatocytes and cholangiocytes simultaneously. While hepato-biliary crosstalk is less understood, it is thought that the presence of one cell type helps to hold the other in an appropriate niche, as the absence of biliary cells has been shown to induce compensatory transdifferentiation of hepatocytes (*167*). Thus, stromally-derived gradient signals allowing for bipotent differentiation of hepatoblasts are likely to play a critical role in maturation after implant. Mimicking these microenvironmental factors *in vitro* may help to drive more complete differentiation in a dish.

For the field of liver tissue engineering, successfully engrafting functional implants with an expandable hepatic cell source is a hugely impactful feat. Current liver cell therapies are generally limited to primary cells that are often unreliable and difficult to source (*90*). Hepatoblast organoids proliferate over months and are easily cryopreserved, bypassing major roadblocks for

cell sourcing. Unfortunately, after implant, engrafted hepatoblasts did not appear to proliferate extensively and were restricted to small, dispersed nodules. While this is an important model to probe hepatic development, it falls short of generating engineered liver tissues with potential for clinical translation, as grafts will need to be large and highly functional to support humans. Research has shown that more mature cell sources tend to have better engraftment outcomes after transplant (*153*, *154*), thus future work will focus on generating a more mature hepatic organoid that can expand in culture while retaining its differentiation state and phenotype.

2.4 METHODS

2.4.1 *2D cell culture*

Primary human umbilical vein endothelial cells (HUVECs, passage 2) were thawed and cultured in EGM-2 media (Lonza). Media was replaced every other day. Cells were passaged once before implantation.

2.4.2 *Hepatoblast organoid establishment and culture*

Hepatoblasts were resuspended in the hepatoblast organoid media, mixed with an equal volume of Growth Factor Reduced Phenol Free Matrigel (Corning), and pipetted into 48 well plates (10,000 cells in 20 μL per well). The plates were placed at 37ºC for fifteen minutes to allow the mixture to set, and subsequently 200 μL of fresh organoid media was added to each well. The culture medium was changed every 48-72 hours, and organoids were mechanically passaged every 7-10 days. Organoids were passaged by scraping the gel away from the plate, pipetting the resulting solution into 1.5 ml tubes, and pipetting the solution up and down to break individual organoids into pieces. If a precise cell number was required, the organoids could alternatively be processed to a single

cell solution with TrypLE, and then re-plated at the required dilution in the 50% Matrigel-medium solution.

2.4.3 *Encapsulation of organoids for implantation*

Hepatoblast organoids were isolated and suspended in 55% matrigel on ice. HUVECs were suspended in 10 mg/ml fibrin hydrogel (human thrombin, Sigma-Aldrich; bovine fibrinogen, Sigma-Aldrich) and mixed with organoids in un-polymerized matrigel at a 20:1 ratio. Cell/fibrin mix containing organoids and HUVECs was polymerized in disks from which 6 mm biopsies were punched to create "organoid tissues". Each 6 mm implant contained approximately 3,500 organoids and 100,000 HUVECs.

2.4.4 *Implantation and induction of liver injury*

All surgical procedures were conducted according to protocols approved by the University of Washington Institutional Animal Care and Use Committees. 14- to 18-week-old female Fah-/-, Rag2-/-, Il2rg-/-, NOD (FRGN) mice (Yecuris) were administered sustained release buprenorphrine and anesthetized with isofluorane. Two or three organoid tissues were sutured onto the gonadal fat pads of each mouse. Three mice received organoid tissues with Donor 2026 hepatoblasts and 2 mice received organoid tissues with Donor 2029 hepatoblasts. Incisions were closed aseptically. Nitisinone (NTBC) was withdrawn from animals' drinking water immediately after implantation of organoid tissues and for 14 days after implantation to induce liver injury. NTBC was then reintroduced to the drinking water to allow for recovery, and then removed again after 4 days for the remainder of the experiment. Animals were sacrificed 27 days after implantation of organoid tissues.

2.4.5 *Immunostaining*

Implants were harvested and fixed in 4% paraformaldehyde for 48 hours at 4°C. Excess fat was trimmed off of the implants, which were then dehydrated in graded ethanol (50-100%), embedded in paraffin, and sectioned using a microtome (6 μm). Some sections were histochemically stained with hematoxylin and eosin. For immunostaining, sections were blocked with normal donkey serum and incubated with primary antibodies against human CK18 (mouse, 1:25; Dako), CK19 (rabbit, 1:50; Abcam), arginase-1 (rabbit, 1:400; Sigma-Aldrich), human albumin (goat, 1:100; Bethyl Laboratories), human alpha-1-antitrypsin (rabbit, 1:100; Dako), or human AFP (rabbit, 1:100; Dako) and followed with species appropriate secondary antibodies conjugated to Alexa Fluor 488, 555, or 647. To semi-quantify CK19 distribution in nodules, graft nodules in which all cells were CK18+/CK19+ were tallied as "+". Nodules with both CK18+/CK19+ and CK18+/CK19- cells were tallied as "+/-". Nodules with only CK18+/CK19- cells were tallied as "-". Nodules in each category were summed across each tissue section and divided by total CK18+ grafts in the section to acquire percentages in each animal, with each data point representing one animal.

2.4.6 *Albumin ELISA*

Blood was drawn retro-orbitally for human albumin ELISA (Bethyl Laboratories) immediately prior to sacrifice at the termination of the experiment (27 days). Serum was separated by centrifugation and levels of human albumin were determined by an enzyme-linked immunosorbent assay (ELISA) using goat polyclonal capture and horseradish peroxidase–conjugated goat anti-human albumin detection antibodies (Bethyl Laboratories). Non-implanted FNRG mouse blood serum was included as a negative control.

2.4.7 *Statistics*

Statistical analyses were performed with an unpaired t-test with unequal variance (Welch's correction). $P < 0.05$ was considered statistically significant.

Chapter 3. GENERATING ORGANOIDS FROM ADULT HUMAN HEPATOCYTES

3.1 INTRODUCTION

As the largest solid organ in the body with hundreds of wide-ranging functions, the liver is essential for the maintenance of healthy human life (*168*). Some of the liver's roles include synthesis of plasma proteins, blood detoxification, drug metabolism, storage of glycogen, bile production and excretion, and cholesterol synthesis. Due to the high functional and metabolic demands on the liver, hepatic injury can have systemic and devastating effects on human health. Liver disease currently causes 3.5% of global mortality, with incidence of both chronic and acute disease continuing to increase annually (*41*). Those living with liver disease experience a severely reduced quality of life, which results in a significant and inequitable healthcare burden across the US and the world (*41*, *42*, *46*, *47*).

The vast majority of the liver's critical metabolic functions are performed by hepatocytes, an epithelial cell comprising ~80% of the liver parenchyma. The functional tasks carried out by hepatocytes arise progressively over human development, in tandem with human hepatocyte fate specification and maturation, with mature adult hepatocytes ultimately performing ~500 functions (*168*). Due to their hundreds of critical roles in human health, a source of mature human hepatocytes for research and translational applications would enable countless studies, ranging from basic liver biology to drug development to therapeutics such as implantable cell-based therapies for treating liver disease (*91*).

To address this need, numerous human hepatocyte sources have been explored. Yet, several of these, such as induced pluripotent stem cell (iPSC)-derived hepatocytes and fetal hepatocytes,

remain immature in phenotype and function (*88*). The immaturity of these cells makes them unsuitable for many applications requiring functionality or robust engraftment *in vivo*, as maturity highly correlates with engraftment success (*153*, *154*). Conversely, primary human hepatocytes isolated from adult livers are functionally mature (*90*, *91*, *153*, *154*), but cannot currently be propagated extensively *in vitro*. Moreover, these cells are typically structurally and functionally impaired upon recovery from cryopreservation and lose their morphology and functionality over days in culture unless supported by highly specialized culture methods or equipment (*78*, *82*, *85*, *99*). A reliable method to culture mature human hepatocytes *in vitro* in a manner that sustains their functionality and potential for later engraftment *in vivo* could transform basic liver biology and regenerative medicine.

One promising approach could be to leverage organoids – 3D "mini-organs" that have revolutionized culture of numerous primary epithelial cell types, ranging from the human intestine to kidney (*104*, *114*, *115*, *169*, *170*). In the liver field, human organoid culture methods have been developed that recapitulate several stages of embryonic and fetal hepatic development, including hepatoblasts (gestational weeks 3-7) (*112*), fetal hepatocytes (gestational weeks 7-20) (*113*), and one pediatric donor (*113*). In adult settings, liver organoids have been generated from cholangiocytes, which are the epithelial cells lining the liver's bile ducts that share epithelial signatures with hepatocytes but are otherwise functionally and phenotypically distinct (*114*, *117*, *168*). Thus far, reproducibly generating organoid cultures from adult human hepatocytes that replicate the diverse and numerous functions of mature human liver has remained elusive.

Here, we addressed this major need in human health. We optimized organoid growth conditions for mature human hepatocytes and tracked organoid growth over time to demonstrate significant expansion. We performed thorough characterization of all organoids that arise in

culture and ultimately determined that hepatocytes grown as organoids conserve the phenotype and function of their cell of origin throughout culture.

3.2 RESULTS

3.2.1 *Assessing developmental organoid medias for adult organoid formation*

We were inspired by recent progress in culturing adult epithelial organoids from cells embedded in droplets of soft extracellular matrix hydrogels (*170–172*). We postulated that culture in a physiologically relevant 3D matrix such as Matrigel, paired with stimulation from appropriate liver regenerative factors could induce adult primary human hepatocytes to form organoids (Figure 3.1) (*173*).

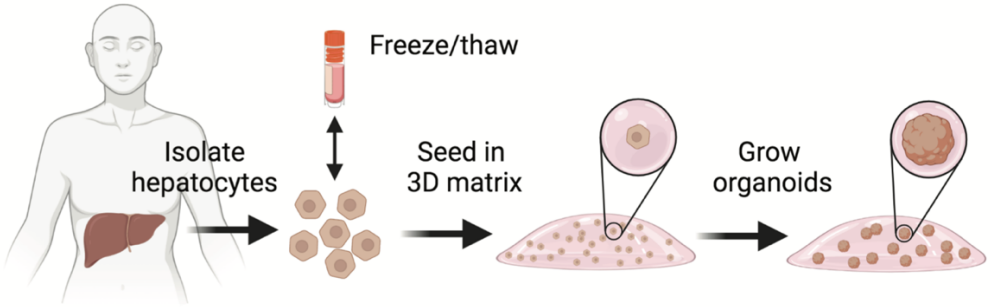

Figure 3.1: Schematic of hepatocyte organoid growth strategy

Hepatocytes are isolated from a human liver, cryopreserved, thawed, and seeded in a Matrigel droplet where single cells or small cell clumps then grow into small organoids.

To identify an ideal cocktail of growth stimuli, we looked to developmental hepatic organoid systems, as many important developmental signaling pathways overlap with those stimulating adult liver regeneration (*49*, *50*, *174*, *175*). First, we tested conditions previously

identified to support human hepatoblast or human fetal hepatocyte organoids for their organoid formation potential on previously cryopreserved primary human hepatocytes from a 34-year-old donor. Wnt and epidermal growth factor (EGF) pathways were stimulated, and rho-associated kinase (ROCK) and transforming growth factor-beta (TGFβ) pathways were inhibited for both hepatoblast and fetal hepatocyte conditions (*112*, *113*), with additional stimulation of hepatocyte growth factor (HGF), fibroblast growth factor (FGF), and transforming growth factor-alpha (TGFα) for fetal hepatocyte culture conditions (*113*) (Figure 3.2A). Over two weeks, single primary hepatocytes seeded in Matrigel formed into small organoids under both culture conditions (Figure 3.2B), though immunostaining revealed that nearly all cells grown under fetal hepatocyte conditions expressed cytokeratin-19 (CK19), a cytoskeletal protein strongly expressed by cholangiocytes and some hepatic progenitor cells, but generally absent in healthy mature hepatocytes (Figure 3.2C, left). Furthermore, many of the CK19+ organoids grown under fetal hepatocyte culture conditions had organized into a single or double layer of small cells forming a hollow cystic structure, a morphology typical of liver ductal cell or cholangiocyte organoids (*114*, *117*) (Figure 3.2C, left, arrow). Organoids grown under hepatoblast culture conditions also displayed ductal morphology, though dense organoids with strong expression of epithelial marker cytokeratin 18 (CK18) and low expression of CK19 were also present (Figure 3.2C, right). Immunostaining demonstrated that cells in dense organoids displayed hepatocyte morphological signatures such as a low nuclear-to-cytoplasmic ratio, strong CK18 expression at cell-cell junctions, and some binucleated cells (Figure 3.2C, right, arrowhead). Media supernatants from organoids cultured under each condition were also analyzed for the presence of human albumin, a protein produced in abundance by human hepatocytes, and thus a first-pass surrogate for querying the presence of functional hepatocytes. Human albumin secretion was consistently lower across

wells grown in fetal hepatocyte conditions, as compared to those grown in hepatoblast conditions, which had significantly higher albumin production, on average. However, albumin levels varied widely from well-to-well, with some containing no measurable albumin (Figure 3.2D). While the presence of occasional organoids with aspects of hepatocyte phenotype in hepatoblast culture conditions was encouraging, the phenotypic and functional consistency across cultures remained low. Thus, we next sought to achieve human hepatocyte organoid cultures with high purity, functionality, and well-to-well consistency across cultures.

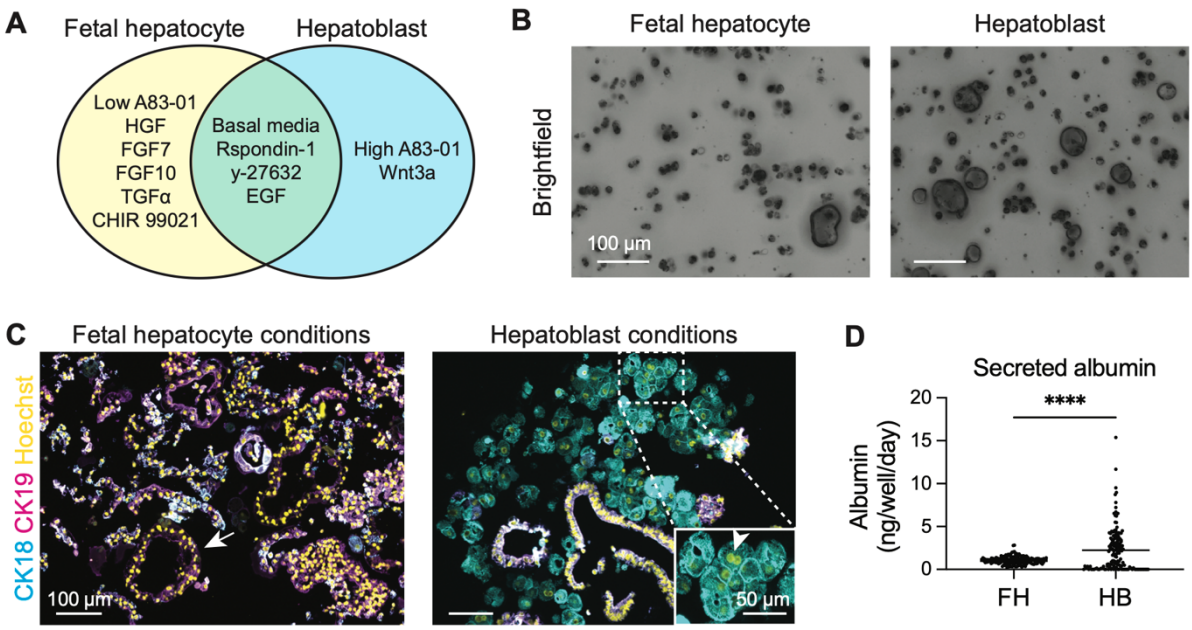

Figure 3.2: Comparing developmental hepatic organoid medias for adult human hepatocyte organoid formation

(A) Venn diagram illustrating media differences between fetal hepatocyte (left, yellow) and hepatoblast (right, blue) organoid medias. Green shows shared media components.

(B) Representative minimum intensity projections of brightfield z-stacks of adult human hepatocytes grown in fetal hepatocyte organoid conditions (left) or hepatoblast organoid conditions (right). Scale bar = 100 µm.

(C) Immunofluorescence images of adult human hepatocytes grown in fetal hepatocyte organoid conditions (left) or hepatoblast organoid conditions (right) stained for CK18 (cyan), CK19 (magenta), and Hoechst (yellow). Arrow on left identifies an intact cystic organoid, arrowhead in right inset indicates binucleated cell. Scale bar = 100 μm, 50 μm for inset.

(D) Albumin secretion measured by human albumin ELISA comparing adult human hepatocytes grown in fetal hepatoblast organoid conditions or hepatoblast organoid conditions. Data represented as mean +/- SEM of 154 replicates at day 12. Welsh's t test, **** $p < 0.0001$.

3.2.2 *Optimizing adult hepatocyte organoid media through growth factor and small molecule screen*

Seeking improved purity, functionality and consistency, we further supplemented hepatoblast media with a portfolio of additional factors implicated in liver development and regeneration, including growth factors HGF, FGF1, FGF2, FGF7, FGF10, TGFα, and the small molecule A83-01 (Table 1). After one week, brightfield imaging identified two conditions that robustly supported gross organoid growth and morphology (Figure 3.3A; conditions 7 and 9). This observation was confirmed with morphometric analysis of brightfield images showing a significant increase in average object area, a metric of organoid size (Figure 3.3B). Organoids cultured under these two conditions also had significantly higher human albumin secretion compared to all other conditions screened (Figure 3.3C). Notably, compared to all others tested, both of these conditions had a lower concentration of A83-01, a small molecule that blocks TGFβ signaling through inhibition of TGFβ receptor 1.

Table 1: Growth factor (GF) and small molecule (SM) components of media screen

Media	Base	HGF	FGF10	FGF7	Low A83-01	TGFα	FGF1	FGF2
1	Base (high A83-01)							
2	Fetal hepatocyte	+	+	+	+	+		
3	No GF or SM							
4	Base	+						
5	Base		+					
6	Base			+				
7	Base				+			
8	Base	+	+	+		+		
9	Base	+	+		+			
10	Base						+	
11	Base							+

Of the two conditions with low A83-01, one (condition 9) was additionally supplemented with HGF and FGF10 and generated organoids that demonstrated intermediate or mixed phenotypes, with the majority of organoids exhibiting dense morphology but heterogenous CK19 expression (Figure 3.3D, left). Conversely, organoids from the second condition (condition 7, with no HGF or FGF10) demonstrated a more consistent morphology in which organoids were predominantly dense and contained CK18+/CK19- cells (Figure 3.3D, right). Due to this phenotypic conservation paired with improved organoid formation and high function, condition 7 was used to culture adult human hepatocytes as organoids for all subsequent phenotypic and functional analyses, which we hereafter refer to as "mature human hepatocyte culture conditions".

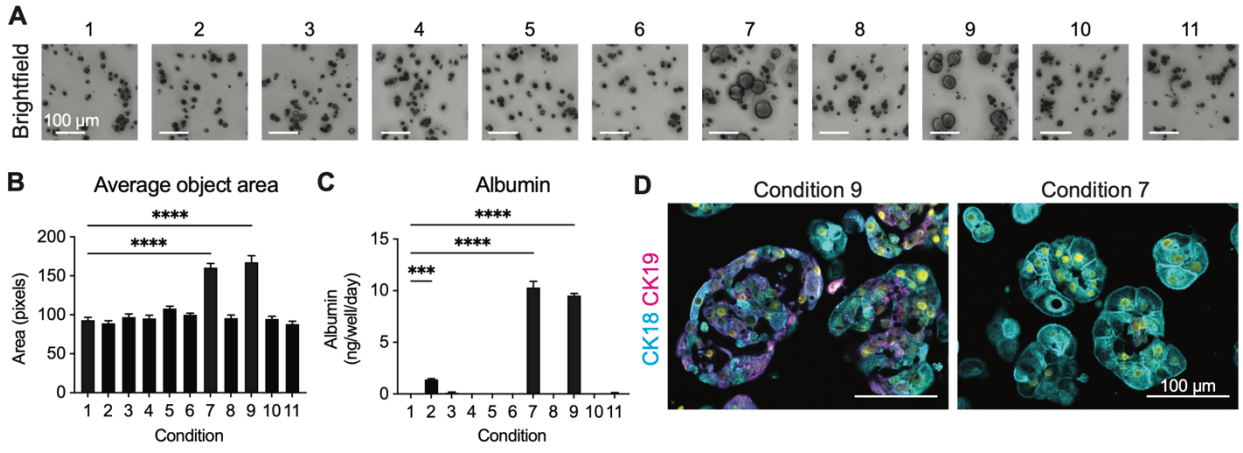

Figure 3.3: *In vitro* screening identifies optimal adult human hepatocyte organoid culture conditions

(A) Representative minimum intensity projections of brightfield z-stacks of adult human hepatocytes grown in 11 different culture conditions listed in Table 1. Scale bar = 100 μm.

(B) Average cross-sectional area of all cellular and multicellular objects in a single well at day 7. Data represented as mean +/- SEM of 16 wells. One-way ANOVA, Dunnett's multiple comparisons test, **** $p < 0.0001$.

(C) Albumin secretion measured by human albumin ELISA comparing adult human hepatocytes grown in 11 different media conditions listed in (E). Data represented as mean +/- SEM of 4 wells at day 9. One-way ANOVA, Dunnett's multiple comparisons test, *** $p < 0.001$, **** $p < 0.0001$.

(D) Immunofluorescence images comparing adult human hepatocyte organoids grown in condition 9 (left) and condition 7 (right) stained for CK18 (cyan), CK19 (magenta), and Hoechst (yellow). Scale bar = 100 μm.

3.2.3 *Analyzing adult hepatocyte organoid growth and phenotype*

We next sought to characterize the growth and phenotype of human hepatocytes cultured under mature human hepatocyte culture conditions. To do this, we grew human hepatocytes from a 19-year-old donor as organoids and then measured the cross-sectional area of cellular or multicellular objects in brightfield images over time. On the first day after cell seeding, the average area of all objects measured was 907 μm^2 (estimated ~34 μm diameter, assuming sphericity) with a normal distribution, reflecting a relatively homogenous population of single hepatocytes or small clumps of a few cells (Figure 3.4A-C). By day 5, however, the cell population had begun to separate into a bimodal distribution, with a lower mode representing inert single cells and an upper mode representing growing organoids. The distribution further stratified by day 14, with ~1/3 of objects forming organoids (Figure 3.4C-E) that ranged from ~50 μm to over 150 μm in diameter.

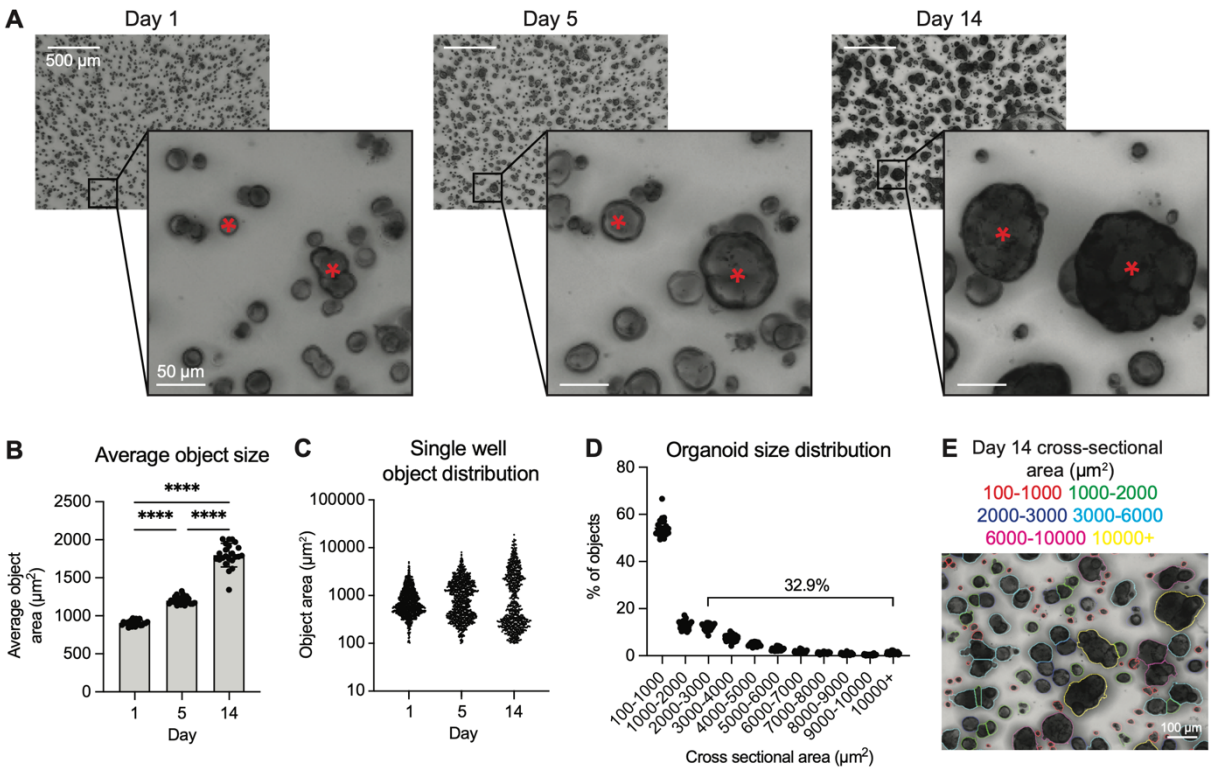

Figure 3.4: Adult human hepatocytes exhibit significant growth throughout organoid culture

(A) Representative minimum intensity projections of brightfield z-stacks used for quantification in (B). Images were taken in the center of Matrigel droplets on days 1, 5, and 14. Red asterisks track individual cells/organoids over time. Scale bars = 500 µm for low magnification and 50 µm for inset images.

(B) Average cross-sectional area of all cellular and multicellular objects in individual wells on days 1, 5, and 14. Data represented as mean +/- SEM of 23 wells. One-way ANOVA, Tukey's multiple comparisons test, **** $p < 0.0001$.

(C) Cross-sectional area of each cellular/multicellular object in a single well at day 1, 5, and 14. Each dot represents a single object.

(D) Distribution of object sizes at day 14 across 24 wells. Each dot represents the percentage of organoids in that size range in a single well. On average 32.9% of objects were larger than 2000 μm^2 and thus were considered organoids.

(E) Minimum intensity projection of brightfield z-stack demonstrating color-coded cross-sectional area ranges used for quantification in (B-D). Scale bar = 100 µm.

To further investigate the phenotypic identity of the cells comprising the organoids, we performed immunostaining for various structural and functional hepatic proteins. Immunostaining for CK18 demonstrated that cells self-organized into densely packed spheroids with large cells and a low nuclear to cytoplasmic ratio, similar to primary hepatocytes (Figure 3.5A). Cells in adult human hepatocyte organoids were largely negative for the biliary/progenitor cell marker CK19, though occasional cells were found that were CK19+, but generally maintained hepatic as opposed to biliary morphology (Figure 3.5A). The majority of cells expressed albumin (Alb), a marker of functional hepatocytes, and arginase-1 (Arg1), an enzyme involved in nitrogen metabolism (Figure 3.5B and C). Adult human hepatocyte organoids also expressed the cell-cell junction protein E-cadherin (E-cad), which was primarily located at the cell membrane and between cells (Figure 3.5C). Multidrug resistance-associated protein 2 (MRP2), an efflux transporter located in the bile canaliculi on the apical domain of polarized hepatocytes, was expressed on the interior of dense organoids (Figure 3.5B). Samples were then immunostained for both albumin and Ki67, a protein associated with the cell cycle and thus used as a marker for proliferating cells. Ki67+ nuclei made up 34% and 1% of all albumin+ nuclei on days 5 and 15, respectively (Figure 3.5D and E). Rare Ki67+ mitotic figures were also identified, suggesting that hepatocytes in organoid culture were actively undergoing cell division (Figure 3.5F).

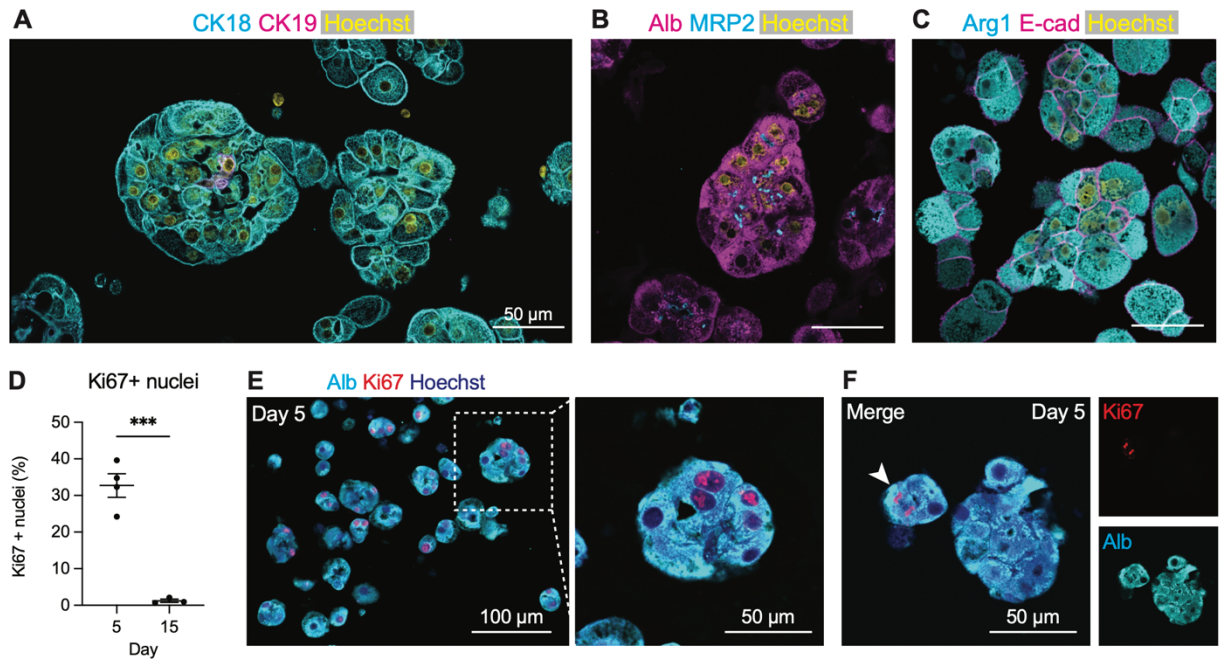

Figure 3.5: Adult human hepatocyte organoids maintain phenotype and morphology despite early proliferation

(A-C) 2D confocal images of day 14 organoids stained for (A) CK18 (cyan) and CK19 (magenta), (B) Alb (magenta) and MRP2 (cyan) (middle), or (C) Arg1 (cyan) and E-cad (magenta) (right). Nuclei stained for Hoechst (yellow) in all images. Scale bars = 50 µm.

(D) Quantification of Ki67+ nuclei in Alb+ cells at days 5 and 15. Data represented as mean +/- SEM of 3 or 4 replicates. Unpaired t test, *** $p < 0.001$.

(E) Immunofluorescence image of day 5 organoid sample stained for Alb (cyan), Ki67 (red), and Hoechst (blue). Scale bar = 100 µm for low magnification, 50 µm for inset image.

(F) Fluorescence image demonstrating mitotic figure (arrowhead) in day 5 organoid stained for Alb (cyan), Ki67 (red), and Hoechst (blue). Image shown merged (left) and with Ki67 and Alb channels separated (right). Scale bar = 50 µm.

Alongside adult human hepatocyte organoids, rare and distinct cystic ductal organoids formed that were CK19, CK18, and E-cad positive, and MRP2, Alb, and Arg1 negative (Figure 3.6), but accounted for only ~0.16% of cellular objects (Figure 3.6A), possibly arising from contaminating cholangiocytes. Overall, imaging and immunostaining demonstrated that adult

human hepatocytes formed organoids that grew over time in culture, and that these cells maintained robust adult primary hepatocyte morphology and phenotype.

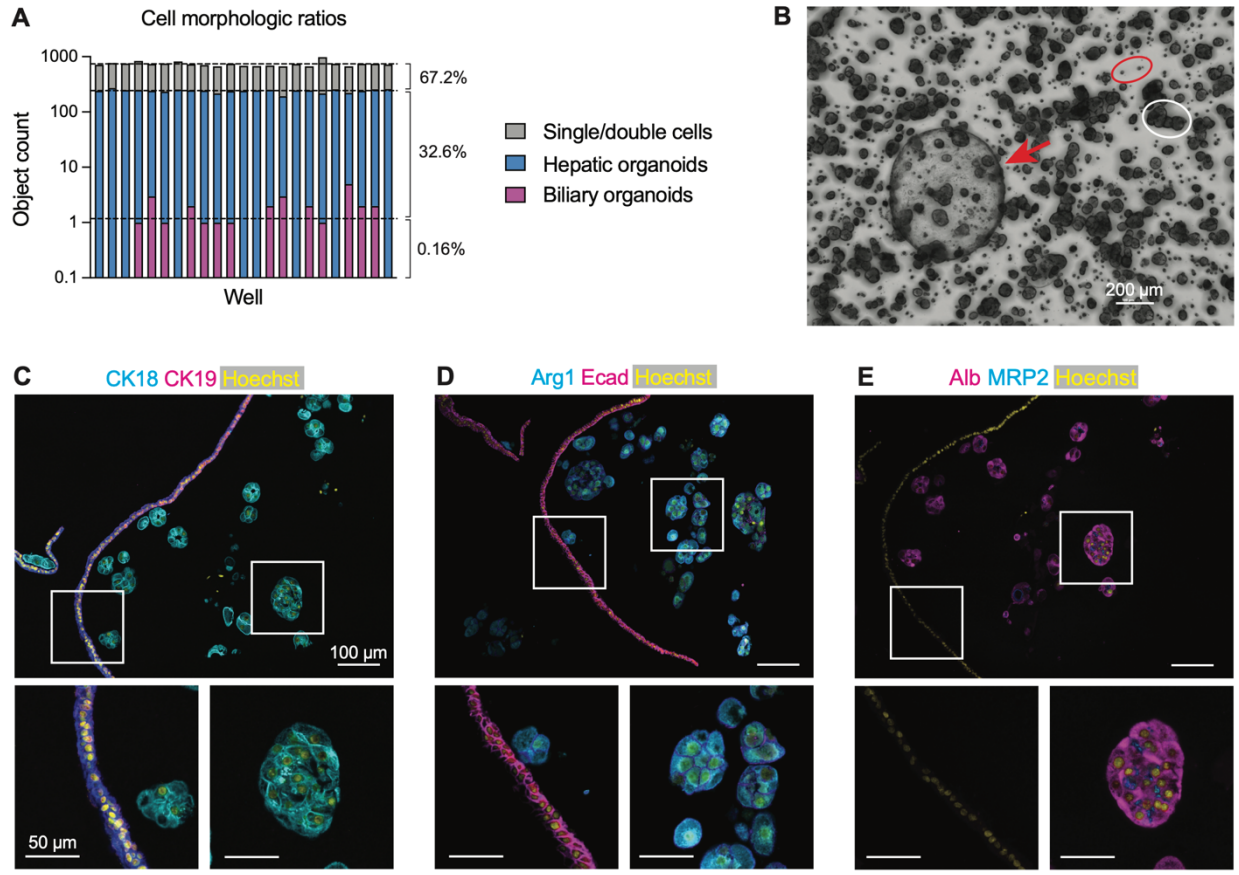

Figure 3.6: Phenotypic characterization of adult human hepatocyte organoid cultures

(A) Distribution of cellular morphologies across 24 wells. Biliary organoids (cystic morphology, pink bars) make up an average of 0.16% of all cellular objects. Hepatic organoids (dense morphology, area > 2000 µm^2, blue bars) make up an average of 32.6% of all cellular objects. Single/double cells (dense morphology, area < 2000 µm^2, grey bars) make up remaining 67.2% of all cellular objects.

(B) Minimum intensity projection of brightfield z-stack demonstrating cellular morphologies used for quantification in (A). Red arrow indicates biliary organoid with cystic morphology. White circle indicates cluster of hepatic organoids with dense morphology. Red circle indicates single/double cells. Scale bar = 200 µm.

(C-E) Fluorescence images of serial day 14 organoid sections stained for (C) CK18 (cyan) and CK19 (magenta), (D) Arg1 (cyan) and Ecad (magenta), and (E) Alb (magenta) and MRP2 (cyan). Nuclei

stained for Hoechst (yellow) in all images. Left insets demonstrate a cystic biliary organoid, right insets demonstrate dense hepatic organoid. Low magnification scale bar = 100 μm, inset scale bars = 50 μm.

To better assess both the 3D morphology and phenotype of cells within organoids, we immunostained, cleared, 3D imaged and computationally reconstructed organoid cultures. These studies further demonstrated conservation of hepatocyte morphology and protein localization, with cytoplasmic Arg1 staining (Figure 3.7A), nuclear expression of hepatocyte transcription factor HNF4α (Figure 3.7B), and strong expression of E-cad at cell-cell junctions throughout the organoid depth and at various sizes (Figure 3.7A and B).

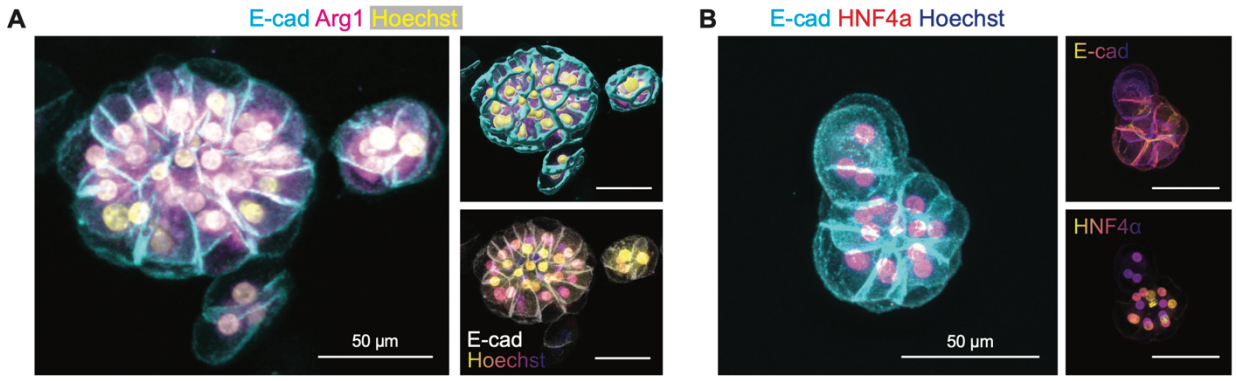

Figure 3.7: 3D imaging of adult human hepatocyte organoids demonstrates hepatocyte phenotype and morphology through organoid depth

(A) 3D reconstructed confocal z-stack of day 14 organoids stained for E-cad (cyan), Arg1 (magenta), and Hoechst (yellow). Visualization methods: maximum intensity projection (left), Imaris surface rendering of E-cad and Hoechst (top right), depth color coding of Hoechst (yellow=top, pink=middle, blue=bottom) with E-cad in white (bottom right). Scale bars = 50 μm.

(B) 3D reconstructed confocal z-stack of day 14 organoids stained for E-cad (cyan), HNF4α (red), and Hoechst (blue). Visualization methods: maximum intensity projection (left), depth color coding of E-cad (top right), and HNF4α (bottom right) (yellow=top, pink=middle, blue=bottom). Scale bars = 50 μm.

3.3 DISCUSSION

Here, we describe a novel adult human hepatocyte organoid culture method that closely maintains the phenotype and morphology of hepatocytes in human liver. Adult human hepatocyte organoids transiently proliferate to significantly expand the cell population. Cholangiocyte organoids also co-arise with hepatocyte organoids, likely emerging from contaminating cholangiocytes in the initial population, but possibly from hepatocyte transdifferentiation (*167*).

Adult human hepatocyte organoids are an excellent new liver model and a significant improvement on previous hepatic organoids (*113*, *114*), but fall short of providing an indefinitely expandable hepatocyte cell source. A high number of Ki67+ cycling nuclei at day 5 decline to almost no cycling hepatocytes by day 15. This is matched by an initial burst of cell expansion, with approximately 30% of seeded hepatocytes forming organoids, suggesting that organoids are not arising from a rare stem cell population, but instead are forming from transient proliferation of normally quiescent hepatocytes. Interestingly, this follows a similar trajectory of hepatocyte growth and remodeling after partial hepatectomy, where all hepatocytes in the remaining liver tissue divide once or twice to recover lost tissue mass then return to quiescence. Adult human hepatocyte organoids may then serve as an *in vitro* model of liver regeneration, a process that is poorly understood in humans.

Simultaneous formation of hepatocyte and cholangiocyte organoids is another unique and occasionally frustrating feature of our culture format. Though hepatocytes and cholangiocytes should co-exist in the liver, cholangiocyte organoids have sustained and rapid proliferation, meaning that they quickly outnumber hepatocytes and prevent passaging. Strategies to limit biliary growth will be discussed in Chapter 8, but it raises the interesting possibility that the presence of cholangiocytes may be critical for maintenance of hepatocytes. As hepatocytes and cholangiocytes

differentiate simultaneously and in adjacent cell layers of the liver bud (*6*), parenchymal signaling between the two cell types may be important for differentiation of each. It has been demonstrated in mice that when the biliary tree fails to develop, hepatocytes can transdifferentiate to cholangiocytes to form a biliary system *de novo* (*167*). Thus, it is possible that in the absence of cholangiocytes, hepatocytes would be induced to adopt a biliary phenotype to fill the missing niche. Our adult human hepatocyte organoid system provides an interesting model to study this hypothesis and gain insight into other poorly understood aspects of human liver regeneration.

3.4 METHODS

3.4.1 *Organoid culture of hepatocytes*

Cryopreserved hepatocytes were thawed into 37°C medium and quickly spun down at 70 x g. Cells were mixed with 45% organoid media and 55% Matrigel and seeded in 20 µl droplets in each well of 48-well plates. After Matrigel had solidified, 200 µl of organoid medium was added to each well. Organoid medium: 40% Basal medium (DMEM/F12, 1x GlutaMAX, 1x HEPES, 1x penicillin-streptomycin, 2% B27, 10 mM nicotinamide, 1.25 mM N-acetyl cysteine, 10 nM gastrin), 50% Wnt3a conditioned medium, 10% Rspo1 conditioned medium, 50 ng/ml EGF, 5 µM A83-01, and 10 µM y-27632. Medium was refreshed every 2-3 days with care not to disturb the Matrigel droplet. Organoid size and growth were quantified from minimum intensity projections of brightfield z-stacks taken on a Nikon Eclipse Ti inverted high-resolution widefield microscope.

3.4.2 *Brightfield microscopy and morphometric analysis*

Brightfield z-stack images were taken in the center of each organoid well at multiple timepoints on a Nikon Eclipse Ti inverted high-resolution widefield microscope. Z-stacks were flattened into

a single image using a minimum intensity projection (MinIP) with FIJI or Nikon NIS-Elements software. Organoid size and growth were quantified from MinIP images in ImageJ software and graphed with GraphPad Prism software.

3.4.3 *Organoid histology, immunofluorescent staining and microscopy*

Organoids were harvested from Matrigel and fixed in 4% PFA at room temperature for 30 minutes, then embedded in HistoGel (VWR). For 2D histology, HistoGel pellets were dehydrated in ethanol, embedded in paraffin, and sectioned using a microtome (5-6mm sections). Immunofluorescence staining of organoids was performed by deparaffinizing sections, performing antigen retrieval, blocking with normal donkey serum for 1 hour at room temperature, then incubating with primary antibody overnight at 4°C. The following day, sections were washed with PBS-T and then incubated with secondary antibody + Hoechst 33342 (Thermo H3570) for 1 hour at room temperature, washed, and mounted with Fluoromount-G (Invitrogen). For 3D imaging, organoids in HistoGel were blocked in bovine serum albumin and normal donkey serum overnight at room temperature then incubated with primary antibodies for 24 hours at 37°C. After washing for 6 hours at room temperature, organoids were incubated with secondary antibodies overnight at 37°C. Finally, organoids were washed for 6 hours at room temperature and then cleared by bathing in Ce3D solution (*176*) overnight at room temperature with Hoechst 33342. All antibody information is included in Table 2. Images were obtained using a Nikon Eclipse Ti inverted high-resolution widefield microscope, a Nikon A1R scanning confocal microscope, or a Leica SP8 confocal microscope. Images were processed using Adobe Photoshop or ImageJ software. For morphometric analyses, images were thresholded and pixels were measured using ImageJ software.

Table 2: Antibody information

Antibody	*Vendor/Product #*	*Species*	*Dilution*
Human cytokeratin-18	Dako M701029-2	Mouse	1:25
Cytokeratin-19	Abcam ab52625	Rabbit	1:100
Human albumin	Bethyl A80-129A	Goat	1:100
Arginase-1	Sigma HPA003595	Rabbit	1:200
MRP2	Thermo TA812520	Mouse	1:500
HNF4a	Abcam ab201460	Rabbit	1:100
Ter119	BD Pharmingen 550565	Rat	1:100
Ecad	R&D AF748	Goat	1:100
Ki67	Abcam ab16667	Rabbit	1:500
Goat anti-mouse 555	Invitrogen A21127	Goat	1:500
Donkey anti-mouse 555	Invitrogen A31570	Donkey	1:1000
Donkey anti-rabbit 594	Invitrogen A21207	Donkey	1:1000
Donkey anti-rabbit 647	Invitrogen A31573	Donkey	1:1000
Donkey anti-goat 488	Invitrogen A11055	Donkey	1:1000
Donkey anti-goat 647	Invitrogen A21447	Donkey	1:1000
Donkey anti-rat 488	Invitrogen A21208	Donkey	1:1000

3.4.4 *Albumin ELISA*

Organoid media was collected every 2-3 days and frozen. Secreted human albumin was then measured in media via enzyme linked immunosorbent assay (ELISA) using a goat anti-human albumin coating antibody and horseradish peroxidase-conjugated goat anti-human albumin detection antibody (Bethyl E80-129).

3.4.5 *Statistical Analysis*

Data in graphs are expressed as the mean ± SEM, as denoted in figure legends. Statistical significance was determined with PRISM software using *t*-test, one-way ANOVA, or two-way ANOVA followed by Sidak's, Dunnett's, or Tukey's multiple comparison test, as denoted in figure legends.

Chapter 4. ADULT HUMAN HEPATOCYTE ORGANOIDS FORM FROM A DIVERSE SET OF POST-ADOLESCENT DONOR HEPATOCYTES AND MAINTAIN ROBUST HEPATIC FUNCTIONS

4.1 INTRODUCTION

A confounding issue for development of adult human hepatocyte therapies and model systems has been major variability in cell viability and the functional quality of primary hepatocytes isolated from different human donor livers (*81*, *177*, *178*). While some functional differences are expected due to natural variation in human biology (*81*, *179*, *180*), research is often stymied by donor hepatocytes that are non-adherent or non-viable in 2D culture, or cells that cannot engraft after implant (*82*, *177*, *181*). This is due in part to cell stress and downregulation of adhesion molecules induced by isolation from the liver (*87*), and exacerbated by damage from cryopreservation and thaw (*82*, *85*). This often leads labs to select a single lot of donor hepatocytes that has the best viability and cell attachment that they use for all studies, reducing biological variability. New strategies to culture adult hepatocytes from diverse samples could recover previously unusable cells and enable longer-term hepatic studies on samples with broader genetic and ancestral variation (*83*, *84*).

Additionally, many studies of hepatic culture methods look at a single metric, such as albumin secretion, to verify function. This can lead to cells or techniques that are biased towards one functional axis and thus do not represent the broad range of functions needed to accurately represent the liver *in vitro*. Thus, we sought to determine whether organoid culture could reliably

generate broadly functional, adult human hepatocyte organoids from an additional set of seven diverse adult donors.

4.2 RESULTS

4.2.1 *Adult human hepatocyte organoids form from a diverse set of post-adolescent donor hepatocytes*

First, we identified human donor lots with reported variation in 2D plating longevity, in which hepatocytes were viable for only 3 days, 5 days, or beyond 5 days of culture as reported by the vendor (Table 3). From these we selected a subset of donors ranging in age from 19-49 years old with varying sex (71% female, 29% male) and racial/ethnic demographics (71% White, 14% Black, 14% Latine/Hispanic) (Table 3).

Table 3: Patient data for human hepatocyte lot screening

Lot	Age	Sex	Race/ Ethnicity	2D viability*	CYP3A induction*
1	49	F	White	5+	x
2	31	M	White	5 days	21.1
3	31	F	Black	5+	4.9
4	37	F	White	3 days	x
5	24	M	Hispanic	5 days	28.1
6	26	F	White	5 days	34.6
7	19	F	White	5+	6.6

* = reported by Invitrogen x = data not available

Plating efficiency in 2D was confirmed to be highly variable (Figure 4.1A). Despite this, after plating hepatocytes from all seven donor lots for 3D culture, adult human hepatocytes formed organoids with compact hepatic morphology across all lots, as observed by brightfield morphology (Figure 4.1B). Immunostaining demonstrated that organoids from all lots expressed the epithelial marker CK18 and that individual cells had adult hepatocyte morphology (Figure 4.1C). Similar to

our earlier studies, cystic ductal organoids expressing CK19 were rare (<0.2%) and found in cultures for all human donor lots (Figure 4.1C). Thus, adult human hepatocytes from seven additional different donors, which in 2D culture demonstrated highly variable 2D plating efficiency, successfully formed organoids when grown in mature human hepatocyte culture conditions.

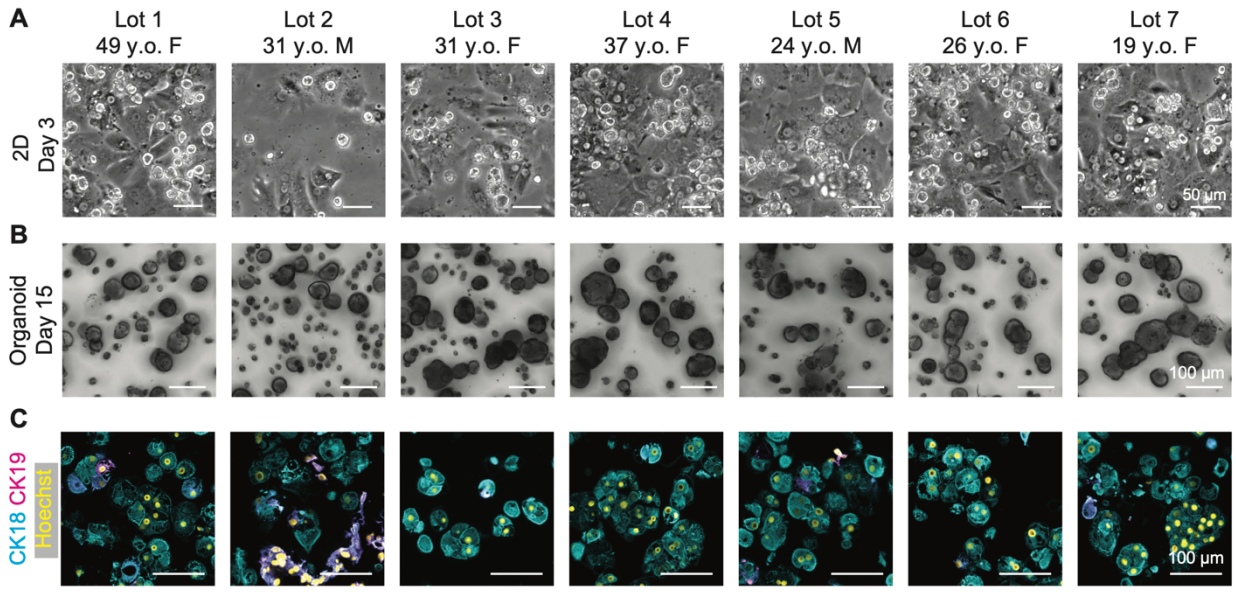

Figure 4.1: Hepatocyte morphology and function are better preserved by organoid culture conditions

(A) Representative brightfield images of cells derived from seven separate donors, Lots 1-7, in 2D culture on collagen coated plates at day 3. Donor age listed above image. Scale bar = 50 µm.

(B) Representative minimum intensity projections of brightfield z-stacks across all seven lots screened. Images were taken in the center of Matrigel droplets on day 15. Scale bars = 100 µm.

(C) Immunofluorescence images across all seven lots screened stained for CK18 (cyan), CK19 (magenta), and Hoechst (yellow). Scale bars = 100 µm.

4.2.2 *Adult human hepatocyte organoids maintain expression of functional and mature hepatic genes*

Although hepatocytes comprise a workforce that performs hundreds of functions within the human liver (*168*), hepatocyte functions decline rapidly in most 2D culture formats *in vitro* in the absence of highly engineered microenvironments, restricting their utility as a liver model (*78*, *99*). Encouraged by the robust adult human hepatocyte organoid formation across all donor lots tested, we next sought to assess hepatocyte functions across the various donors.

We first assessed gene expression across different hepatocyte functional axes and compared adult human hepatocyte organoid gene expression to hepatic cells from various stages of liver development, including human hepatoblast organoids (HBO) representing early development (*112*), freshly thawed primary adult human hepatocytes (PHH), and whole adult human liver RNA (HuLiv). We first assessed expression of a panel of genes encoding secreted proteins that are upregulated in development and stay highly expressed in hepatocytes throughout adulthood, *ALB, ARG1, SERPINA1*, and *TF* (*112*, *182*), which provide instructions for making the proteins albumin, arginase-1, alpha-1 antitrypsin, and transferrin, respectively. Adult human hepatocyte organoids from all lots had high and remarkably similar expression for all adult protein-encoding genes (Figure 4.2). Next, we assessed genes known to be differentially expressed between fetal and adult liver (*183*). Alpha-fetoprotein (*AFP*), is expressed at high levels in fetal liver, declines post-natally and is generally absent in adult hepatocytes (*112*, *182*). As expected, human hepatoblast controls exhibited high expression of *AFP* (Figure 4.2). Conversely, adult human hepatocyte organoids had little to no *AFP* expression, similar to adult mature hepatocyte and human liver controls (Figure 4.2). We next sought to interrogate gene expression of two enzymes responsible for the metabolism of ~40% of drugs in humans, cytochrome P450 genes *CYP1A2* and *CYP3A4* (*184*). The majority of CYP enzymes, aside from fetal isoforms such as

CYP3A7, are expressed at low levels in fetal developmental stages and increase with hepatocyte maturation (*28*, *185–188*). Consistent with embryonic and fetal liver stages, human hepatoblasts had low to no *CYP1A2* or *CYP3A4* expression. In contrast and importantly, adult human hepatocyte organoids exhibited high gene expression in all lots, and at similar levels as adult controls (Figure 4.2). This maintenance of mature gene expression and dearth of fetal genes demonstrates successful preservation of adult liver transcription across all lots and differentiates adult human hepatocyte organoid culture from models with an immature phenotype.

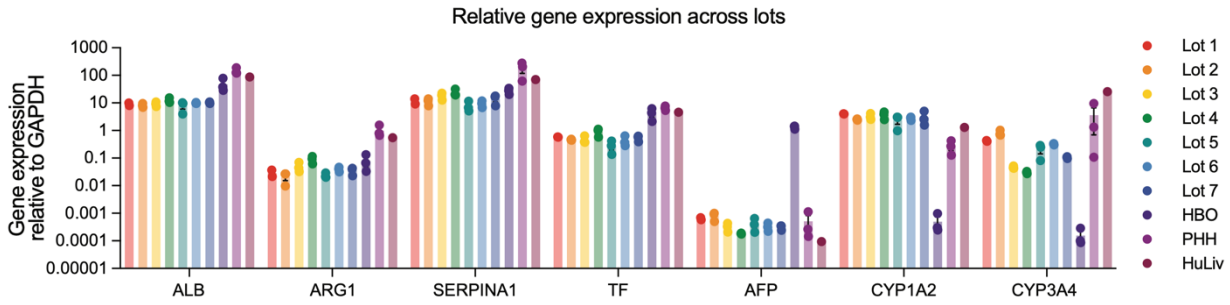

Figure 4.2: Hepatic gene expression demonstrates maturity across all hepatocyte donor lots

Gene expression analysis by qRT-PCR on genes of interest across all lots compared to RNA from hepatoblast organoids (HBO), freshly thawed primary human hepatocytes (PHH), and whole liver RNA (HuLiv). Gene expression relative to *GAPDH* for each sample. Data represented as mean +/- SEM of 2 or 3 replicates, each measured in technical triplicate.

4.2.3 *Screening hepatic functional axes in adult human hepatocyte organoids*

Next, we explored a panel of functional assays to assess the extent to which hepatocytes maintain important liver functions after organoid culture. Human albumin protein was measured over time to explore the secretory function of adult human hepatocyte organoids. All lots increased albumin production as organoids grew, with an average of 150-fold increase over 2 weeks (Figure 4.3A).

The lots with the highest albumin secretion at day 14 were also found to have the highest percentage of hepatocytes expressing Ki67 at day 5 (correlation coefficient R2 = 0.8831), suggesting that the substantive increase in albumin over time was at least partly due to cell growth and organoid expansion (Figure 4.3B). Synthesis of urea, a byproduct of ammonia detoxification, was also present in cultures derived from all lots, with differential patterns of urea secretion across lots mirroring trends of albumin secretion for each donor (Figure 4.3C).

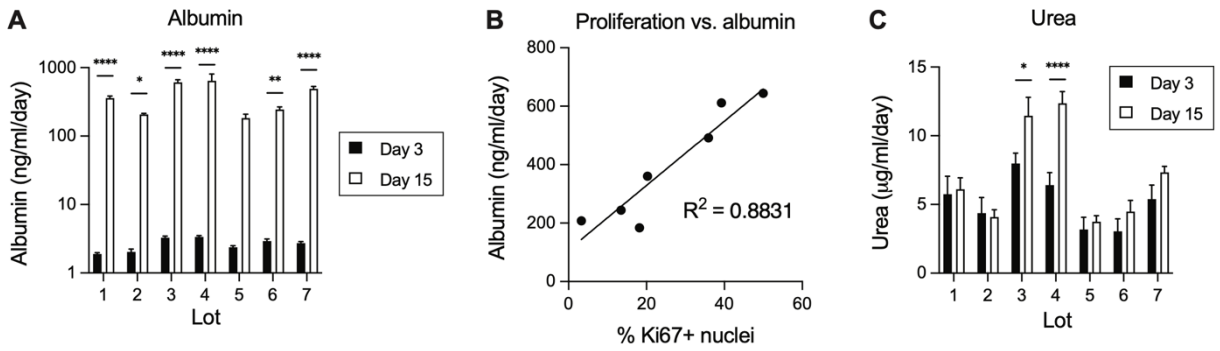

Figure 4.3: Secretory functions of adult human hepatocyte organoids increase with organoid growth

(A) Albumin secretion across all lots measured by human albumin ELISA. Data represented as mean +/- SEM of 8 replicates at day 3 (black) and day 15 (white). Two-way ANOVA, Sidak's multiple comparisons test, * $p < 0.05$, ** $p < 0.01$, **** $p < 0.0001$.

(B) Scatter plot of albumin secretion at day 15 vs percent of Ki67+ nuclei at day 5 across the 7 donor lots shows correlation coefficient $R^2 = 0.8831$.

(C) Urea secretion across all lots measured by BUN assay. Data represented as mean +/- SEM of 8 replicates on day 3 (black) and day 15 (white). Two-way ANOVA, Sidak's multiple comparisons test, * $p < 0.05$, **** $p < 0.0001$.

To assess hepatic xenobiotic metabolism, we next explored the activity of CYP3A4, the enzyme responsible for 30-60% of drug metabolism in the human liver (189). CYP3A4 activity

can be strongly induced or inhibited by certain drugs, altering pharmacokinetics and making accurate prediction of CYP3A4 activity critical for human liver models (190). Adult human hepatocyte organoids from four donors were exposed to known CYP3A4 inducers rifampin and dexamethasone, and CYP3A4 activity was measured. All lots exhibited induction by both drugs, with inter-donor variability in induction levels, as would be expected for mature adult human hepatocytes in which function has been maintained (Figure 4.4A and B). Importantly, of these, CYP3A4 rifampin induction for lot 4 was not reported by the vendor due to its limited 2D viability but we were able to observe 20-fold induction in organoids (Table 3, Figure 4.4B). Thus, human adult human hepatocyte organoids capture reported variability in CYP3A4 activity between donors (80, 81, 178, 191, 192) and, importantly, can also be used to assay CYP3A4 activity in lots that were not amenable to 2D culture.

After modifications by CYP enzymes and other biotransformations, many xenobiotics are excreted from hepatocytes by efflux transporters in the multidrug resistance protein (MRP) family (193, 194). MRP2, a transporter that usually exports substrates from within hepatocytes out to bile canaliculi (194), was assessed through incubation of adult human hepatocyte organoids with fluorescent MRP2 substrate, carboxy dichlorofluorescein diacetate (CDFDA). Fluorescent signal localized to networks or puncta on the interior of the organoids, indicating active MRP2-driven efflux and validating the morphological polarity observed with MRP2 immunostaining (Figure 4.4C). Finally, glycogen accumulation and low-density lipoprotein (LDL) uptake were observed with periodic acid Schiff (PAS) staining and Dil-LDL incubation, respectively, as assessments of hepatocyte functions (Figure 4.4D and E).

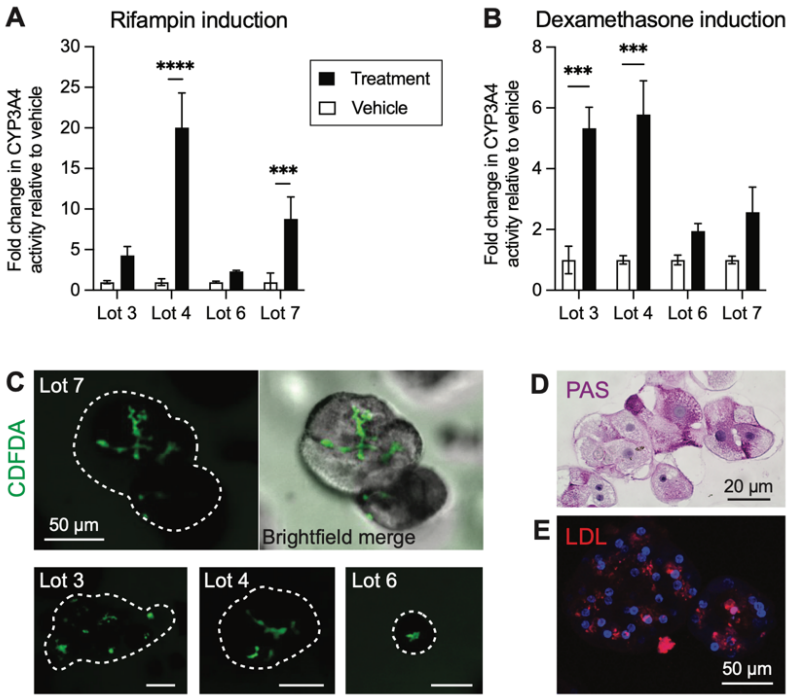

Figure 4.4: Drug metabolic activity conserved across lots screened

(A-B) Analysis of CYP3A4 activity after (A) rifampin or (B) dexamethasone induction in four organoid lots by P450-Glo assay. Data normalized to vehicle control, represented as mean fold change +/- SEM with 3 replicates each of vehicle (white) and treatment (black). Two-way ANOVA, Sidak's multiple comparisons test, *** $p < 0.001$, **** $p < 0.0001$.

(C) Confocal maximum intensity projection of CDFDA (green) accumulation in organoids, overlaid with minimum intensity projection of brightfield z-stack for lot 7 (top right). CDFDA maximum intensity projection for lots 3, 4, and 6 on bottom. Organoids outlined with white dashed line. Scale bars = 50 µm.

(D) Glycogen storage in organoids, visualized with PAS stain (pink) and Hematoxylin counterstain (blue). Scale bar = 20 µm.

(E) Low density lipoprotein (LDL) accumulation in organoids, visualized with Dil-LDL staining (red) and Hoechst (blue). Scale bar = 50 µm.

In sum, adult human hepatocyte organoids from diverse donors demonstrated maintenance of a wide variety of hepatic functions, illustrating their potential as a model of functional human hepatocytes and as a tool for basic research applications and drug screening.

4.3 DISCUSSION

Here, we have shown that adult human hepatocyte organoid culture is compatible with a broad set of donor hepatocytes that exhibited variable plating efficiency and viability in 2D culture. Human hepatocytes grown as organoids also maintain multiple axes of hepatic function *in vitro*, demonstrated through gene expression and direct functional measurement. This was particularly significant for the drug metabolism axis, as organoid lots exhibited high gene expression of mature cytochrome enzymes in contrast to the low expression of immature controls. Cytochrome induction was observed in all lots tested, which distinguished organoid culture from 2D, where the viability of one lot was too short-lived to run such an assay.

We hypothesize that the improved viability and longevity of hepatocytes in organoid culture are potentially mediated by cellular recovery from cryopreservation-induced injury; after isolation, freezing, and thawing, hepatocytes experience ice crystal formation and anoikis (*85–87*) and downregulation of important adhesion molecules such as E-cadherin (*82*, *85*), leading to poor cryo-recovery and plating efficiency after thaw. We observe that adult human hepatocyte organoids strongly express E-cadherin across multiple human donors, suggesting that organoid culture may help to recover hepatocytes from cryo-induced injury and downregulation of adhesion molecules.

Though many other cells are more amenable to 2D culture, plating on polystyrene can stimulate phenotypic activation of cells in response to non-physiological stiffness and ECM interactions (*195*, *196*). Thus, it is possible that the soft Matrigel substrate used in organoid culture is a better mimic of the homeostatic hepatic microenvironment, eliminating the additional stress of 2D culture and thereby allowing cellular recovery. Future experiments could tune the substrate stiffness that organoids are grown in to probe this potential cryo-recovery mechanism and explore

the phenotypic and functional response of hepatocytes to pathological stiffnesses, as seen in liver diseases like cirrhosis.

4.4 METHODS

4.4.1 *Previously described*

Methods used in this chapter but described previously include Organoid culture of hepatocytes, Brightfield microscopy and morphometric analysis, Organoid histology, immunofluorescent staining and microscopy, and Albumin ELISA.

4.4.2 *Primary hepatocytes*

Cryopreserved primary human hepatocytes were purchased through Thermo Fisher (Cat# HMCPIS (lots Hu8366, Hu8373, Hu8300, Hu8287, and Hu1880) HMCPMS (lot Hu8360), and HMCPTS (lots Hu8339 and Hu 8375)) and cultured as organoids, as described below.

4.4.3 *RNA isolation and qPCR*

Organoids were lysed in Qiazol (QIAGEN) or Trizol (Thermo) and RNA was extracted using the phenol-chloroform extraction method. RNA was reverse transcribed into cDNA using random hexamer primers and a Superscript III first-strand synthesis kit (Thermo 18080093) according to manufacturer's instructions. qPCR was performed using SYBR-green (BioRad 1725122). The 2^{dCT} method (*197*) was used to report fold change in gene expression compared to internal control gene *GAPDH*. Primer sequences are included in Table 4 below.

Table 4: Primer sequences

Gene	Forward primer	Reverse primer
SERPINA1	GATCAACGATTACGTGGAGAAGG	CCTAAACGCTTCATCATAGGCA
AFP	AGTGAGGACAAACTATTGGCCT	ACACCAGGGTTTACTGGAGTC
ALB	GAGACCAGAGGTTGATGTGATG	AGTTCCGGGGCATAAAAGTAAG
ARG1	GCCAAGTCCAGAACCATAGG	AGCAGACCAGCCTTTCTCAA
KRT19	TCCGAACCAAGTTTGAGACG	CCCTCAGCGTACTGATTTCCT
CYP3A4	CAGCCTGGTGCTCCTCTATC	ACCATCATAAAAGCCCCACA
CYP1A2	ACCTTGTGACCAAGCCTGAG	AAGGAGGAGTGTCGGAAGGT
TF	TGATTGCATCAGGGCCATTG	GCCAGGTAAGCATCATACACCA

4.4.4 *CYP3A4 induction and activity assessment*

CYP3A4 induction was assessed by adding CYP inducers (25 μM rifampin or 25 μM dexamethasone) or vehicle controls (DMSO or EtOH) to organoid cultures for 3 days after which CYP3A4 activity was measured using the P450-Glo CYP3A4 Assay (Promega V9001). Variability in cell numbers was normalized using the CellTiter-Glo assay (Promega G9681).

4.4.5 *CDFDA visualization*

Bile canalicular transport was assessed by incubating organoids for 30 minutes with 2 μg/ml 5-[and-6]-car-boxy-2',7'-dichlorofluorescein diacetate (CDFDA, Sigma 21884), a fluorescent MRP2 substrate. After incubation organoids were imaged on a Nikon Eclipse Ti inverted microscope with a Yokogawa W1 spinning disk head.

4.4.6 *Low density lipoprotein visualization*

Low-density lipoprotein (LDL) uptake was assessed by incubating organoids with 20 μg/ml Dil-LDL, a fluorescently labelled LDL (Thermo L3482), for 3 hours at 37ºC with Hoechst 33342 diluted 1:1000. After incubation organoids were imaged on a Leica SP8 confocal microscope.

4.4.7 *Periodic acid Schiff staining*

Glycogen accumulation was assessed with periodic acid-Schiff staining (PAS, Sigma, 395B-1KT) according to manufacturer's instructions. Stained organoids were imaged on a light microscope.

4.4.8 *Urea analysis*

After media collection and freezing, urea secretion was measured using a BUN assay on organoid media (Fisher SB0580250) according to manufacturer's instructions.

4.4.9 *Statistical Analysis*

Data in graphs are expressed as the mean ± SEM, as denoted in figure legends. Statistical significance was determined with PRISM software using two-way ANOVA followed by Sidak's multiple comparison test, as denoted in figure legends.

Chapter 5. SINGLE-CELL RNA-SEQUENCING REVEALS TRANSCRIPTIONAL MATURITY AND FUNCTIONAL HETEROGENEITY IN ADULT HUMAN ORGANOID HEPATOCYTES

5.1 INTRODUCTION

Hepatocytes exhibit functional heterogeneity throughout the liver lobule to distribute the heavy functional workload of the liver. Bulk genomic techniques mask these cell-to-cell differences by averaging expression across the entire cell population. Thus, we were interested in further exploring the distribution of hepatic functions on a cell-to-cell basis across the entire transcriptome. Using the 10X Genomics Chromium platform, we performed single cell RNA sequencing (scRNAseq) on our organoid population and found multiple cell types present in our adult human organoid populations. Organoid hepatocytes clustered closely with hepatocytes found in the adult human liver and had contrasting expression of genes that stratify hepatic maturity when compared to fetal hepatoblasts.

5.2 RESULTS

5.2.1 *Single cell RNA sequencing of adult human hepatocyte organoids reveals distinct cell types that cluster closely with human liver samples*

After analysis by principal component analysis (PCA) and clustering with uniform manifold approximation and projection (UMAP), cells segregated into six distinct populations (Figure 5.1A and B). We characterized each cluster by examining differential gene expression and identifying known cell type-specific markers. Clusters 1, 2, and 5 represented hepatocytes with high

expression of hepatic markers such as *ALB, ALDH1A1, APOC1,* and *ASGR1*. Clusters 0 and 3 were composed of cholangiocytes, with low expression of the above hepatic markers and high expression of biliary markers *KRT7, EPCAM,* and *TFF1-3*. Cluster 4 was composed of a stromal population expressing *COL3A1, IGFBP7,* and *DCN* (Figure 5.1B).

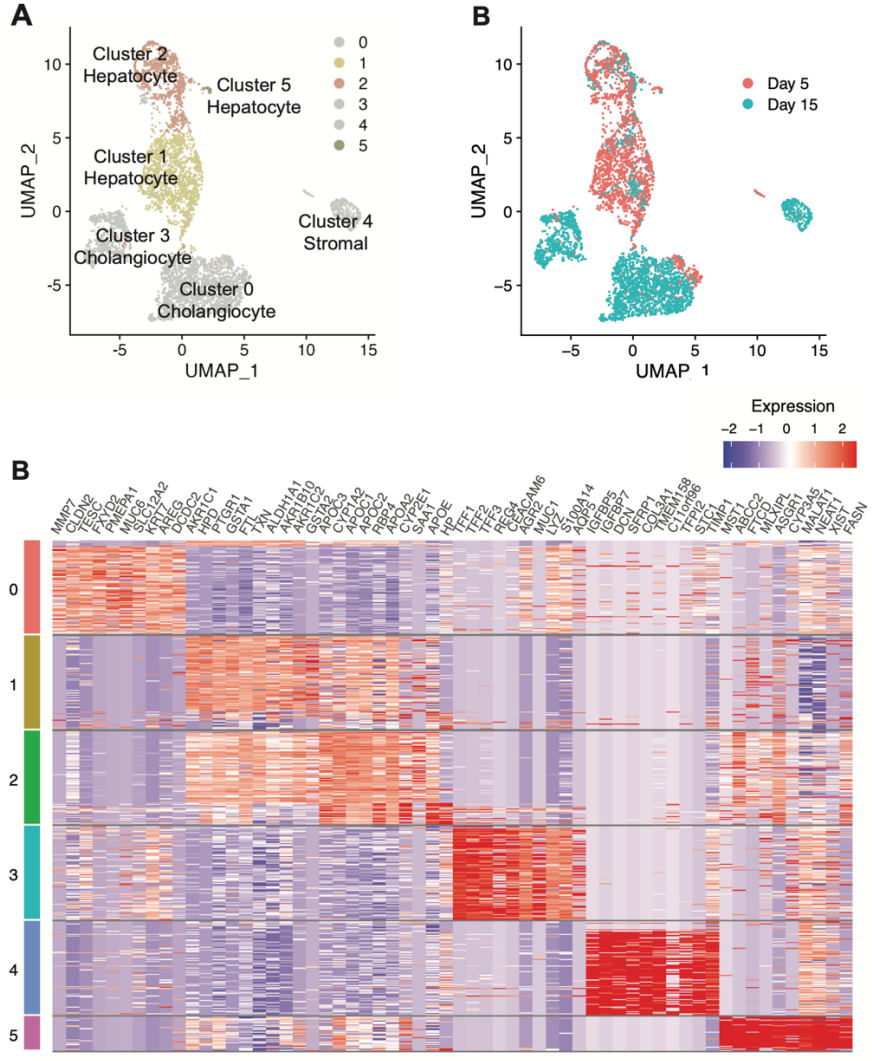

Figure 5.1: Single cell RNA sequencing demonstrates cellular heterogeneity in adult human hepatocyte organoids

(A) UMAP clustering of single cells from adult human hepatocyte organoids at day 5 and day 15 in culture. Green, pink, and yellow clusters represent hepatocytes.

(B) UMAP clustering of single cells from adult human hepatocyte organoids at day 5 (pink) and day 15 (blue) in culture.

(C) Heat map of expression of top 10 most differentially expressed genes between clusters 0-5 in UMAP from Figures 3A and S4A.

Having classified the cells in our adult human hepatocyte organoids based on known hepatocyte markers, we next sought to compare the transcriptional profiles of the organoid hepatocytes to hepatocytes from adult liver using a non-biased approach. We first compiled and integrated seven published scRNAseq libraries of adult human liver (198–200). We then clustered this adult human liver data with our adult human hepatocyte organoid samples as well as with a fetal hepatoblast organoid library as a comparison for maturity (Figure 5.2A) (112). Cells clustered into 11 distinct populations, which we identified as hepatocytes, cholangiocytes, stromal/endothelial cells, and immune cells based on cell-type-specific gene expression (Figure 5.2B) (201). Cells from our adult human organoid population clustered with adult liver hepatocytes, cholangiocytes, and stromal cells, validating that each population retains transcriptional similarity to its primary cell of origin (Figure 5.2C). Hepatocytes from adult human organoids were distributed across the hepatocyte clusters from all adult datasets, despite significant variability in the individual adult human liver libraries (Figure 5.2C).

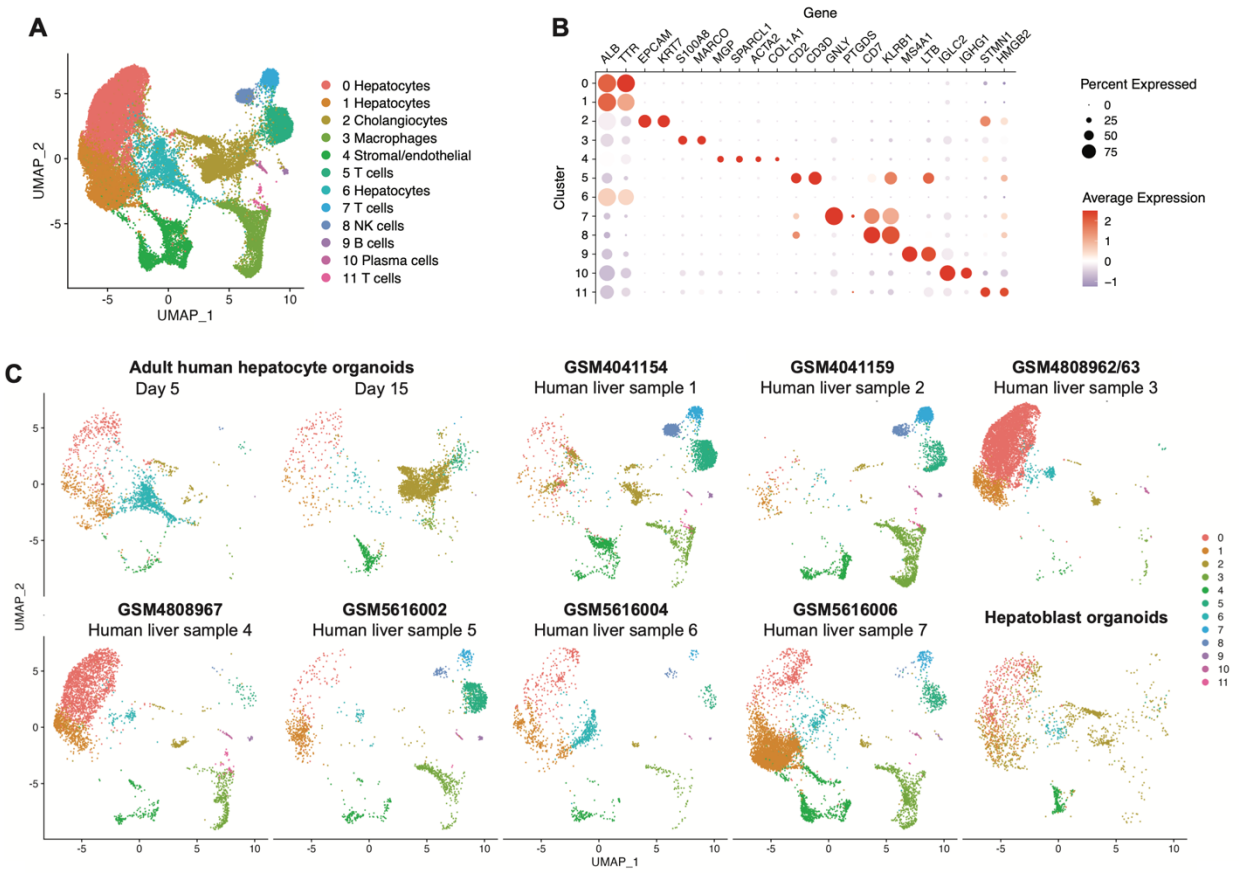

Figure 5.2: Adult human hepatocyte organoids cluster closely with human liver samples and hepatoblast organoids

(A) UMAP of adult human hepatocyte organoids at day 5 and day 15 clustered with fetal hepatoblast organoids and primary adult hepatocytes from 7 human liver samples.

(B) Dot plot demonstrating average expression and percent of cells expressing genes of interest in each cluster from UMAP in (D). Genes selected as representative markers for different cell types of the liver, informing cluster identities in bottom right.

(C) UMAP from (A) separated by sample for visualization of clustering differences.

5.2.2 *Hepatocyte subclusters demonstrate transcriptional maturity and functional heterogeneity of adult human organoid hepatocytes*

To further explore the distribution of functional gene expression specifically in the hepatocyte populations, the three hepatocyte clusters (0, 1, and 6) were subset from the complete dataset (Figure 5.3A). In the resulting UMAP projection, adult human organoid hepatocytes were again found to distribute evenly with hepatocytes from adult liver datasets (Figure 5.3B). Genes involved in important hepatic processes were then compared between adult human organoid hepatocytes, fetal hepatoblast organoids, and hepatocytes from the integrated adult liver datasets by visualizing the distribution of expression of genes representing various axes of hepatocyte metabolic function. Secreted plasma protein genes *ALB, TTR*, and *RBP4* represent key hepatocyte functions and serve as early indicators of endodermal commitment toward hepatic cell fate in development (*19*). All three genes had strong expression across the majority of cells in the hepatocyte clusters and exhibited similar gene expression to adult liver and fetal controls (Figure 5.3C). Similarly, genes involved in lipid and fatty acid metabolism that are expressed in the fetal liver and throughout adult life, *APOA2, APOC1,* and *FABP1,* were strongly expressed across the entire hepatocyte population and at similar levels to adult liver and fetal controls (Figure 5.3D) (*112*, *202*). Genes involved in glutathione and amino acid metabolism, *GAMT, MGST1,* and *HPD*, all had high expression in adult human organoid hepatocytes with similar expression to hepatocytes from adult liver. Interestingly, *HPD*, an enzyme involved in tyrosine metabolism, had distinctly lower expression in fetal hepatoblast organoids compared to all other conditions including adult human hepatocyte organoids, which again highlighted the mature phenotype of human hepatocyte organoids (Figure 5.3E). We thus set out to more carefully query functional genes with known expression changes over the course of hepatocyte development and maturation.

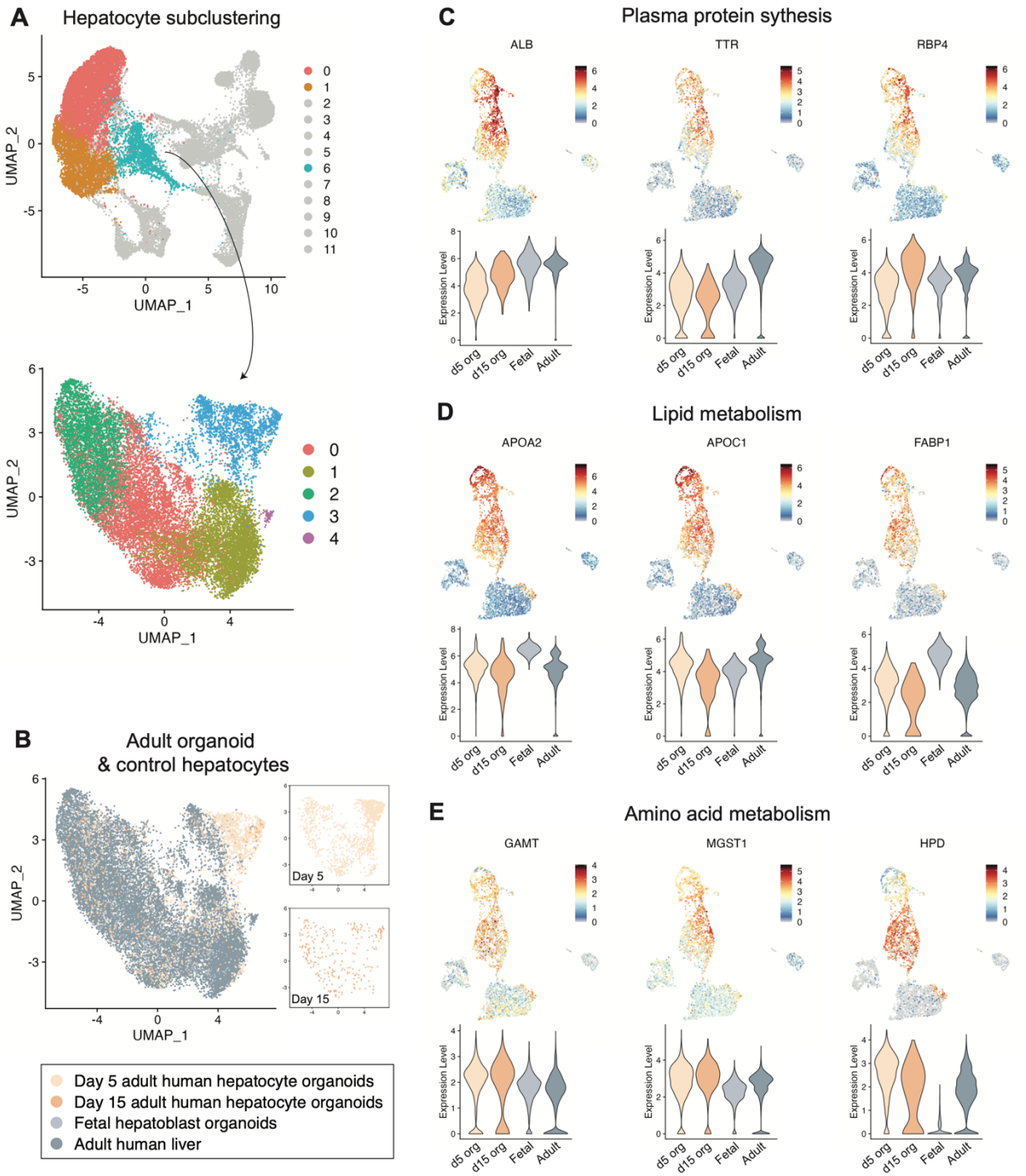

Figure 5.3: Single-cell RNA sequencing demonstrates functionality of adult human hepatocytes grown as organoids

(A) Schematic illustrating the re-clustering of all hepatocyte clusters from UMAP in Figure 5.2A into the projection used in (B).

(B) UMAP of adult human hepatocyte organoids on day 5 (light orange) and day 15 (dark orange) clustered with fetal hepatoblast organoids (light grey) and primary adult hepatocytes (dark grey) from seven human liver samples. Insets of adult human hepatocyte organoids for clearer visualization.

(C-E) UMAP plots of adult human hepatocyte organoids from Figure 5.1A, emphasizing expression of individual genes of interest, and violin plots from (B) showing distribution of expression compared to controls. Genes divided by hepatic functional axis: (C) plasma protein synthesis, (D) lipid metabolism, and (E) amino acid metabolism. Violin plot groups color-coded as in (B) with d05 org = Day 5 adult human hepatocyte organoids, d15 org = Day 15 adult human hepatocyte organoids, Fetal = Fetal hepatoblast organoids, and Adult = Adult human liver.

As the liver develops and matures pre- and postnatally, many functional genes upregulate or downregulate to adjust to the hepatic requirements for the corresponding stage of development. Regulation of cytochrome enzymes and other genes involved in drug metabolism is especially dynamic as the liver matures. For example, gene expression of enzymes *CYP2E1* and *CES1* does not rise in the liver until after birth, while *CYP3A7* is expressed highly in fetal liver and downregulates postnatally (*112*). We observed that expression of mature drug-metabolizing genes *CYP2E1* and *CES1* was high in adult human organoid hepatocytes after several weeks of culture, similar to hepatocytes in human liver samples, while fetal controls had little to no expression (Figure 5.4A). In contrast, expression of fetal drug-metabolizing enzyme CYP3A7, as well as other fetal hepatic genes AFP, H19, GPC3, DLK1, and SPINK1, was low or absent in adult human organoid hepatocytes and control hepatocytes from adult liver (Figure 5.4B). All fetal hepatic genes had high expression in fetal controls (Figure 5.4B).

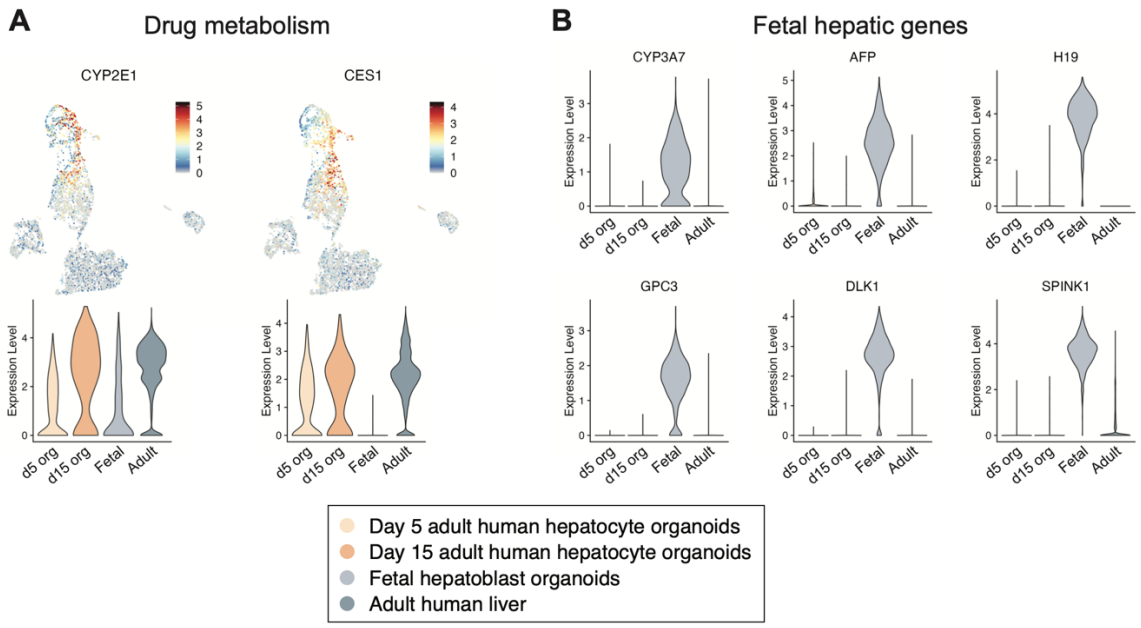

Figure 5.4: Single-cell RNA sequencing demonstrates transcriptomic maturity of adult human hepatocytes grown as organoids

(A) UMAP plots of adult human hepatocyte organoids from Figure 5.1A, emphasizing expression of drug metabolism genes, and violin plots from (B) showing distribution of expression compared to controls. Violin plot groups color-coded as in Figure 5.3B with d05 org = Day 5 adult human hepatocyte organoids, d15 org = Day 15 adult human hepatocyte organoids, Fetal = Fetal hepatoblast organoids, and Adult = Adult human liver.

(B) Violin plots from Figure 5.3B showing distribution of fetal hepatic gene expression in adult human hepatocyte organoids compared to controls. Groups color coded as in (A).

In addition to maturity, hepatocytes in late-stage organoids were found to have high expression of many genes involved in liver regeneration and the liver's response to inflammation. These included transcription factors *FOS, JUN, JUNB,* and *JUND* (Figure 5.5A), which are known to be upregulated in liver regeneration, as well as genes associated with the acute phase of inflammation, *APCS*, *CP*, *CLU*, *HP*, and *SERPINA1* (Figure 5.5B) (*203*, *204*). Fibrinogen genes, *FGA, FGB,* and *FGG,* and complement factor genes *CFB, CFH,* and *C3*, which are involved in blood clotting and wound healing (*204*) were also more highly expressed by hepatocytes in later

stages of organoid culture (Figure 5.5C and D). Most of these inflammatory genes had low expression in day 5 organoids but had substantially increased by day 15. These results indicate that the organoid growth observed between day 5 and day 15 may be triggered by inflammatory and/or regenerative signaling pathways.

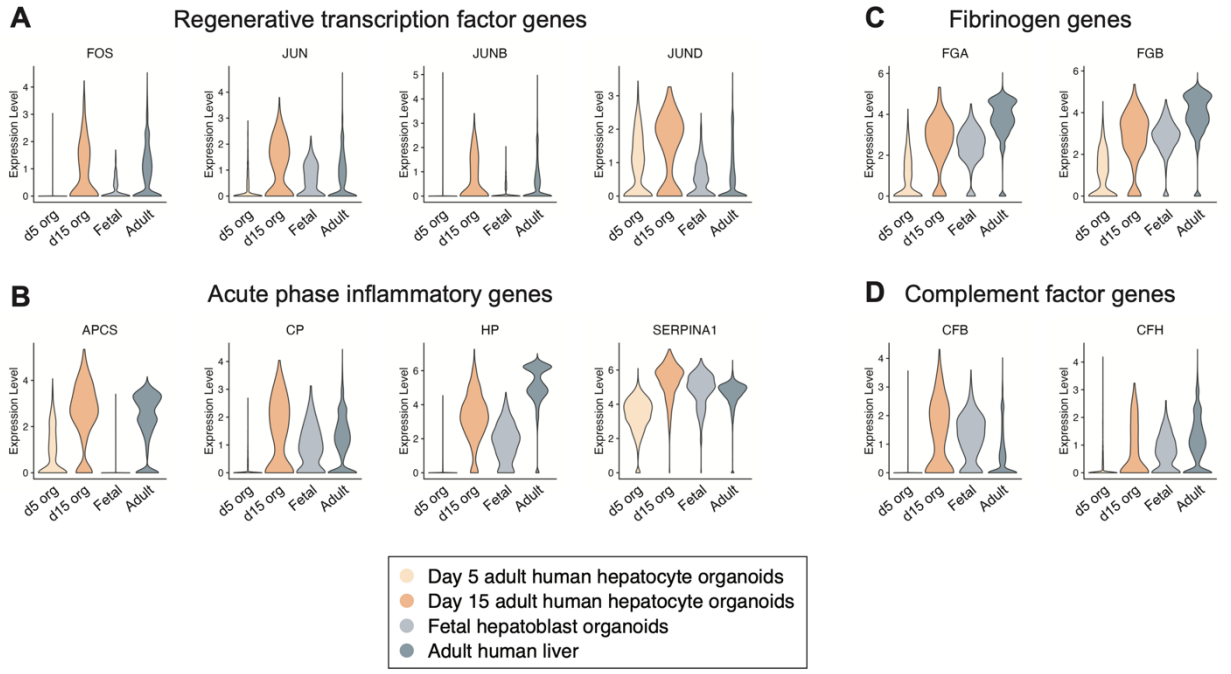

Figure 5.5: Genes for inflammatory proteins and regenerative transcription factors are highly expressed in late-stage adult human organoid hepatocytes

Violin plots of adult human hepatocyte organoids and controls from clustering in from Figure 5.3B showing distribution of expression of (A) regenerative transcription factor genes, (B) acute phase inflammatory genes, (C) fibrinogen genes, and (D) complement factor genes. Violin plots color-coded as in Figure 5.3B with d05 org = Day 5 adult human hepatocyte organoids, d15 org = Day 15 adult human hepatocyte organoids, Fetal = Fetal hepatoblast organoids, and Adult = Adult human liver.

Taken together, these results validate that adult human hepatocyte organoids maintain differentiated and mature transcription across multiple axes of liver function. In particular, the

expression of developmentally dynamic drug-metabolizing genes emphasizes the value of adult human hepatocyte organoids for pharmaceutical applications such as drug screening.

5.3 Discussion

In this chapter, we use scRNAseq to transcriptionally explore functionality and maturity in adult human hepatocyte organoids. The cell population in organoids is found to contain ductal cells that cluster closely with adult cholangiocytes, stromal cells that cluster with hepatic fibroblasts, and organoid hepatocytes that cluster closely with hepatocytes from the adult human liver. The organoid hepatocytes demonstrate similar distributions of functional gene expression when compared to hepatocytes from human liver. Importantly, expression of genes that are indicative of mature functions such as drug metabolism were high in organoid hepatocytes, while immature genes such as AFP were low. The opposite was true for fetal hepatoblast controls, confirming that hepatocytes grown as organoids maintain their differentiated state.

In addition to demonstrating transcriptional maturity, our single-cell RNA sequencing data highlighted that drug metabolism genes shift expression over time in organoids. Downregulation of CYP enzymes during liver regeneration in rodents is a well-documented phenomenon as cells undergo significant growth (*62–64*). Thus, adult human hepatocyte organoids may be similarly shifting metabolism towards cell growth and away from xenobiotic metabolism in the early days of culture, then returning to normal adult liver transcription and function as hepatocytes reach homeostasis. Additionally, low expression of fetal genes in adult human hepatocyte organoids confirms their maturity but also validates that while growing they do not adopt a malignant transcriptional profile, as fetal genes such as *AFP, H19,* and *GPC3* are often upregulated when adult hepatic cells become cancerous (*19*, *25*). Future work will explore the transcriptional

differences between early and late stages of organoid hepatocytes to begin to tease apart the transcriptional signatures of proliferating hepatocytes and direct experiments to sustain cell expansion.

5.4 METHODS

5.4.1 *Organoid digestion and barcoding*

Organoids were grown in Matrigel under mature human hepatocyte culture conditions for 5 or 15 days, as described above. At each timepoint, organoids were pooled and suspended in TrypLE (Thermo) for 20-30 minutes until they had digested to single cells. The single-cell suspension was mixed with 1% BSA to prevent clumping and sticking to tubes/tips. Immediately before partitioning, cells were filtered through a FlowMi Cell Strainer (Belart) to remove cell clumps and debris. Cells were counted then loaded into a 10X Chromium flow cell using the Single Cell 3' v3 kit. 10X genomics barcoding and library construction were performed according to manufacturer's recommendations and generated libraries from 2327 cells at day 5 and 3411 cells at day 15 in culture.

5.4.2 *Single cell RNA sequencing and bioinformatics*

Libraries were sequenced using an Illumina NextSeq 2000. Reads were aligned to the human genome GRCh38-2020-A and counted with the 10X Cell Ranger pipeline version 6.1.1 (*205*). The day 5 organoid library generated 74,577 mean reads per cell with 1,320 median genes per cell. The day 15 organoid library generated 41,264 mean reads per cell with 2,296 median genes per cell. Cell Ranger outputs were loaded into R using the Seurat v4.0 package (*206*) and all bioinformatic analysis was performed following the recommended vignettes for data integration and clustering

as described by the Satija lab. First, cell filtering was performed on individual libraries to remove cells with >500 genes and >25% mitochondrial RNA content to exclude fragments and dying cells from analysis; 1849 and 2796 cells remained from days 5 and 15, respectively. Next, global-scaling normalization and highly variable feature selection were performed. Cells were assigned a cell cycle score which was regressed during data scaling to lessen the influence of these genes from clustering and prevent cell cycle genes from masking variations in liver gene signatures between cells. Two integrated datasets were generated: an integrated day 5 and day 15 organoid sample, and an integrated sample of day 5 and day 15 organoids, a publicly available hepatoblast sample (ArrayExpress under accession E-MTAB-7189), and multiple human liver datasets (GEO under accession numbers GSM4808962 and GSM4808963, GSM4808967, GSM5615002, GSM5616004, GSM5616006, GSM4041154, and GSM4041159). Integrated datasets were scaled, principal component analysis was performed, followed by UMAP clustering, and gene expression was visualized to assign cluster identities to known liver cell types. All plots were generated using R Studio and the Seurat package.

Chapter 6. ADULT HUMAN HEPATOCYTE ORGANOIDS IN ENGINEERED LIVER TISSUES RAPIDLY ADOPT LIVER MORPHOLOGY AND FUNCTIONAL MATURITY

6.1 INTRODUCTION

When the liver is damaged beyond repair via end-stage liver disease, organ transplantation is the only curative treatment. However, an acute global shortage of donor organs leaves many patients waiting for transplants while their liver function and quality of life continue to decline (*44*). An exciting alternative approach to overcome the scarcity of donor livers is cell-based therapy, wherein hepatic cells are engrafted orthotopically or ectopically into a patient with liver disease to assume partial responsibility for the lacking liver functions (*91*, *102*, *106*, *156*, *164*). As liver cell-based therapies move closer to clinical translation, it will be essential to establish a reliable source of human hepatocytes. Mature hepatocytes have been shown to engraft more efficiently and with better function that immature cells (*153*, *154*), so adult human hepatocytes are the current best option for transplant. Unfortunately, primary hepatocytes exhibit extreme variability in viability and function after isolation and cryopreservation (*82*, *85*, *87*), stymying clinical translation.

Adult human hepatocyte organoids have demonstrated robust growth and function *in vitro* and are able to form from a diverse set of donor hepatocytes. Thus, we hypothesized that organoid culture may serve as an effective pre-treatment that could stabilize and expand hepatocytes before implantation in engineered liver tissues. Here, we demonstrated that adult human hepatocyte organoids from two different donors robustly engraft in a mouse model of chronic liver injury. Hepatocytes exhibit significantly better function after engraftment when grown as organoids, as opposed to those grown in traditional aggregate culture.

6.2 RESULTS

6.2.1 *Adult human hepatocyte organoids in engineered liver tissues demonstrate robust engraftment and functionality after implant*

We chose to examine the utility of adult human hepatocyte organoids as a cell source within engineered liver tissues, which could serve as an ectopic therapeutic option for patients suffering from a variety of forms of liver disease (*102*, *106*). To test the engraftment potential of hepatocytes grown as organoids within engineered tissues, adult human hepatocyte organoids were grown from a 34-year-old donor and encapsulated within fibrin hydrogel to create engineered liver tissues. These tissues were then implanted in the gonadal fat pad of FRGN (Fah-/-, Rag2-/-, Il2rg-/-, NOD) mice, a strain that experiences chronic liver injury (tyrosinemia) unless administered the treatment drug nitisinone (*164*). Human albumin was then measured in mouse blood from weekly blood draws as a measure of the function of human hepatocytes within the implanted engineered tissues. Human albumin increased over 4 weeks *in* vivo, suggesting both a functional increase over time as well as a connection to host vasculature (Figure 6.1A). Excised grafts displayed large areas in which most cells stained positively for antigens expressed by hepatocytes, CK18 and Arg1 (Figure 6.1B and C). Occasional CK19+ cells with hepatocyte morphology were also present in grafts, perhaps suggesting that some engrafted cells adopt a progenitor phenotype (*207*). The mouse red blood cell marker Ter119 stained small, localized areas throughout the graft between Arg1+ hepatocytes, indicating that implanted cells were being supplied with host blood (Figure 6.1B).

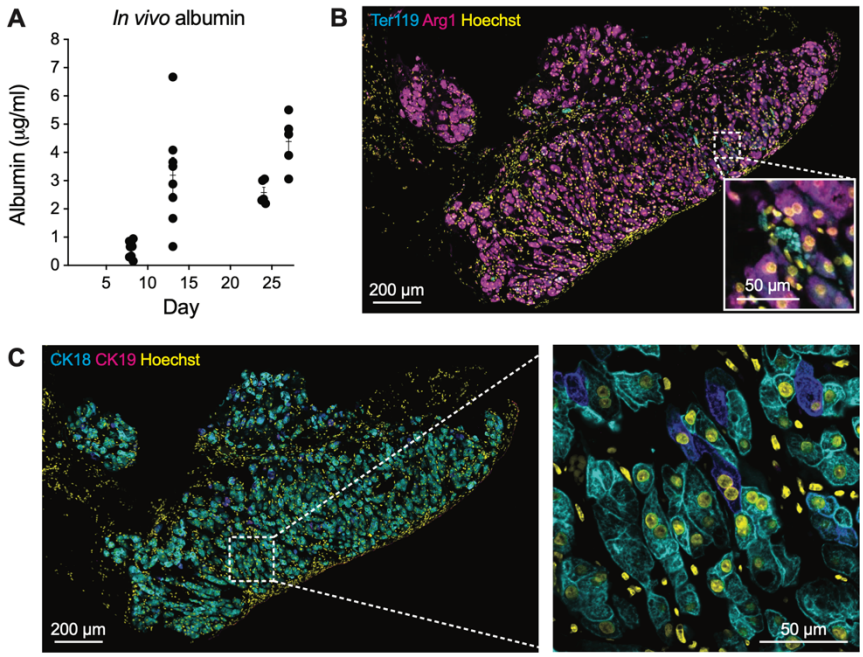

Figure 6.1: Engineered liver tissues fabricated with adult human hepatocyte organoids engraft and function *in vivo* in a mouse model of chronic liver injury.

(A) Secreted human albumin measured in mouse blood by human albumin ELISA. Data represented as mean +/- SEM of each mouse at different timepoints across 28 days.

(B) Immunofluorescence image of explanted graft stained for Arg1 (magenta), Ter119 (cyan), and Hoechst (yellow). Low magnification scale bar = 200 µm, inset scale bar = 50 µm.

(C) Immunofluorescence image of explanted graft stained for CK18 (cyan), CK19 (magenta), and Hoechst (yellow). Low magnification scale bar = 200 µm, inset scale bar = 50 µm.

6.2.2 *Adult human hepatocyte organoids do not require xenogenous cell support and serve as better parenchymal cell source in engineered liver tissues than traditional models*

We were surprised by the substantive size of grafts in this initial study (Figure 6.1), given that we had not included any cell populations beyond adult human hepatocyte organoids themselves within the engineered tissues. Previous studies had shown that optimal engraftment of engineered tissues built from other hepatocyte sources (e.g., primary human hepatocyte aggregates) (100, 102) and

iPS-derived hepatocytes (106) required the addition of endothelial and stromal cells (e.g., fibroblasts, mesenchymal stromal cells) prior to tissue transplantation. The ability to remove these cell populations from engineered tissues would greatly simplify the clinical development and approval pipeline by creating a simpler product and would also reduce safety concerns of tumorigenicity and stromal cell overgrowth (100, 102, 208). We thus set out next to directly compare engraftment efficiency of engineered tissues derived using two different primary adult human hepatocyte culture methods – adult human hepatocyte organoids developed here, or "aggregates" developed previously (102) – both in the presence and absence of non-parenchymal cells (NPC) (Figure 6.2A and B).

We built engineered tissues that contained either adult human hepatocyte organoids or aggregates with or without fibroblasts and endothelial cells, collectively referred to as non-parenchymal cells (NPCs) (Figure 6.2A and B). Both organoids and aggregates were generated from the same 19-year-old human hepatocyte donor. Notably, this was a different donor than was used in the previous in vivo experiment (Figure 6.1), thus together these studies enabled assessment of engraftment of two different adult donors. Again, blood was drawn from implanted mice to assess human liver protein (albumin) production as a metric for hepatic functionality of implants. After one week of engraftment, the group of animals receiving engineered tissues with only adult human hepatocyte organoids had on average >2-fold more human albumin than the organoid + NPC group or either aggregate group (Figure 6.2C). By week two the differences between groups were even more pronounced with the organoid-only group producing ~6x more albumin than the organoid + NPC group, as well as significantly more than both aggregate +/- NPC control groups, at up to ~25x more albumin (Figure 6.2C). Similarly, human alpha-1 antitrypsin (A1AT) was also identified in the mouse blood of the organoid-only group at ~6x more

than the organoid + NPC, and greater than both aggregate +/- NPC groups (up to ~12x difference; Figure 6.2D).

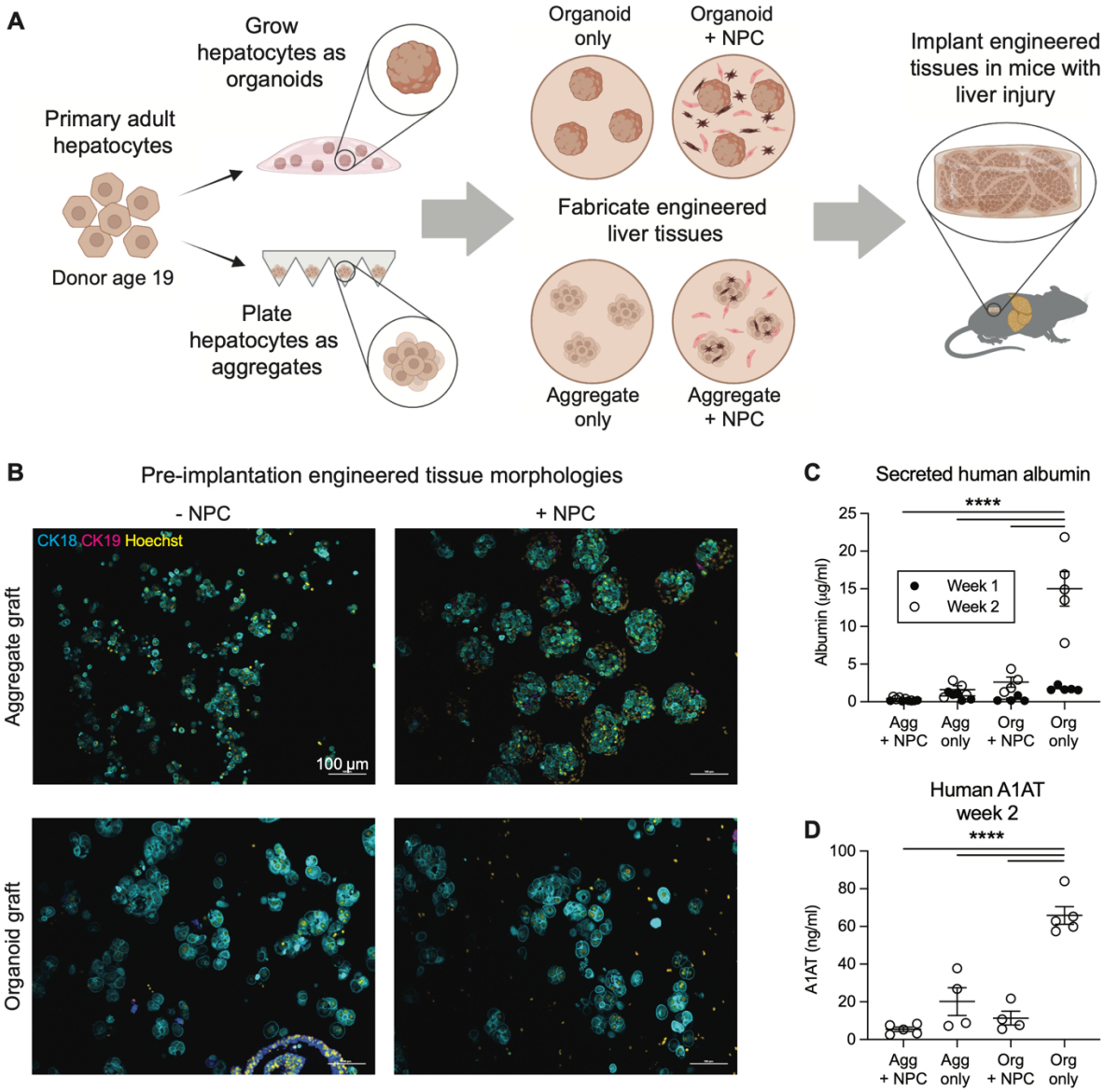

Figure 6.2: Engineered liver tissues fabricated with adult human hepatocyte aggregates vs. organoids with and without NPCs demonstrate significant differences in *in vivo* functionality

(A) Schematic illustrating the *in vitro* culture of adult human hepatocytes as either organoids or aggregates and the subsequent fabrication and implantation of engineered liver tissues with either aggregates or organoids, with or without non-parenchymal cells.

(B) Representative fluorescence images of each group (aggregates or organoids +/- NPC) at implant stained for CK18 (cyan), CK19 (magenta), and Hoechst (yellow). Scale bars = 100 μm.

(C) Secreted human albumin measured in mouse blood by human albumin ELISA. Data represented as mean +/- SEM of each mouse at week 1 (black) and week 2 (white). Two-way ANOVA, Sidak's multiple comparisons test, **** $p < 0.0001$.

(D) Secreted human A1AT measured in mouse blood by human A1AT ELISA. Data represented as mean +/- SEM of each mouse at week 2. One-way ANOVA, Tukey's multiple comparisons test, **** $p < 0.0001$.

To further explore the engraftment efficiency of human cells within tissue grafts from each group, implanted tissues were excised and immunostained. Human CK18, a marker of both hepatocytes and cholangiocytes, was identified in grafted areas in all mice (Figure 6.3A). Using CK19 as a marker to differentiate between hepatocyte and biliary areas, graft size and phenotype were quantified in all groups. Importantly, and in corroboration with secreted protein data (Figure 6.2C and D), hepatic graft area (CK18+/CK19-) was found to be significantly larger in organoid-only grafts compared to all other groups (Figure 6.3B). Significant biliary area (CK18+/CK19+) was also found in both organoid groups, comprising 13.5% of organoid + NPC grafts and 7.6% percent of organoid-only grafts (Figure 6.3B-D).

While the presence of secreted human proteins albumin and A1AT in mouse blood suggested that the CK18+/CK19- cells, which constituted >86% of the human cell area in organoid grafts, were indeed human hepatocytes in engrafted tissues, we sought to further establish their hepatocyte identity via immunostaining (Figure 6.3E). We found that these cells also expressed hepatocyte functional proteins Alb and Arg-1, transcription factor HNF4α, and epithelial cell-cell junction protein E-cad, and were generally negative for CK19, all consistent with a human hepatocyte phenotype (Figure 6.3E). Furthermore, cells that stained positively for CK18, Alb, Arg1, HNF4α, and E-cad also exhibited hepatocyte morphology with a low nuclear-to-

cytoplasmic ratio, occasional binucleation, and tightly packed cells that collectively self-assembled to form elongated structures reminiscent of hepatocyte cords in the mature liver (Figure 6.3E).

Conversely, CK19+ cells were negative for hepatocyte markers but positive for E-cad (Figure 6.3E, insets) and had small, densely packed cuboidal cell morphologies, all consistent with cholangiocytes. In explanted tissue grafts, these cells were generally found in self-assembled tubular structures resembling bile ducts, with diameters ranging from ~15 μm-800 μm. Notably, the percent of biliary area in organoid-only grafts was significantly lower than in the organoid + NPC group (Figure 6.3D and E), suggesting that non-parenchymal cells may play a role in regulating the ratio of human hepatocyte versus cholangiocyte populations in engrafted tissues.

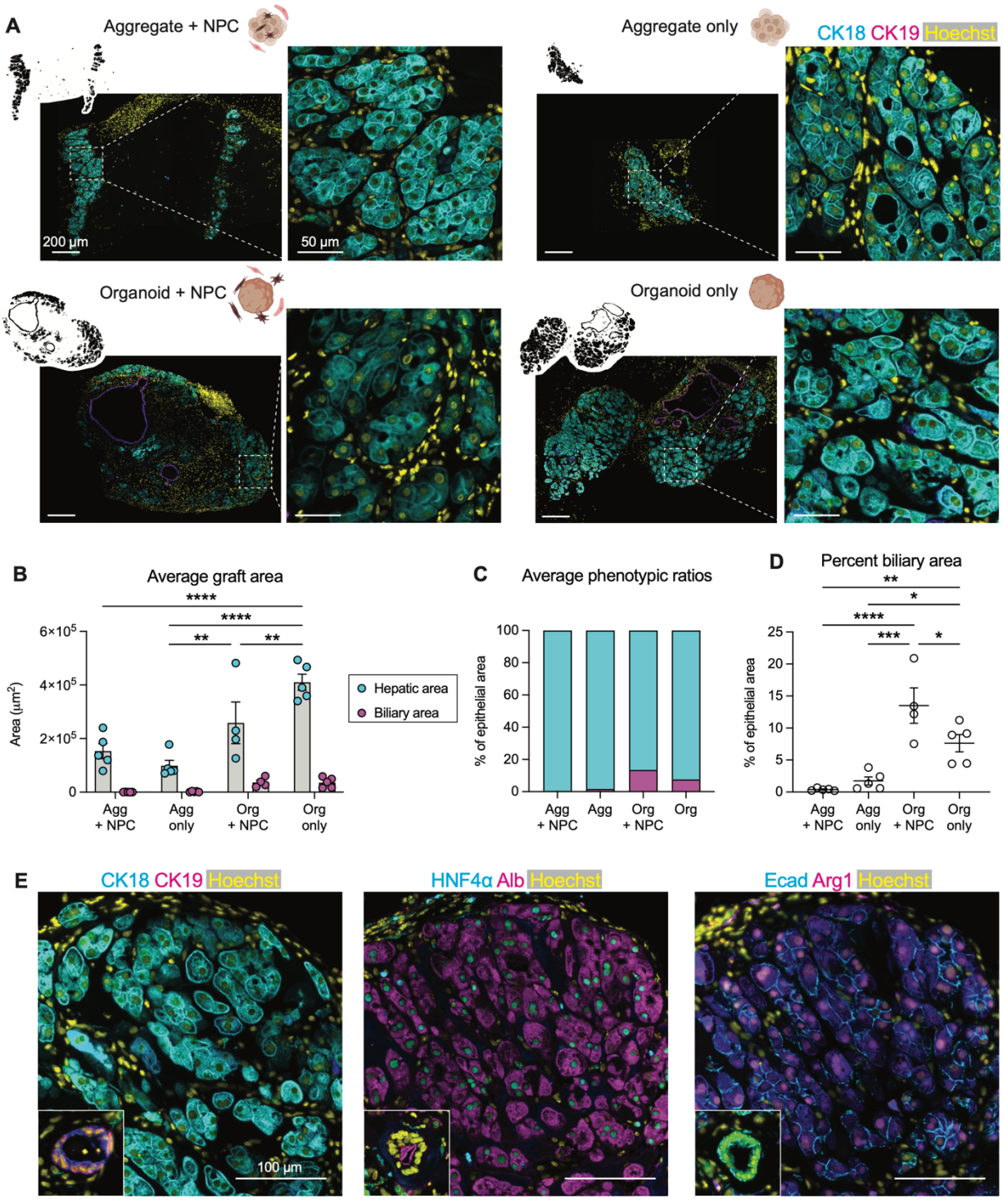

Figure 6.3: Adult human hepatocyte organoids maintain phenotype after implant and generate larger engineered liver tissues with more biliary area than hepatic aggregates

(A) Representative fluorescence images used for quantification in (B-D). CK18 (cyan), CK19 (magenta), and Hoechst (yellow). Scale bars = 200 μm for low magnification, 50 μm for inset images. Example masks used for quantification in upper left corner of each image.

(B) Average graft area calculated from immunofluorescence images. Hepatic area measured as CK18+/CK19- area (cyan). Biliary area measured as CK18+/CK19+ area (magenta). Each data point represents the average graft area of all grafts found in a single mouse. Data represented as mean +/- SEM of each mouse at week 2. Two-way ANOVA, Sidak's multiple comparisons test, ** $p < 0.01$, **** $p < 0.0001$.

(C) Average hepatic area and biliary area as a ratio of total epithelial area (CK18+) in each group. Hepatic area measured as CK18+/CK19- area (cyan). Biliary area measured as CK18+/CK19+ area (magenta).

(D) Percent biliary area calculated from immunofluorescence images as CK18/CK19+ area / CK18+ area. Each data point represents the average percent biliary area of all grafts found in a single mouse. Data represented as mean +/- SEM of each mouse at week 2. One-way ANOVA, Tukey's multiple comparisons test, * $p < 0.05$, ** $p < 0.01$, *** $p < 0.001$, **** $p < 0.0001$.

(E) Confocal images of serial sections of organoid-only graft stained for CK18 (cyan) and CK19 (magenta) (left), Alb (magenta) and HNF4α (cyan) (middle), or Arg1 (magenta) and E-cad (cyan) (right). Nuclei stained for Hoechst (yellow) in all images. Scale bars = 100 μm. Inset shows serial sections of neighboring biliary area at the same scale.

Taken together, these findings demonstrate that "priming" adult human hepatocytes *in vitro* as organoids provides a highly functional cell source in engineered liver tissues that robustly engrafts and spatially reorganizes to create structures that morphologically, phenotypically, and functionally resemble both human hepatocyte and cholangiocytes populations and that exogenous non-parenchymal cell populations are not needed to facilitate tissue engraftment or assembly.

6.3 DISCUSSION

Our findings demonstrating that organoid culture primes hepatocytes for superior engraftment outcomes have powerful translational implications, as enhancing hepatic engraftment efficiency would simultaneously reduce the cell sourcing production burden. One potential mechanistic

reason that organoid culture may prime hepatocytes for superior engraftment is that organoid culture recovers hepatocytes that have been damaged by cryopreservation, as discussed in Chapter 4.3. Additionally, organoid culture may serve as a purification step to enrich healthy, expandable hepatocytes and dilute those cells that could not recover from cryopreservation, improving the ratio of healthy:damaged hepatocytes in engineered liver tissues. Those enriched, healthy hepatocytes also demonstrate an improvement in transcriptional maturity throughout the culture timeline, which has been suggested to improve cell transplantability and engraftment in engineered liver tissues (*153*, *154*). Thus, organoid culture may prime hepatocytes for implant by purifying healthy cells and/or providing an environment in which hepatocytes can recover from cryo-damage and can re-establish maturity, homeostatic cell-cell adhesions, morphology, and function.

Another impactful and surprising finding in this work was the demonstration that adult human hepatocyte organoids exhibit significant functional improvement when implanted without non-parenchymal cell support. Historically, implanted hepatic cells – either primary human hepatocytes or iPSC-derived hepatic endoderm – have demonstrated decreased function in the absence of non-parenchymal cells. Our results demonstrate a functional, phenotypic, and translational advantage of adult human hepatocyte organoids, as exclusion of superfluous cell types may save time and cost in engineered tissue production, as well as speed FDA approval.

Interestingly, we further found that the addition of fibroblasts and endothelial cells increased the ratio of biliary to hepatic cells within engrafted engineered tissues composed of adult human hepatocyte organoids. This finding is particularly notable when considered together with findings from the Huch lab, which demonstrated that paracrine signals between mouse ductal cell organoids and nearby mouse portal fibroblasts induce biliary proliferation (*172*). Together, these findings suggest that exogenous fibroblasts in engineered liver tissues may stimulate proliferation

of residual cholangiocytes within implanted adult human hepatocyte organoids, thus expanding the proportion of cholangiocytes in the resultant graft (*172*). This has major clinical ramifications, as such cellular interactions could be leveraged to finely tune the identities, proportions, and morphogenesis of several liver cell populations within engineered tissues, similar to multicellular assembly processes in human liver development and regeneration (*6*, *19*, *49*).

As liver cell therapy moves closer to patients, further improvements such as generating adult human hepatocyte organoids at therapeutically relevant, human-organ scales, will accelerate translation. The adult human hepatocyte organoids described here could broadly enable basic and clinical studies in areas such as therapeutic regenerative medicine, pharmaceutical screening, and generating patient-specific organoids for precision medicine.

6.4 METHODS

6.4.1 *2D Cell culture*

Human umbilical vein endothelial cells (HUVEC, Lonza C2519A) were grown in EGM-2 media (Lonza) and neonatal normal human dermal fibroblasts (NHDF, Lonza CC-2509) were grown in DMEM + 10% FBS + 1% penicillin-streptomycin. HUVECs and NHDFs were used in engineered liver tissues between passage 4-8.

6.4.2 *Cell aggregation and organoid culture*

To generate hepatocyte aggregates, primary human hepatocytes were thawed, counted, and plated into pyramidal microwells as described previously (*100*, *102*) at a concentration of 100 hepatocytes per microwell. If cells were aggregated with fibroblasts, NHDFs were trypsinized, counted, and added to pyramidal microwells at a concentration of 160 NHDFs per microwell immediately

before adding hepatocytes. Cells were incubated at 37ºC overnight to form aggregates. Organoids were grown as written previously in Chapter 2 “Organoid culture”.

6.4.3 *Engineered liver tissue fabrication*

Hepatocyte organoids were digested out of Matrigel (Corning) with Cell Recovery Solution (Corning), washed once in PBS, and resuspended in diluted fibrinogen. If HUVECs or NHDFs were included in engineered liver tissues, they were suspended in diluted thrombin. Diluted thrombin with or without non-parenchymal cells was mixed with an equal volume of hepatocyte organoids in diluted fibrinogen and 60 ul was pipetted into 6mm PDMS gaskets. After 30 minutes of incubation, fibrin/cell gels were released from gaskets and implanted in mice as engineered liver tissues. Final cell concentrations were 1.25 million HUVECs/ml, 3.6 million NHDFs/ml, or 2.25 million hepatocytes/ml. Fibrin was used at a final concentration of 10 mg/ml.

6.4.4 *Implantation and induction of liver injury*

12- to 20-week-old FRGN mice (Fah -/-, Rag1-/-, Il2rg-/-, on a NOD background) were anesthetized with isofluorane. Three organoid tissues were sutured onto the gonadal fat pads of each mouse. Immediately after surgery, nitisinone (NTBC) was withdrawn from animals’ drinking water for 14 days to induce liver injury. For experiments that extended beyond 14 days, NTBC was then reintroduced to the drinking water to allow for mouse recovery, then removed again after 4 days for the remainder of the experiment.

6.4.5 *Albumin and A1AT ELISA*

Blood was drawn weekly from the saphenous vein of each mouse. Blood was centrifuged to isolate serum, then frozen until analysis. Albumin and A1AT ELISAs (Bethyl E80-129 and E88-122)

were then performed on serum according to manufacturer's instructions, as above in Chapter 2 "Albumin ELISA".

6.4.6 *Tissue harvesting, histology, and immunostaining*

Organoid tissues were identified using the surgical suture as a landmark then were excised and fixed in 4% paraformaldehyde for 48 hours at 4°C. Excess fat was removed from around the implant. Trimmed grafts were then dehydrated, paraffin-embedded, and sectioned on a microtome. Sections were then immunostained with antibodies listed in Table 2 according to the methods in Chapter 3 "Organoid histology, immunofluorescent staining and microscopy".

6.4.7 *Morphometric analysis*

Collected immunofluorescence images were analyzed using ImageJ software. Images were thresholded and masks were generated for each channel. Epithelial area was measured from CK18+ masks. Hepatic area was measured from CK18+ masks – CK19+ masks. Biliary area was measured from CK18+/CK19+ masks.

6.4.8 *Statistical Analysis*

Data in graphs are expressed as the mean ± SEM, as denoted in figure legends. Statistical significance was determined with PRISM software using one-way ANOVA or two-way ANOVA followed by Sidak's or Tukey's multiple comparison test, as denoted in figure legends.

Chapter 7. SCALING UP ENGINEERED LIVER TISSUES USING 3D PRINTED VASCULATURE

7.1 INTRODUCTION

While ectopic engineered liver tissues are an appealing alternative for the future of organ transplant, the current scale of hepatic implants is simply too small for human translation. Implanted hepatocyte organoids reached a peak albumin level of 15 μg/ml in mice (**Error! Reference source not found.**C), which would need to be scaled up more than 2000x to reach standard mouse albumin levels and 5,000,000x to reach human equivalence (*209*, *210*). Though the obvious solution is to fabricate larger tissues, transport limitations are quickly encountered upon scale up (*211*). Small tissues can be vascularized relatively quickly by the host, enabling delivery of necessary oxygen and nutrients, but large tissues will take more time to vascularize and thus develop necrosis in the core (*211*).

Researchers are working towards a solution to this problem by engineering vasculature that can rapidly anastamose with host vessels upon implant (*212*). The fields of 3D printing and bioprinting have made great progress towards developing techniques to engineer vasculature that can be quickly scaled up to meet the needs of tissue engineers. One method in particular, called sacrificial scaffolding, 3D prints a dissolvable negative mold around which a cellularized gel can be cast (*163*, *213*). After solidification, which can take seconds or minutes depending on the gel chosen, the 3D printed sacrificial scaffold is washed out, leaving an empty network within a cellularized gel. That network can then be filled with endothelial cells and serve as a primitive vascular network that can mature and integrate with the host circulation upon implantation (*163*).

We gravitated toward this method to generate vascularized engineered tissues due to the material freedom and rapid fabrication time. We partnered with the Miller Lab at Rice University who had recently developed a new technique to generate sacrificial sugar scaffolds with laser-sintered carbohydrate powder, called selectively laser-sintered carbohydrate sacrificial templating, or SLS-CaST (Figure 7.1) (*126*). With these networks we then explored how primitive vascular structures can help support hepatic cells *in vitro* with the goal to eventually fabricate large, vascularized, engineered hepatocyte organoid tissues for therapeutic rescue.

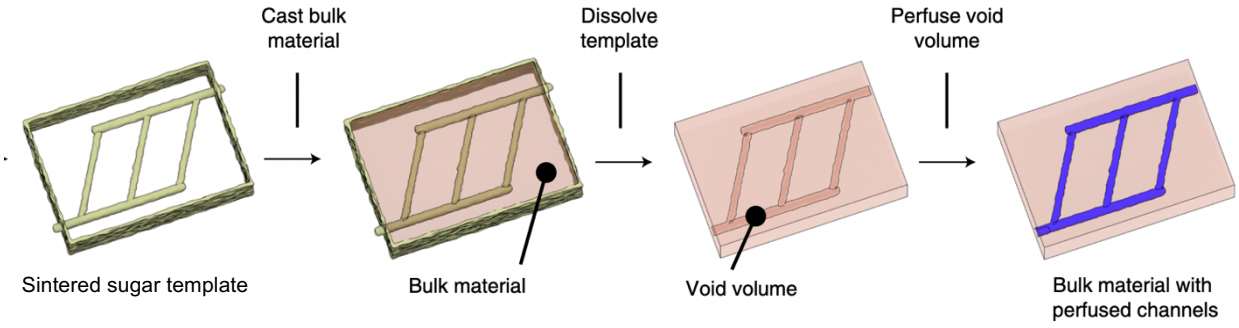

Figure 7.1: Schematic of SLS-CaST process

Process by which SLS-CaST gels are fabricated. First a carbohydrate template is generated through laser sintering. A gel is cast around the template and after solidification is dissolved and flushed out, leaving a void, perfusable network.

7.2 Results

7.2.1 *Perfusion of dendritic networks to support primary hepatocyte cultures.*

It is notoriously difficult to metabolically support and preserve native hepatic phenotype *ex vivo* (*214*), so supporting these cells serves as an important validation of the laser-sintering technique. Moreover, contemporary methods for *in vitro* hepatocyte culture use multicellular aggregates to leverage the beneficial effects of cell–cell interactions (*215*). The rapid casting approach is well

suited for handling these large and delicate multi-cellular aggregates, which may be incompatible with other biofabrication processes.

We began with a comparative study of the metabolic activity and phenotype of hepatic aggregates (comprising primary rat hepatocytes and normal human dermal fibroblasts) (*100*, *102*) in perfused versus statically cultured agarose gels (Figure 7.2A). Perfused aggregate gels showed negligible loss of metabolic function over 7 days of perfusion, whereas statically cultured gels exhibited widespread metabolic loss over the same time period, measured by MTT assay (Figure 7.2B and C). We also observed marked phenotypic differences: perfused gel aggregates stained positive for E-cadherin (a marker of hepatocyte intercellular junctions) across the gel (Figure 7.2D) with substantive signal localized at the cell membrane (Figure 7.2E), as well as for cytokeratin 18 (Figure 7.2F; hepatocyte cytoskeleton) and vimentin (Figure 7.2E; fibroblast cytoskeleton). By contrast, statically cultured aggregates appeared less compacted with diminished membrane-localized E-cadherin and vimentin staining. Notably, the distinctive capsule structure formed by fibroblasts around the outer surface of aggregates in perfused gels appeared to occur with lower frequency in the statically cultured aggregates, which may account for their less cohesive morphology. Over the 7 day culture duration, perfused gels also produced significantly more albumin (a key hepatic functional marker) than their static counterparts (Figure 7.2G).

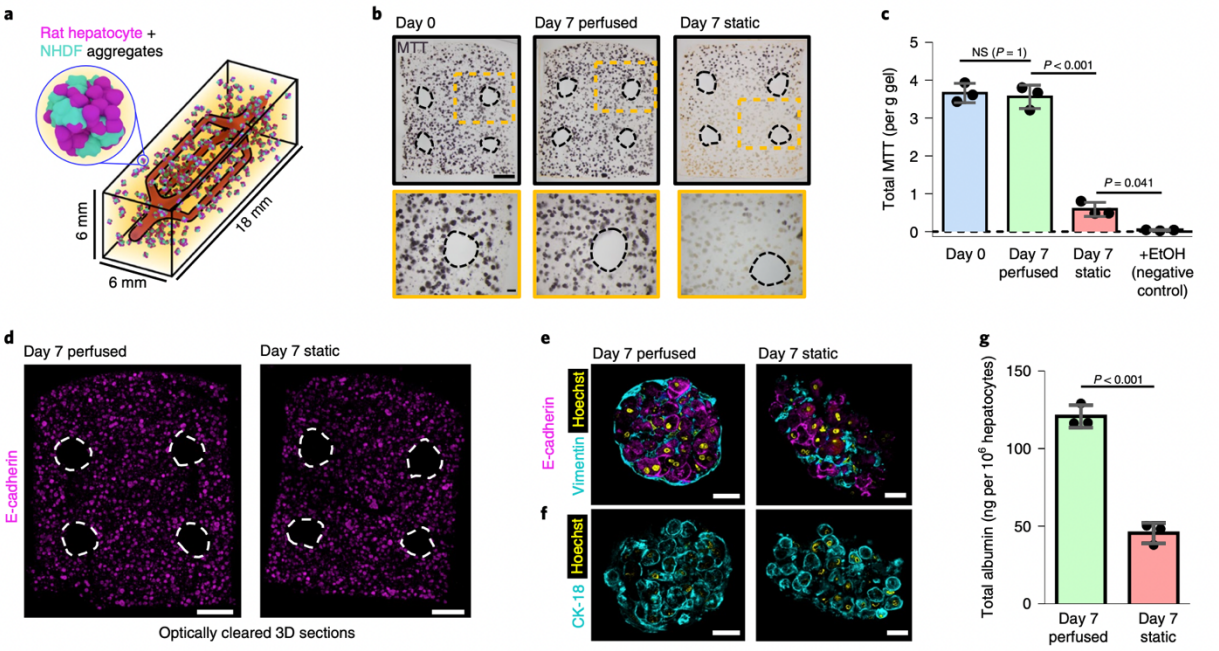

Figure 7.2: Perfusion through dendritic networks to support primary hepatocyte cultures

(A) Encapsulated hepatic aggregates, comprising primary rat hepatocytes and normal human dermal fibroblasts (NHDF), were cultured statically or under perfusion in agarose gels.

(B, C) MTT staining (B) of hepatic aggregates (500-µm sections) demonstrates robust metabolic activity in perfused gels but not in static gels after 7 d of culture. Scale bar, 1 mm (top), 200 µm (bottom). (C) No significant drop in metabolic output was recorded between day 0 and day 7 perfused gels. Data are mean ± s.d. of n = 3 technical gel replicates; significance determined by one-way ANOVA with Bonferroni post hoc test.

(D) Hepatic aggregates stain positively for e-cadherin throughout perfused and static gels. Scale bars, 1 mm; images show maximum intensity projection.

(E, F) Representative images of aggregates in 6-µm sections of perfused gels show that some cells (presumably hepatocytes) have positive staining for e-cadherin (E) and cytokeratin 18 (CK-18) (F) that is largely membrane localized, as well as positive staining for the fibroblast marker vimentin (E). Aggregates in static gels show disruption in vimentin connectivity with decreased membrane localization of e-cadherin. Scale bars, 20 µm. Approximately 15 aggregates across 3 gels were imaged.

(G) Over 7 days, perfused gels secreted significantly more albumin than static gels (mean ± s.d., unpaired two-tailed t-test).

7.2.2 *Generating vascularized, therapeutic-scale engineered liver tissues for in vitro hepatocyte support*

The apparent compatibility of SLS-CaST with primary hepatocytes in a relatively simple gel architecture motivated us to explore our capacity to support much larger volumes of primary hepatocyte cultures using dendritic vascular topologies. We used mutual tree attraction to generatively design a larger, more extensively branched dendritic network (Figure 7.2H). We demonstrated that this network can be laser-sintered at a scale large enough to generate a 6.5ml gel. Crucially, while the fabrication time for these sacrificial templates was significantly longer than for smaller dendritic networks, the time required to actually cast the corresponding tissues was only slightly longer; gels of all sizes were fabricated in less than 5 minutes despite the increased volume and vascular complexity. With the 6.5ml high-density dendritic architecture, we fabricated 6 hepatic tissues, each containing 65 million hepatocytes and 32.5 million fibroblasts, and then perfused them on a continuous flow loop for 3 or 7 days.

Similar to the previous experiment, we found that perfusion through the dendritic network supported the metabolism of primary hepatic aggregates (Figure 7.3I and J). The high-density dendritic network appears to be well spaced at its center for this density of hepatic aggregates since only a thin region of non-viable cells appeared around the exterior surfaces of an optimally perfused sample, which were not in direct contact with medium (Figure 7.3I). A perfusion apparatus that also bathes the gel exterior in medium would thus be expected to boost metabolic activity at the day 7 time point. We estimated the metabolically active distance to be on the order of 800-1,000 μm; the relatively high variability may stem from the polydispersity of the aggregates themselves and potential inhomogeneities in their initial seeding density. Positive E-cadherin staining was observed at day 3 and day 7, although the staining was more variegated across the gel at the later time point (Figure 7.3K). We measured accumulation of albumin and found

substantially more albumin at both day 3 and day 7 compared with blank gels (Figure 7.3M), demonstrating that hepatocytes in gels with dendritic networks retained measurable hepatic function until at least day 7. However, we also found that albumin production decreased over time in these gels, which, together with the observed decrease in E-cadherin staining suggests that hepatocytes may undergo a loss of phenotype ('de-differentiation') in the current gel formulation, indicative of a longstanding and ongoing challenge in the field of in vitro hepatocyte culture (*78*, *100*). Despite decreasing albumin secretion, hepatic aggregates generally retained expression of membrane-localized E-cadherin (Figure 7.3N) and cytokeratin 18 after 7d of culture. Aggregates also maintained a packed morphology (Figure 7.3L) with well-defined vimentin staining in a fibrillar network forming the characteristic capsule-like structure around the perimeter of the aggregate (Figure 7.3N).

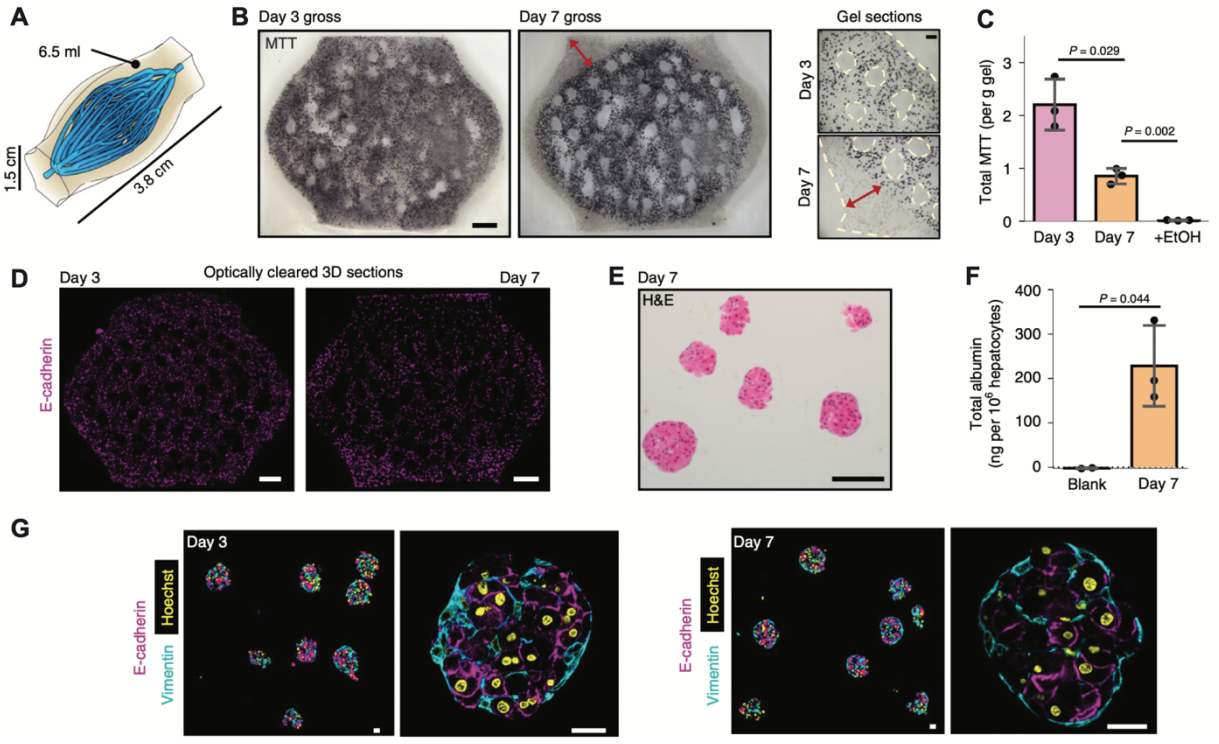

Figure 7.3: Therapeutic scale-up of vascularized engineered liver tissues

(A) Perfusion culture of hepatic aggregates was scaled up to a high-density 3D dendritic network.

(B, C) Uniform positive MTT staining was observed across the gels at day 3, whereas day 7 MTT staining was confined to the vicinity of perfused channels ((B); scale bars, 1 mm (gross), 500 μm (sections)). Red arrows indicate the region of metabolically inactive aggregates which extends around the gel perimeter; dashed lines mark gel boundaries. Here we illustrate an optimally perfused sample. (C) Quantification corroborates the visualized drop in metabolic output near the outer gel surface (mean ± s.d. for n = 3 technical gel replicates; one-way ANOVA with Bonferroni post hoc test).

(D) Aggregates in cleared thick sections stain positively for e-cadherin at day 3 (left) and day 7 (right), with less expression at day 7. Scale bars, 2 mm.

(E) Hematoxylin and eosin (H&E) staining demonstrates compacted aggregate morphology at day 7. Scale bar, 50 μm.

(F) Hepatic aggregates produce albumin after 7 days of flow loop perfusion (mean ± s.d., unpaired two-tailed t-test).

(G) Aggregates stain positively for hepatocyte marker e-cadherin and fibroblast marker vimentin, with some loss of e-cadherin staining at day 7. Scale bars, 20 μm. Approximately 15 aggregates across 3 gels were imaged. Technical replicates refer to the use of a single pooled primary hepatocyte isolate for all gels within a trial to eliminate donor-to-donor variability.

Together, the results of these two experiments demonstrate that perfusion improves aggregate metabolism and maintenance of hepatic markers, and that perfusion though dendritic vascular networks can meet the mass transport needs of these highly metabolic cells. We postulate that the decline in function should not be attributed to poor oxygen or nutrient transport, but rather to a suboptimal microenvironment for the aggregates, as shown previously in other hepatocyte culture systems (*78*, *100*, *216*). As a materials-agnostic fabrication strategy, SLS-CaST is well suited for investigating the intersection between mass transport and the hepatic microenvironment for optimizing hepatic stabilization (*217*). Given our recent progress in hepatocyte organoid culture, we expect that SLS-CaST will offer a fabrication strategy to translate these advances in biology towards the scale of therapeutic utility.

7.3 DISCUSSION

As a proof of concept, this work has demonstrated the utility of 3D printing and vascularization for scale up of engineered liver tissues. Using SLS-CaST, large tissues can be fabricated within minutes, limiting the hypoxia and cell stress that accompanies laborious fabrication techniques such as extrusion printing. Additionally, sacrificial scaffolding is compatible with any polymerizable substrate, opening material possibility that were previously incompatible with light-based methods such as stereolithographic printing. Due to these new advantages, we expect that SLS-CaST will be highly compatible with our newly developed adult human hepatocyte organoids, and by uniting the two technologies we can generate larger scale engineered liver tissues to move toward clinical translation.

Another advantage of SLS-CaST for liver tissue engineering is the precise resolution in all three dimensions. Previous sugar-based scaffolds were limited in the z-dimension, leading to planar scaffolds with non-physiologic scaffold junctions (*125*). This precision enables recreation of complex hepatic architectural features, including hierarchical vasculature and independent but intertwined networks. These features will allow tissue engineers to thoroughly pre-vascularize implants and will offer a template that could be independently seeded with endothelial cells and cholangiocytes to replicate portal veins and bile ducts within a single tissue.

7.4 METHODS

7.4.1 *Preparation of hepatocyte aggregates*

Primary rat hepatocytes were isolated through portal vein cannulation and two-step collagenase digestion as previously described (*218*). Hepatocytes were resuspended in hepatocyte culture media (DMEM (VWR), 10% fetal bovine serum (Biowest), 1% ITS supplement (insulin,

transferrin, sodium selenite, VWR), 7 ng/mL glucagon (Sigma), 0.04 g/mL dexamethasone (Sigma), and 1% antibiotic/antimycotic solution (Sigma). Normal human dermal fibroblasts (NHDF, Lonza) were trypsinized and resuspended in hepatocyte culture media. Cellular aggregates containing approximately 150 hepatocytes and 75 NHDFs per aggregate were created with aggrewell molds as previously described (*100*).

7.4.2 *Gel casting*

Cell-laden agarose gels were prepared by resuspending the appropriate number of hepatocyte/NHDF aggregates in ITS media to half the desired gel volume. This cell suspension was combined with an equal volume of sterile low-melt agarose (4 wt% in PBS, heated to 60 °C, then cooled to 37-42 °C before mixing with cells). The cell suspension and agarose were vigorously mixed for approximately 60 seconds using a positive displacement pipettor prior to dispensing around a carbohydrate template and cooling to 4 °C for 5-10 minutes. The carbohydrate template was removed by incubation in media for 10-15 minutes, assisted by gently flushing through the channels with media via syringe. All experiments used a final cell density of approximately 10e6 hepatocytes/mL and 5e6 NHDF/mL, and acellular agarose gels ("blank") were cast as negative controls for albumin measurement. For comparison of static and perfused gels, one set of gels was perfused with hepatocyte culture media at 20 μL/min with a multichannel peristaltic pump. A second set of gels was identically catheterized and a 1mL syringe of hepatocyte media was connected at the inlet and outlet to permit only diffusive transport of nutrients into the gel. For longitudinal albumin measurement, outflow media was collected each from the perfused gels, and the static gels were flushed through with fresh media to capture accumulated albumin. High density dendritic gels were connected in a flow loop configuration with 50 mL hepatocyte culture media continuously recirculated using a custom designed peristaltic pump at 1 mL/min.

Each day, 10-20 mL media was sterilely removed from the flow loop for albumin measurement and replaced with an equal volume of fresh media.

7.4.3 *Albumin measurements.*

Rat albumin in sampled media was quantified by an enzyme-linked immunosorbent assay (ELISA) using goat polyclonal capture and horseradish peroxidase-conjugated goat anti-rat albumin detection antibodies (Bethyl Laboratories).

7.4.4 *Immunostaining and imaging*

Primary hepatocyte gels were removed from their perfusion chambers and sliced into 1–2-mm-thick sections with a microtome blade. Slices were fixed in 4% paraformaldehyde for 48 h at 4 °C followed by two PBS washes. Slices used for paraffin sectioning were dehydrated in graded ethanol (50–100%), embedded in paraffin, then sectioned (6 μm) using a microtome for immunohistochemical staining. Sections were histochemically stained with hematoxylin and eosin or immunostained by first blocking with normal donkey serum (VWR) and then incubating with primary antibodies against cytokeratin 18 (rabbit, 1:100; Abcam), E-cadherin (goat, 1:100; R&D) and/or vimentin (rabbit, 1:200; Abcam) and followed with Hoechst and species-appropriate secondary antibodies conjugated to Alexa Fluor 594 or Alexa Fluor 647. Antibody-stained sections were imaged on a Nikon A1R scanning confocal microscope or Nikon Ti-E inverted high-resolution wide-field microscope. Gel slices used for tissue clearing and 3D imaging were removed from PBS, placed in blocking solution (0.1 M tris (VWR), 1% BSA (Sigma), 1% normal donkey serum (VWR), 0.3% Triton-X (VWR)), stained with a primary antibody against E-cadherin (goat, 1:100; R&D) followed by Alexa Fluor 647 secondary antibody, and cleared using the Ce3D

method (*176*). Cleared gels were imaged on a Leica SP8 confocal microscope and images were processed with Imaris image analysis software.

7.4.5 *Gel sectioning and measurement of metabolic activity.*

Before staining, gels were removed from culture and live sectioned by hand or into 500 μm slices on a vibrating microtome (VT1000S, Leica). Immediately after sectioning, gel slices were stained with MTT solution to measure metabolic output. To prepare MTT stock solution, MTT (Bio Basic) was dissolved in PBS (5 mg/ml), sterile filtered and stored at −20 °C. MTT staining solution was prepared by mixing equal volumes of thawed stock solution with sectioning medium and added to gel slices until they were entirely submerged. After 30 min MTT staining solution was aspirated and gel slices were fixed in paraformaldehyde (4%; Electron Microscopy Sciences) for 30 min. Stained gel slices were imaged on a stereoscopic microscope (SteREO Discovery.V8; Zeiss) equipped with a DSLR camera (EOS 5DSR; Canon). MTT formazan signal was imaged for each slice without disturbing the slice position. Total MTT signal was measured from imaging data by summing the relevant pixel intensities and independently by optical absorbance. Gel slices were incubated in acidified isopropanol (100 mM HCl) for 2–4 h at 37 °C to dissolve the formazan product. Following centrifugation of the remaining gel material, the supernatant was transferred to a 96-well plate and absorbance was measured at 590 nm on a plate reader (Tecan). When MTT formazan was dissolved from variable amounts of starting gel material, the absorbance value was reported as absorbance units per unit mass of gel in g.

Chapter 8. CONCLUSION

8.1 SUMMARY OF CURRENT WORK

Though the burden of liver disease has continued to grow globally over the last few decades, treatment for late-stage liver disease has remained limited to one curative option: transplant (*41*). Unfortunately, the number of organs available for transplant is stagnant while the number of patients awaiting transplant grows annually as disease incidence increases. To alleviate this burden and close the donor organ gap, we must prevent disease onset, reverse disease progression, and/or develop alternatives to transplant such as implantable engineered liver tissues. However, research efforts are stymied by the inability to culture and expand high quality hepatic cell, which are necessary to better understand the liver in health and disease, and to generate functional engineered liver tissues. To address this challenge, in this body of work we explore organoid culture as a means to grow hepatic cells, model the human liver *in vitro*, and prime hepatic cells for implant in engineered liver tissues. We also demonstrate the potential of 3D printing technologies for scale up of engineered liver tissues to move closer to clinical translation.

In Chapter 2, we use newly developed hepatoblast organoids as an expandable hepatic cell source in engineered liver tissues and as a model of hepatic development. Hepatoblast organoids were shown to survive after implant and produce human protein measurable in mouse blood serum, suggesting successful engraftment and connection to host vasculature. Hepatoblasts, which incompletely differentiate *in vitro*, generated both hepatocytes and cholangiocytes in engineered liver tissues absent of external stimuli. This indicates that the *in vivo* microenvironment produces differentiation and maturation signals that were absent from *in vitro* culture. This was the first demonstration of engraftment of human fetal liver organoids in ectopic engineered liver tissues

and established a new model with which to better understand hepatic development and maturation. However, engrafted organoids exhibited minimal expansion and morphogenesis after implant, suggesting that more mature hepatic organoids may be a better parenchymal cell source for engineered liver tissues.

Towards this end, in Chapter 3 we developed and characterized adult human hepatocyte organoids. We first tested developmental growth conditions on adult human hepatocytes and established a base culture which was then optimized through toggling of the TGFβ pathway. Resulting organoids were shown to express proliferation-associated marker Ki-67 during the first week of culture and correspondingly exhibited significant growth over 2 weeks. Most organoids demonstrated a densely packed morphology with cells that stained positively for a variety of hepatocyte markers and negative for biliary markers. Alongside dense organoids, cystic organoids also grew that were composed of smaller cells that stained positive for cholangiocyte markers, demonstrating that both hepatocytes and cholangiocytes can be cultured as organoids in our established conditions.

In Chapter 4, adult human hepatocyte organoids were screened for a variety of mature liver functions across a diverse set of donor hepatocytes to test our culture method for robustness. Hepatocytes from seven different donors that exhibited variable plating in 2D were grown in organoid conditions and found to consistently generate adult human hepatocyte organoids with maintenance of the phenotype characterized in Chapter 3. Organoids from all donor hepatocytes exhibited strong expression of a handful of hepatic functional genes, similar to primary hepatocyte controls and in contrast to fetal hepatoblast controls when the genes correlated with maturity. To corroborate our transcriptional findings, we then directly measured liver function across multiple axes including albumin secretion and drug metabolizing activity and found that adult human

hepatocytes robustly maintained hepatic functions through organoid culture. Collectively, this demonstrates that our adult human hepatocyte organoid culture method can be used to grow highly functional and mature organoids from a diverse set of donor hepatocytes.

To more completely explore functional heterogeneity within our adult human hepatocyte organoid cultures, in Chapter 5 we used single cell RNA sequencing to assess the transcriptome of single cells after being grown as organoids. We identified hepatocytes, cholangiocytes, and fibroblasts within the culture that each clustered closely with their corresponding cell type from adult liver in UMAP. The organoid hepatocytes exhibited a similar distribution of expression of a variety of functional genes when compared to hepatocytes from adult liver. Drug metabolizing genes, known to arise late in development or after birth, were low in fetal hepatoblast controls but similarly high in organoid hepatocytes and adult liver hepatocytes. Conversely, fetal genes that were high in fetal hepatoblast controls were low in organoid hepatocytes, validating that organoid culture maintains the transcriptional maturity of hepatocytes.

As more mature hepatic cells tend to demonstrate better function and engraftment after transplant, in Chapter 6 we tested the performance of adult human hepatocyte organoids in implanted engineered liver tissues. Engrafted organoids had high function after implant, measured through production of human albumin and A1AT, and adopted aspects of liver morphology such as cord architecture. Critically, organoids formed significantly larger and more highly functional grafts than aggregates that were generated from the same hepatocyte donor. Additionally, when non-parenchymal cells were excluded from implants, organoid grafts had better function and less of the graft area was composed of biliary cells. We were excited by this demonstration that adult human hepatocyte organoids could be a robust parenchymal cell source for liver tissue engineering.

Having identified an improved hepatic cell source, in Chapter 7 we address another significant barrier for the tissue engineering field: tissue scale up and vascularization. We utilized a newly developed 3D printing technology based on sacrificial scaffolding called SLS-CaST, that uses laser sintering to precisely build carbohydrate scaffolds. We used the SLS-CaST to fabricate negative vascular molds, cast a bulk gel with hepatic aggregates around the network, and then dissolve out the carbohydrate, leaving behind an empty vasculature network surrounded by hepatic aggregates. Using these tissues, we explored the effects of fluid transport within our fabricated tissues and found that media perfusion enhances the morphology and function of aggregates. Additionally, using SLS-CaST we designed macro tissues that were ~100x larger than the engineered liver tissues used in Chapter 2 and Chapter 6, and demonstrated that perfusion through dense dendritic vascular networks could support large scale engineered tissues. This served as a proof of concept for future experiments that can focus on scale up of organoid tissues for more therapeutically relevant implantation.

8.2 REMAINING CHALLENGES AND FUTURE DIRECTIONS

Though the work presented here offers major improvements to multiple issues faced by the liver tissue engineering field, a significant hurdle still stands in the way of clinical translation: hepatocyte abundance. Organoid culture transiently expands adult human hepatocytes *in vitro* and primes them for implant but they are not yet proliferative long-term and therefore are not producible on a scale that is relevant for clinical translation. Adapting organoid culture for compatibility with high throughput manufacturing processes will enable mass generation of hepatocytes but will be better optimized in a dedicated industrial facility. Thus, below I focus on

experimental approaches to induce prolonged organoid growth and passage-ability to exponentially expand the input cell population.

8.2.1 *Media screening in high throughput*

When hepatocytes replicate in partial hepatectomy, they undergo one or two rounds of cell division and return to senescence (*51*). However, serial transplantation of hepatocytes has demonstrated that they have the potential to continue cell division when exposed to the appropriate stimulation (*72*). Thus, we will explore signals that are high in the early phases of liver regeneration, such as HGF, EGF, Wnt, TGFα, TNFα, IL6, norepinephrine, serotonin, and insulin, as well as maturation factor OSM (*49*). Additionally, we will probe the signals known to terminate liver regeneration. These signals are less understood, but studies into the "hepatostat" – an observed phenomenon where the liver almost perfectly returns to its original size after resection (*66*) – can give us clues as to the signals that may be preventing indefinite proliferation in organoids. Signals and pathways found to misregulate the hepatostat include: TGFβ (*49*, *66*), sensation of bile acids through FXR and FGF19 (*219*), glycipcan-3 (*69*), Yap/Hippo (*67*), and stretch-induced activation of endothelial β1 integrin and VEGFR3 (*52*). Through a combination of activated "go" signals and inhibited "stop" signals, we aim to induce sustained hepatocyte proliferation and mimic a prolonged growth phase of regeneration.

One potential issue that we may face is that induction of indefinite proliferation as is seen during serial transplantation may require repeated, cyclical stimulation of regenerative pathways. If this is the case, growth factors will need to be temporally adjusted in the organoid media and may require a full cycle of priming, growth, and termination signals before another regenerative phase is induced. Testing all of the potential combinations of signals and additionally augmenting them over time will lead to thousands of different conditions to screen, a task that would be

impossible for an academic-sized lab. Thus, another important step for optimization of adult human hepatocyte organoid culture will be adapting organoid culture for high throughput screening. Similar adjustments have been made for other organoid systems, enabling rapid optimization of culture conditions, screening of genetic mutations, and testing pharmaceutical interventions (*220–222*). Using established high throughput compatible organoids as a template, future work should focus on making adult human hepatocyte organoid culture compatible with 384-well plates and robotic handling stations as well as optimizing endpoints for high throughput analysis.

8.2.2 *Strategies to control the ratio of hepatocytes, cholangiocytes, and stromal cells in organoid culture*

Another strategy to prolong the lifespan of hepatocyte organoids is to purify the culture and control or eliminate contaminating cholangiocytes and stromal cells. The reasons for this are twofold: (1) cholangiocytes and stromal cells are more proliferative in organoid culture, and thus dilute and rapidly out-compete hepatocytes after a single passage, and (2) paracrine signals and/or direct contact from cholangiocytes and stromal cells may introduce signals or stimuli that influence proliferation or transdifferentiation. This second hypothesis is inspired by a recent paper from the Huch lab that demonstrated that indirect, paracrine signaling between fibroblasts and ductal organoids stimulated cholangiocyte proliferation, but that direct cell-cell contact between ductal organoids and fibroblasts inhibits their proliferation (*172*). Spatial regulation of soluble and physical stimuli is known to be critical in development (*223–225*), and makes sense in the context of liver physiology, where cholangiocytes in homeostasis are non-proliferative when in contact with portal fibroblasts, but can lose those contacts after injury, when they must proliferate to return to homeostatic contact (*49*, *172*).

During development, hepatocytes and cholangiocytes both differentiate from a common progenitor cell, the hepatoblast (*5–7*). This differentiation is spatially regulated, and hepatoblasts nearest the portal mesenchyme become cholangiocytes through TGFβ and Notch signaling – signals that primarily originate from fibroblasts (*7*, *14*). Hepatoblasts more removed from the portal mesenchyme and therefore more distant from fibroblast signals differentiate into hepatocytes (*7*). Experiments in mice have shown that TGFβ, a cytokine produced by fibroblasts, can induce direct transdifferentiation of hepatocytes to cholangiocytes (*167*). *In vitro* experiments have shown that TGFβ can induce cellular senescence, epithelial-to-mesenchymal transition, and apoptosis in hepatocytes (*226–228*). Additionally, our *in vivo* experiments in Chapter 6 demonstrated that inclusion of stromal cells reduced hepatic function and graft growth. Thus, we hypothesize that contaminating fibroblasts in our organoid cultures provide spatially misregulated paracrine signals to hepatocytes. This may induce transdifferentiation, dedifferentiation, apoptosis, or senescence – all outcomes that would prevent hepatocyte organoid propagation.

On the other hand, the absence of a biliary network *in vivo* has also been shown to induce hepatocyte transdifferentiation to cholangiocytes (*167*). While the rapid growth of cholangiocytes in culture are certainly unfavorable, it is possible that complete elimination of cholangiocytes from our organoid culture could drive transdifferentiation of hepatocytes to fill the missing biliary niche. Thus, we wish to control the ratios of contaminating fibroblasts and cholangiocytes in our hepatocyte organoid culture to explore these hypotheses and ultimately enable prolonged growth and passaging of adult human hepatocyte organoids.

To do this, we can design a lentiviral vector expressing puromycin resistance under the albumin promoter, with constitutively active red-fluorescent protein (RFP). Cells will be transduced in suspension, then plated as organoids. Only transduced cells expressing albumin

should possess antibiotic resistance, so occasional exposure to puromycin should eliminate non-transduced and non-albumin producing cells, leaving behind only hepatocytes. Reintroducing non-transduced populations with controlled ratios of fibroblasts and cholangiocytes will enable toggling of cell stoichiometry and exploration of the influence fibroblasts and cholangiocytes have on hepatocytes in culture.

8.2.3 *Fabrication of ideal hepatic microenvironment in engineered liver tissues*

In Chapter 6 we demonstrated that engineered liver tissues fabricated with organoids exhibited significant differences in function and morphology with and without exogenous non-parenchymal cells. This exciting result raises many questions about the role that non-parenchymal cells play in engineered liver tissues and whether controlling their architecture or ratios will influence cell fate or function. However, testing all possible permutations in a controlled *in vivo* experiment would take hundreds of mice and likely many years. To surpass this bottleneck, Colleen O'Connor in the Stevens lab has developed an *in vivo* array platform called "Highly Parallel Tissue Grafting" (HPTG), which can screen up to 43 different cell or material combinations in one mouse. Using this technology, we can test dozens of different cell- or material-based combinations with altered ratios of fibroblasts, endothelial cells, and adult human hepatocyte organoids to optimize the microenvironment of engineered liver tissues.

In parallel to optimizing the cell stoichiometry of implanted organoids, we can also use SLS-CaST to incorporate architectural complexity for better biomimicry in engineered liver tissues. Separate vascular structures can be seeded with endothelial cells and cholangiocytes in independent networks within hepatocyte organoid-dense hydrogels to generate more physiological engineered liver tissues. Such tissues can be rapidly fabricated and used for implantation or can serve as *in vitro* models to study cell-cell interactions and morphogenesis in the human liver.

In sum, the work summarized here demonstrates significant progress for liver tissue engineering and opens many new possibilities for exciting research into the biology and pathology of mature hepatocytes in the human liver.

BIBLIOGRAPHY

1. J. Jung, M. Zheng, M. Goldfarb, K. S. Zaret, Initiation of mammalian liver development from endoderm by fibroblast growth factors. *Science (1979)*. **284**, 1998–2003 (1999).

2. J. M. Rossi, N. R. Dunn, B. L. M. Hogan, K. S. Zaret, Distinct mesodermal signals, including BMPs from the septum transversum mesenchyme, are required in combination for hepatogenesis from the endoderm. *Genes & Development*. **15**, 1998–2009 (2001).

3. V. A. McLin, S. A. Rankin, A. M. Zorn, Repression of Wnt/β-catenin signaling in the anterior endoderm is essential for liver and pancreas development. *Development*. **134**, 2207–2217 (2007).

4. E. A. Ober, H. Verkade, H. A. Field, D. Y. R. Stainier, Mesodermal Wnt2b signalling positively regulates liver specification. *Nature 2006 442:7103*. **442**, 688–691 (2006).

5. E. A. Ober, F. P. Lemaigre, Development of the liver: Insights into organ and tissue morphogenesis. *Journal of Hepatology*. **68**, 1049–1062 (2018).

6. M. Gordillo, T. Evans, V. Gouon-Evans, Orchestrating liver development. *Development*. **142**, 2094–108 (2015).

7. Y. Zong, B. Z. Stanger, Molecular mechanisms of liver and bile duct development. *Wiley Interdisciplinary Reviews: Developmental Biology*. **1**, 643–655 (2012).

8. A. Micsenyi, X. Tan, T. Sneddon, J. H. Luo, G. K. Michalopoulos, S. P. S. Monga, β-Catenin is temporally regulated during normal liver development. *Gastroenterology*. **126**, 1134–1146 (2004).

9. W. Goessling, T. E. North, A. M. Lord, C. Ceol, S. Lee, G. Weidinger, C. Bourque, R. Strijbosch, A. P. Haramis, M. Puder, H. Clevers, R. T. Moon, L. I. Zon, APC mutant zebrafish uncover a changing temporal requirement for wnt signaling in liver development. *Developmental Biology*. **320**, 161–174 (2008).

10. K. Matsumoto, R. Miki, M. Nakayama, N. Tatsumi, Y. Yokouchi, Wnt9a secreted from the walls of hepatic sinusoids is essential for morphogenesis, proliferation, and glycogen accumulation of chick hepatic epithelium. *Developmental Biology*. **319**, 234–247 (2008).

11. T. Berg, C. B. Rountree, L. Lee, J. Estrada, F. G. Sala, A. Choe, J. M. Veltmaat, S. de Langhe, R. Lee, H. Tsukamoto, G. M. Crooks, S. Bellusci, K. S. Wang, Fibroblast growth factor 10 is critical for liver growth during embryogenesis and controls hepatoblast survival via beta-catenin activation. *Hepatology*. **46**, 1187–1197 (2007).

12. C. Schmidt, F. Bladt, S. Goedecke, V. Brinkmann, W. Zschiesche, M. Sharpe, E. Gherardi, S. Goedecke, Scatter factor/hepatocyte growth factor is essential for liver development. *Nature 1995 373:6516*. **373**, 699–702 (1995).

13. K. Matsumoto, H. Yoshitomi, J. Rossant, K. S. Zaret, Liver Organogenesis Promoted by Endothelial Cells Prior to Vascular Function. *Science (1979)*. **294**, 559–563 (2001).

14. Y. Zong, A. Panikkar, J. Xu, A. Antoniou, P. Raynaud, F. Lemaigre, B. Z. Stanger, Notch signaling controls liver development by regulating biliary differentiation. *Development*. **136**, 1727–1739 (2009).

15. Y. Kodama, M. Hijikata, R. Kageyama, K. Shimotohno, T. Chiba, The role of notch signaling in the development of intrahepatic bile ducts. *Gastroenterology*. **127**, 1775–1786 (2004).

16. F. Clotman, P. Jacquemin, N. Plumb-Rudewiez, C. E. Pierreux, P. van der Smissen, H. C. Dietz, P. J. Courtoy, G. G. Rousseau, F. P. Lemaigre, Control of liver cell fate decision by a gradient of TGF beta signaling modulated by Onecut transcription factors. *Genes Dev*. **19**, 1849–54 (2005).

17. A. Antoniou, P. Raynaud, S. Cordi, Y. Zong, F. Tronche, B. Z. Stanger, P. Jacquemin, C. E. Pierreux, F. Clotman, F. P. Lemaigre, Intrahepatic Bile Ducts Develop According to a New Mode of Tubulogenesis Regulated by the Transcription Factor SOX9. *Gastroenterology* (2009), doi:10.1053/j.gastro.2009.02.051.

18. M. Yanai, N. Tatsumi, N. Hasunuma, K. Katsu, F. Endo, Y. Yokouchi, FGF signaling segregates biliary cell-lineage from chick hepatoblasts cooperatively with BMP4 and ECM components in vitro. *Developmental Dynamics*. **237**, 1268–1283 (2008).

19. K. Si-Tayeb, F. P. Lemaigre, S. A. Duncan, Organogenesis and Development of the Liver. *Developmental Cell*. **18**, 175–189 (2010).

20. N. Tanimizu, K. Kaneko, T. Itoh, N. Ichinohe, M. Ishii, T. Mizuguchi, K. Hirata, A. Miyajima, T. Mitaka, Intrahepatic bile ducts are developed through formation of homogeneous continuous luminal network and its dynamic rearrangement in mice. *Hepatology*. **64**, 175–188 (2016).

21. A. Kamiya, F. J. Gonzalez, TNF-α regulates mouse fetal hepatic maturation induced by oncostatin M and extracellular matrices. *Hepatology*. **40**, 527–536 (2004).

22. A. Kamiya, T. Kinoshita, A. Miyajima, Oncostatin M and hepatocyte growth factor induce hepatic maturation via distinct signaling pathways. *FEBS Letters*. **492**, 90–94 (2001).

23. D. Shin, S. Pal, S. Monga, Cellular and Molecular Basis of Liver Development Anteroposterior Endoderm Patterning (2013), doi:10.1002/cphy.c120022.

24. X. Tan, Y. Yuan, G. Zeng, U. Apte, M. D. Thompson, B. Cieply, D. B. Stolz, G. K. Michalopoulos, K. H. Kaestner, S. P. S. Monga, β-Catenin Deletion in Hepatoblasts Disrupts Hepatic Morphogenesis and Survival During Mouse Development. *Hepatology*. **47**, 1667–1679 (2008).

25. B. T. Spear, L. Jin, S. Ramasamy, A. Dobierzewska, Transcriptional control in the mammalian liver: liver development, perinatal repression, and zonal gene regulation. *Cellular and Molecular Life Sciences CMLS 2006 63:24*. **63**, 2922–2938 (2006).

26. L. Peng, B. Yoo, S. S. Gunewardena, H. Lu, C. D. Klaassen, X. B. Zhong, RNA Sequencing Reveals Dynamic Changes of mRNA Abundance of Cytochromes P450 and Their Alternative Transcripts during Mouse Liver Development. *Drug Metabolism and Disposition*. **40**, 1198 (2012).

27. J. E. Moscovitz, L. M. Aleksunes, Establishment of Metabolism and Transport Pathways in the Rodent and Human Fetal Liver. *International Journal of Molecular Sciences*. **14**, 23801 (2013).

28. D. Choudhary, I. Jansson, I. Stoilov, M. Sarfarazi, J. B. Schenkman, Expression patterns of mouse and human CYP orthologs (families 1–4) during development and in different adult tissues. *Archives of Biochemistry and Biophysics*. **436**, 50–61 (2005).

29. K. Elvevold, B. Smedsrød, I. Martinez, The liver sinusoidal endothelial cell: A cell type of controversial and confusing identity. *American Journal of Physiology - Gastrointestinal and Liver Physiology*. **294**, 391–400 (2008).

30. S. Benhamouche, T. Decaens, C. Godard, R. Chambrey, D. S. Rickman, C. Moinard, M. Vasseur-Cognet, C. J. Kuo, A. Kahn, C. Perret, S. Colnot, Apc Tumor Suppressor Gene Is the "Zonation-Keeper" of Mouse Liver. *Developmental Cell*. **10**, 759–770 (2006).

31. Z. D. Burke, K. R. Reed, T. J. Phesse, O. J. Sansom, A. R. Clarke, D. Tosh, Liver Zonation Occurs Through a β-Catenin–Dependent, c-Myc–Independent Mechanism. *Gastroenterology*. **136**, 2316-2324.e3 (2009).

32. T. Matsumura, R. G. Thurman, Measuring rates of O2 uptake in periportal and pericentral regions of liver lobule: stop-flow experiments with perfused liver. *https://doi.org/10.1152/ajpgi.1983.244.6.G656*. **7** (1983), doi:10.1152/AJPGI.1983.244.6.G656.

33. S. Ben-Moshe, S. Itzkovitz, Spatial heterogeneity in the mammalian liver. *Nature Reviews Gastroenterology & Hepatology 2019 16:7*. **16**, 395–410 (2019).

34. K. B. Halpern, R. Shenhav, O. Matcovitch-Natan, B. Tóth, D. Lemze, M. Golan, E. E. Massasa, S. Baydatch, S. Landen, A. E. Moor, A. Brandis, A. Giladi, A. Stokar-Avihail, E. David, I. Amit, S. Itzkovitz, Single-cell spatial reconstruction reveals global division of labour in the mammalian liver. *Nature 2017 542:7641*. **542**, 352–356 (2017).

35. B. S. Hijmans, A. Grefhorst, M. H. Oosterveer, A. K. Groen, Zonation of glucose and fatty acid metabolism in the liver: Mechanism and metabolic consequences. *Biochimie*. **96**, 121–129 (2014).

36. A. Treyer, A. Müsch, Hepatocyte Polarity. *Compr Physiol*. **3**, 243–287 (2013).

37. P. Gissen, I. M. Arias, Structural and functional hepatocyte polarity and liver disease. *Journal of Hepatology*. **63**, 1023–1037 (2015).

38. National Library of Medicine, Liver Disease, (available at https://medlineplus.gov/liverdiseases.html).

39. A. Sharma, S. Nagalli, Chronic Liver Disease. *StatPearls* (2021) (available at https://www.ncbi.nlm.nih.gov/books/NBK554597/).

40. A. Marengo, C. Rosso, E. Bugianesi, Liver Cancer: Connections with Obesity, Fatty Liver, and Cirrhosis. *Annu Rev Med*. **67**, 103–117 (2016).

41. S. K. Asrani, H. Devarbhavi, J. Eaton, P. S. Kamath, Burden of liver diseases in the world. *Journal of Hepatology*. **70**, 151–171 (2019).

42. M. Stepanova, L. de Avila, M. Afendy, I. Younossi, H. Pham, R. Cable, Z. M. Younossi, Direct and Indirect Economic Burden of Chronic Liver Disease in the United States. *Clinical Gastroenterology and Hepatology*. **15**, 759-766.e5 (2017).

43. Organ Procurement and Transplant Network (2019), (available at https://optn.transplant.hrsa.gov).

44. J. Brown, J. H. Sorrell, J. McClaren, J. W. Creswell, Waiting for a liver transplant. *Qualitative Health Research*. **16**, 119–136 (2006).

45. C. Warren, A. M. Carpenter, D. Neal, K. Andreoni, G. Sarosi, A. Zarrinpar, Racial Disparity in Liver Transplantation Listing. *J Am Coll Surg*. **232**, 526 (2021).

46. L. D. Nephew, M. Serper, Racial, Gender, and Socioeconomic Disparities in Liver Transplantation. *Liver Transplantation*. **27**, 900–912 (2021).

47. L. Dakhoul, S. Gawrieh, K. R. Jones, M. Ghabril, C. McShane, E. Orman, E. Vilar-Gomez, N. Chalasani, L. Nephew, Racial Disparities in Liver Transplantation for Hepatocellular Carcinoma Are Not Explained by Differences in Comorbidities, Liver Disease Severity, or Tumor Burden. *Hepatology Communications*. **3**, 52–62 (2019).

48. W. R. Kim, T. M. Therneau, J. T. Benson, W. K. Kremers, C. B. Rosen, G. J. Gores, E. R. Dickson, Deaths on the liver transplant waiting list: An analysis of competing risks. *Hepatology*. **43**, 345–351 (2006).

49. G. K. Michalopoulos, Liver regeneration. *Journal of Cellular Physiology*. **213**, 286–300 (2007).

50. N. Tanimizu, A. Miyajima, Molecular Mechanism of Liver Development and Regeneration. *International Review of Cytology*. **259**, 1–48 (2007).

51. N. Fausto, J. S. Campbell, K. J. Riehle, Liver regeneration. *Hepatology*. **43**, 45–53 (2006).

52. L. Lorenz, J. Axnick, T. Buschmann, C. Henning, S. Urner, S. Fang, H. Nurmi, N. Eichhorst, R. Holtmeier, K. Bódis, J. H. Hwang, K. Müssig, D. Eberhard, J. Stypmann, O. Kuss, M. Roden, K. Alitalo, D. Häussinger, E. Lammert, Mechanosensing by β1 integrin induces angiocrine signals for liver growth and survival. *Nature 2018 562:7725*. **562**, 128–132 (2018).

53. F. Braet, M. Shleper, M. Paizi, S. Brodsky, N. Kopeiko, N. Resnick, G. Spira, Liver sinusoidal endothelial cell modulation upon resection and shear stress in vitro. *Comp Hepatol*. **3**, 7 (2004).

54. B.-S. Ding, D. J. Nolan, J. M. Butler, D. James, A. O. Babazadeh, Z. Rosenwaks, V. Mittal, H. Kobayashi, K. Shido, D. Lyden, T. N. Sato, S. Y. Rabbany, S. Rafii, Inductive angiocrine signals from sinusoidal endothelium are required for liver regeneration. *Nature*. **468**, 310–315 (2010).

55. W. M. Mars, M.-L. Liu, R. P. Kitson, R. H. Goldfarb, M. K. Gabauer, G. K. Michalopoulos, Immediate early detection of urokinase receptor after partial hepatectomy and its implications for initiation of liver regeneration. *Hepatology*. **21**, 1695–1701 (1995).

56. T. H. Kim, W. M. Mars, D. B. Stolz, G. K. Michalopoulos, Expression and activation of pro-MMP-2 and pro-MMP-9 during rat liver regeneration. *Hepatology*. **31**, 75–82 (2000).

57. D. Beer Stolz, W. M. Mars, B. E. Petersen, T.-H. Kim, G. K. Michalopoulos, Growth Factor Signal Transduction Immediately after Two-Thirds Partial Hepatectomy in the Rat. *Cancer Research*. **59**, 3954–3960 (1999).

58. J. L. Cruise, K. A. Houck, G. K. Michalopoulos, Induction of DNA Synthesis in Cultured Rat Hepatocytes Through Stimulation of α1 Adrenoreceptor by Norepinephrine. *Science (1979)*. **227**, 749–751 (1985).

59. W. Huang, K. Ma, J. Zhang, M. Qatanani, J. Cuvillier, J. Liu, B. Dong, X. Huang, D. D. Moore, Nuclear receptor-dependent bile acid signaling is required for normal liver regeneration. *Science (1979)*. **312**, 233–236 (2006).

60. M. Lesurtel, R. Graf, B. Aleil, D. J. Walther, Y. Tian, W. Jochum, C. Gachet, M. Bader, P. A. Clavien, Platelet-derived serotonin mediates liver regeneration. *Science (1979)*. **312**, 104–107 (2006).

61. M. Kohjima, T. H. Tsai, B. C. Tackett, S. Thevananther, L. Li, B. H. J. Chang, L. Chan, Delayed liver regeneration after partial hepatectomy in adipose differentiation related protein-null mice. *Journal of Hepatology*. **59**, 1246–1254 (2013).

62. S. L. Habib, N. S. Srikanth, F. A. Scappaticci, M. B. Faletto, A. Maccubbin, E. Farber, A. K. Ghoshal, H. L. Gurtoo, Altered Expression of Cytochrome P450 mRNA during Chemical-Induced Hepatocarcinogenesis and Following Partial Hepatectomy. *Toxicology and Applied Pharmacology*. **124**, 139–148 (1994).

63. I. J. Marie, C. Dalet, J. M. Blanchard, C. Astre, A. Szawlowski, B. saint Aubert, H. Joyeux, P. Maurel, Inhibition of cytochrome P-450p (P450IIIA1) gene expression during liver regeneration from two-thirds hepatectomy in the rat. *Biochemical Pharmacology*. **37**, 3515–3521 (1988).

64. C. Trautwein, T. Rakemann, P. Obermayer-Straub, M. Niehof, M. P. Manns, Differences in the regulation of cytochrome P450 family members during liver regeneration. *J Hepatol*. **26**, 48–54 (1997).

65. R. Solhi, M. Lotfinia, R. Gramignoli, M. Najimi, M. Vosough, Metabolic hallmarks of liver regeneration Endocrinology & Metabolism. *Trends in Endocrinology & Metabolism*. **32**, 731–745 (2021).

66. G. K. Michalopoulos, Hepatostat: Liver regeneration and normal liver tissue maintenance. *Hepatology*. **65**, 1384–1392 (2017).

67. D. Zhou, C. Conrad, F. Xia, J. S. Park, B. Payer, Y. Yin, G. Y. Lauwers, W. Thasler, J. T. Lee, J. Avruch, N. Bardeesy, Mst1 and Mst2 Maintain Hepatocyte Quiescence and Suppress Hepatocellular Carcinoma Development through Inactivation of the Yap1 Oncogene. *Cancer Cell*. **16**, 425–438 (2009).

68. D. Yimlamai, C. Christodoulou, G. G. Galli, K. Yanger, B. Pepe-Mooney, B. Gurung, K. Shrestha, P. Cahan, B. Z. Stanger, F. D. Camargo, Hippo pathway activity influences liver cell fate. *Cell*. **157**, 1324–1338 (2014).

69. B. Liu, A. W. Bell, S. Paranjpe, W. C. Bowen, J. S. Khillan, J. H. Luo, W. M. Mars, G. K. Michalopoulos, Suppression of liver regeneration and hepatocyte proliferation in hepatocyte-targeted glypican 3 transgenic mice. *Hepatology*. **52**, 1060–1067 (2010).

70. W. E. Naugler, B. D. Tarlow, L. M. Fedorov, M. Taylor, C. Pelz, B. Li, J. Darnell, M. Grompe, Fibroblast Growth Factor Signaling Controls Liver Size in Mice With Humanized Livers. *Gastroenterology*. **149**, 728–740 (2015).

71. M. A. Goodell, H. Nguyen, N. Shroyer, Somatic stem cell heterogeneity: diversity in the blood, skin and intestinal stem cell compartments. *Nature Reviews Molecular Cell Biology 2015 16:5*. **16**, 299–309 (2015).

72. K. Overturf, M. Al-Dhalimy, C. N. Ou, M. Finegold, M. Grompe, Serial transplantation reveals the stem-cell-like regenerative potential of adult mouse hepatocytes. *The American Journal of Pathology*. **151**, 1273 (1997).

73. J. Font-Burgada, S. Shalapour, S. Ramaswamy, K. Deisseroth, I. M. Verma, M. Karin, B. Hsueh, D. Rossell, A. Umemura, K. Taniguchi, H. Nakagawa, M. A. Valasek, L. Ye, J. L. Kopp, M. Sander, H. Carter, Hybrid Periportal Hepatocytes Regenerate the Injured Liver without Giving Rise to Cancer. *Cell*. **162**, 766–779 (2015).

74. B. Wang, L. Zhao, M. Fish, C. Y. Logan, R. Nusse, Self-renewing diploid Axin2 cells fuel homeostatic renewal of the liver, doi:10.1038/nature14863.

75. S. Lin, M. Nascimento, C. R. Gajera, L. Chen, P. Neuhöfer, A. Garbuzov, S. Wang, S. E. Artandi, Distributed hepatocytes expressing telomerase repopulate the liver in homeostasis and injury. *Nature* (2018), doi:10.1038/s41586-018-0004-7.

76. W. M. Lee, Drug-Induced Hepatotoxicity. *New England Journal of Medicine*. **349**, 474–485 (2003).

77. E. S. Björnsson, Hepatotoxicity by Drugs: The Most Common Implicated Agents. *International Journal of Molecular Sciences*. **17** (2016), doi:10.3390/IJMS17020224.

78. S. R. Khetani, S. N. Bhatia, Microscale culture of human liver cells for drug development. *Nature Biotechnology*. **26**, 120–126 (2008).

79. A. S. Serras, J. S. Rodrigues, M. Cipriano, A. v. Rodrigues, N. G. Oliveira, J. P. Miranda, A Critical Perspective on 3D Liver Models for Drug Metabolism and Toxicology Studies. *Frontiers in Cell and Developmental Biology*. **9**, 203 (2021).

80. G. R. Wilkinson, Drug metabolism and variability among patients in drug response. *N Engl J Med*. **352**, 2211–2221 (2005).

81. J. H. Lin, A. Y. H. Lu, Interindividual variability in inhibition and induction of cytochrome P450 enzymes. *Annu Rev Pharmacol Toxicol*. **41**, 535–567 (2001).

82. C. Terry, R. D. Hughes, R. R. Mitry, S. C. Lehec, A. Dhawan, Cryopreservation-Induced Nonattachment of Human Hepatocytes: Role of Adhesion Molecules. *Cell Transplantation*. **16**, 639–647 (2007).

83. E. Moore, J. B. Allen, C. J. Mulligan, E. C. Wayne, Ancestry of cells must be considered in bioengineering. *Nature Reviews Materials 2021 7:1*. **7**, 2–4 (2021).

84. H. Ryan, D. Bister, S. A. Holliday, J. Boehlein, A. Lewis, J. Silberman, J. B. Allen, E. Moore, Ancestral Background Is Underreported in Regenerative Engineering. *Regenerative Engineering and Translational Medicine*. **1**, 1 (2021).

85. X. Stéphenne, M. Najimi, E. M. Sokal, Hepatocyte cryopreservation: Is it time to change the strategy? *World Journal of Gastroenterology : WJG*. **16**, 1 (2010).

86. K. Yoshida, F. Ono, T. Chouno, B. R. Perocho, Y. Ikegami, N. Shirakigawa, H. Ijima, Cryoprotective enhancing effect of very low concentration of trehalose on the functions of primary rat hepatocytes. *Regenerative Therapy*. **15**, 173–179 (2020).

87. F. N. Smets, Y. Chen, L. J. Wang, H. E. Soriano, Loss of cell anchorage triggers apoptosis (anoikis) in primary mouse hepatocytes. *Mol Genet Metab*. **75**, 344–352 (2002).

88. M. Baxter, S. Withey, S. Harrison, C. P. Segeritz, F. Zhang, R. Atkinson-Dell, C. Rowe, D. T. Gerrard, R. Sison-Young, R. Jenkins, J. Henry, A. A. Berry, L. Mohamet, M. Best, S. W. Fenwick, H. Malik, N. R. Kitteringham, C. E. Goldring, K. Piper Hanley, L. Vallier, N. A. Hanley, Phenotypic and functional analyses show stem cell-derived hepatocyte-like cells better mimic fetal rather than adult hepatocytes. *Journal of Hepatology*. **62**, 581–589 (2015).

89. J. L. Corbett, S. A. Duncan, iPSC-Derived Hepatocytes as a Platform for Disease Modeling and Drug Discovery. *Frontiers in Medicine*. **6**, 265 (2019).

90. V. Iansante, A. Chandrashekran, A. Dhawan, Cell-based liver therapies: past, present and future. *Philosophical Transactions of the Royal Society B: Biological Sciences*. **373** (2018), doi:10.1098/RSTB.2017.0229.

91. B. J. Dwyer, M. T. Macmillan, P. N. Brennan, S. J. Forbes, Cell therapy for advanced liver diseases: Repair or rebuild. *Journal of Hepatology*. **74**, 185–199 (2021).

92. N. Sayed, C. Liu, J. C. Wu, Translation of Human-Induced Pluripotent Stem Cells: From Clinical Trial in a Dish to Precision Medicine. *J Am Coll Cardiol*. **67**, 2161–2176 (2016).

93. L. Guo, S. Dial, L. Shi, W. Branham, J. Liu, J. L. Fang, B. Green, H. Deng, J. Kaput, B. Ning, Similarities and Differences in the Expression of Drug-Metabolizing Enzymes between Human Hepatic Cell Lines and Primary Human Hepatocytes. *Drug Metabolism and Disposition*. **39**, 528–538 (2011).

94. D. R. Berger, B. R. Ware, M. D. Davidson, S. R. Allsup, S. R. Khetani, Enhancing the functional maturity of induced pluripotent stem cell-derived human hepatocytes by controlled presentation of cell-cell interactions in vitro. *Hepatology*. **61**, 1370–1381 (2015).

95. D. Runge, D. M. Runge, D. Jäger, K. A. Lubecki, D. Beer Stolz, S. Karathanasis, T. Kietzmann, S. C. Strom, K. Jungermann, W. E. Fleig, G. K. Michalopoulos, Serum-free, long-term cultures of human hepatocytes: Maintenance of cell morphology, transcription factors, and liver-specific functions. *Biochemical and Biophysical Research Communications*. **269**, 46–53 (2000).

96. P. Krause, F. Saghatolislam, S. Koenig, K. Unthan-Fechner, I. Probst, Maintaining hepatocyte differentiation in vitro through co-Culture with hepatic stellate cells. *In Vitro Cellular and Developmental Biology - Animal*. **45**, 205–212 (2009).

97. R. N. B. Bhandari, L. A. Riccalton, A. L. Lewis, J. R. Fry, A. H. Hammond, S. J. B. Tendler, K. M. Shakesheff, Liver Tissue Engineering: A Role for Co-culture Systems in Modifying Hepatocyte Function and Viability. *https://home.liebertpub.com/ten*. **7**, 345–357 (2004).

98. P. Godoy, N. J. Hewitt, U. Albrecht, M. E. Andersen, N. Ansari, S. Bhattacharya, J. G. Bode, J. Bolleyn, C. Borner, J. Böttger, A. Braeuning, R. A. Budinsky, B. Burkhardt, N. R. Cameron, G. Camussi, C.-S. Cho, Y.-J. Choi, J. Craig Rowlands, U. Dahmen, G. Damm, O. Dirsch, M. T. Donato, J. Dong, S. Dooley, D. Drasdo, R. Eakins, K. S. Ferreira, V. Fonsato, J. Fraczek, R. Gebhardt, A. Gibson, M. Glanemann, C. E. P. Goldring, M. J. Gómez-Lechón, G. M. M. Groothuis, L. Gustavsson, C. Guyot, D. Hallifax, S. Hammad, A. Hayward, D. Häussinger, C. Hellerbrand, P. Hewitt, S. Hoehme, H.-G. Holzhütter, J. B. Houston, J. Hrach, K. Ito, H. Jaeschke, V. Keitel, J. M. Kelm, B. Kevin Park, C. Kordes, G. A. Kullak-Ublick, E. L. LeCluyse, P. Lu, J. Luebke-Wheeler, A. Lutz, D. J. Maltman, M. Matz-Soja, P. McMullen, I. Merfort, S. Messner, C. Meyer, J. Mwinyi, D. J. Naisbitt, A. K. Nussler, P. Olinga, F. Pampaloni, J. Pi, L. Pluta, S. A. Przyborski, A. Ramachandran, V. Rogiers, C. Rowe, C. Schelcher, K. Schmich, M. Schwarz, B. Singh, E. H. K. Stelzer, B. Stieger, R. Stöber, Y. Sugiyama, C. Tetta, W. E. Thasler, T. Vanhaecke, M. Vinken, T. S. Weiss, A. Widera, C. G. Woods, J. J. Xu, K. M. Yarborough, J. G. Hengstler, Recent advances in 2D and 3D in vitro systems using primary hepatocytes, alternative hepatocyte sources and non-parenchymal liver cells and their use in investigating mechanisms of hepatotoxicity, cell signaling and ADME. *Archives of Toxicology*. **87**, 1315–1530 (2013).

99. G. H. Underhill, S. R. Khetani, Bioengineered Liver Models for Drug Testing and Cell Differentiation Studies. *Cellular and Molecular Gastroenterology and Hepatology*. **5**, 426-439.e1 (2018).

100. K. R. Stevens, M. D. Ungrin, R. E. Schwartz, S. Ng, B. Carvalho, K. S. Christine, R. R. Chaturvedi, C. Y. Li, P. W. Zandstra, C. S. Chen, S. N. Bhatia, InVERT molding for scalable control of tissue microarchitecture. *Nature Communications*. **4**, 1847 (2013).

101. W. R. Proctor, A. J. Foster, J. Vogt, C. Summers, B. Middleton, M. A. Pilling, D. Shienson, M. Kijanska, S. Ströbel, J. M. Kelm, P. Morgan, S. Messner, D. Williams, Utility of spherical human liver microtissues for prediction of clinical drug-induced liver injury. *Arch Toxicol*. **91**, 2849–2863 (2017).

102. K. R. Stevens, M. A. Scull, V. Ramanan, C. L. Fortin, R. R. Chaturvedi, K. A. Knouse, J. W. Xiao, C. Fung, T. Mirabella, A. X. Chen, M. G. McCue, M. T. Yang, H. E. Fleming, K. Chung, Y. P. de Jong, C. S. Chen, C. M. Rice, S. N. Bhatia, In situ expansion of engineered human liver tissue in a mouse model of chronic liver disease. *Sci Transl Med*. **9**, eaah5505 (2017).

103. G. K. Michalopoulos, W. C. Bowen, K. Mulè, D. B. Stolz, Histological Organization in Hepatocyte Organoid Cultures. *The American Journal of Pathology*. **159**, 1877–1887 (2001).

104. T. Sato, D. E. Stange, M. Ferrante, R. G. J. Vries, J. H. van Es, S. van den Brink, W. J. van Houdt, A. Pronk, J. van Gorp, P. D. Siersema, H. Clevers, Long-term Expansion of Epithelial Organoids From Human Colon, Adenoma, Adenocarcinoma, and Barrett's Epithelium. *Gastroenterology*. **141**, 1762–1772 (2011).

105. Method of the Year 2017: Organoids. *Nature Methods 2018 15:1*. **15**, 1–1 (2018).

106. T. Takebe, K. Sekine, M. Enomura, H. Koike, M. Kimura, T. Ogaeri, R.-R. Zhang, Y. Ueno, Y.-W. Zheng, N. Koike, S. Aoyama, Y. Adachi, H. Taniguchi, Vascularized and functional human liver from an iPSC-derived organ bud transplant. *Nature*. **499**, 481–484 (2013).

107. T. Takebe, K. Sekine, M. Kimura, E. Yoshizawa, S. Ayano, M. Koido, S. Funayama, N. Nakanishi, T. Hisai, T. Kobayashi, T. Kasai, R. Kitada, A. Mori, H. Ayabe, Y. Ejiri, N. Amimoto, Y. Yamazaki, S. Ogawa, M. Ishikawa, Y. Kiyota, Y. Sato, K. Nozawa, S. Okamoto, Y. Ueno, H. Taniguchi, Massive and Reproducible Production of Liver Buds Entirely from Human Pluripotent Stem Cells. *Cell Reports*. **21**, 2661–2670 (2017).

108. J. G. Camp, K. Sekine, T. Gerber, H. Loeffler-Wirth, H. Binder, M. Gac, S. Kanton, J. Kageyama, G. Damm, D. Seehofer, L. Belicova, M. Bickle, R. Barsacchi, R. Okuda, E. Yoshizawa, M. Kimura, H. Ayabe, H. Taniguchi, T. Takebe, B. Treutlein, Multilineage communication regulates human liver bud development from pluripotency. *Nature*. **546**, 533–538 (2017).

109. H. Koike, K. Iwasawa, R. Ouchi, M. Maezawa, K. Giesbrecht, N. Saiki, A. Ferguson, M. Kimura, W. L. Thompson, J. M. Wells, A. M. Zorn, T. Takebe, Modelling human hepato-biliary-pancreatic organogenesis from the foregut–midgut boundary. *Nature 2019 574:7776*. **574**, 112–116 (2019).

110. D. Vyas, P. M. Baptista, M. Brovold, E. Moran, B. Gaston, C. Booth, M. Samuel, A. Atala, S. Soker, Self-assembled liver organoids recapitulate hepatobiliary organogenesis in vitro. *Hepatology*. **67**, 750–761 (2018).

111. F. Wu, D. Wu, Y. Ren, Y. Huang, B. Feng, N. Zhao, T. Zhang, X. Chen, S. Chen, A. Xu, Generation of hepatobiliary organoids from human induced pluripotent stem cells. *Journal of Hepatology*. **70**, 1145–1158 (2019).

112. B. T. Wesley, A. D. B. Ross, D. Muraro, Z. Miao, S. Saxton, R. A. Tomaz, C. M. Morell, K. Ridley, E. D. Zacharis, S. Petrus-Reurer, J. Kraiczy, K. T. Mahbubani, S. Brown, J. Garcia-Bernardo, C. Alsinet, D. Gaffney, O. C. Tysoe, R. A. Botting, E. Stephenson, D.-M. Popescu, S. Macparland, G. Bader, I. D. Mcgilvray, D. Ortmann, F. Sampaziotis, K. Saeb-Parsy, M. Haniffa, K. R. Stevens, M. Zilbauer, S. A. Teichmann, L. Vallier, ✉ Affiliations, *bioRxiv*, in press, doi:10.1101/2022.03.08.482299.

113. H. Hu, H. Gehart, B. Artegiani, C. Lopez-Iglesias, F. Dekkers, O. Basak, J. van Es, S. M. Chuva de Sousa Lopes, H. Begthel, J. Korving, M. van der Born, C. Zou, C. Quirk, L. Chiriboga, C. M. Rice, S. Ma, A. Rios, P. J. Peters, Y. P. de Jong, H. Clevers, Long-Term Expansion of Functional Mouse and Human Hepatocytes as 3D Organoids. *Cell*. **175** (2018), doi:10.1016/j.cell.2018.11.013.

114. M. Huch, H. Gehart, R. van Boxtel, K. Hamer, F. Blokzijl, M. M. A. Verstegen, E. Ellis, M. van Wenum, S. A. Fuchs, J. de Ligt, M. van de Wetering, N. Sasaki, S. J. Boers, H. Kemperman, J. de Jonge, J. N. M. Ijzermans, E. E. S. Nieuwenhuis, R. Hoekstra, S. Strom, R. R. G. Vries, L. J. W. van der Laan, E. Cuppen, H. Clevers, Long-Term Culture of Genome-Stable Bipotent Stem Cells from Adult Human Liver. *Cell*. **160**, 299–312 (2015).

115. A. Marsee, F. J. M. Roos, M. M. A. Verstegen, F. Roos, M. Verstegen, H. Clevers, L. Vallier, T. Takebe, M. Huch, W. C. Peng, S. Forbes, F. Lemaigre, E. de Koning, H. Gehart, L. van der Laan, B. Spee, S. Boj, P. Baptista, K. Schneeberger, C. Soroka, M. Heim, S. Nuciforo, K. Zaret, Y. Saito, M. Lutolf, V. Cardinale, B. Simons, S. van IJzendoorn, A. Kamiya, H. Chikada, S. Wang, S. J. Mun, M. J. Son, T. T. Onder, J. Boyer, T. Sato, N. Georgakopoulos, A. Meneses, L. Broutier, L. Boulter, D. Grün, J. IJzermans, B. Artegiani, R. van Boxtel, E. Kuijk, G. Carpino, G. Peltz, J. Banales, N. Man, L. Aloia, N. LaRusso, G. George, C. Rimland, G. Yeoh, A. Grappin-Botton, D. Stange, N. Prior, J. E. E. Tirnitz-Parker, E. Andersson, C. Braconi, N. Hannan, W. Y. Lu, S. Strom, P. Sancho-Bru, S. Ogawa, V. Corbo, M. Lancaster, H. Hu, S. Fuchs, D. Hendriks, S. J. Forbes, L. J. W. van der Laan, Building consensus on definition and nomenclature of hepatic, pancreatic, and biliary organoids. *Cell Stem Cell*. **28**, 816–832 (2021).

116. F. Sampaziotis, D. Muraro, O. C. Tysoe, S. Sawiak, T. E. Beach, E. M. Godfrey, S. S. Upponi, T. Brevini, B. T. Wesley, J. Garcia-Bernardo, K. Mahbubani, G. Canu, R. Gieseck, N. L. Berntsen, V. L. Mulcahy, K. Crick, C. Fear, S. Robinson, L. Swift, L. Gambardella, J. Bargehr, D. Ortmann, S. E. Brown, A. Osnato, M. P. Murphy, G. Corbett, W. T. H. Gelson, G. F. Mells, P. Humphreys, S. E. Davies, I. Amin, P. Gibbs, S. Sinha, S. A. Teichmann, A. J. Butler, T. C. See, E. Melum, C. J. E. Watson, K. Saeb-Parsy, L.

Vallier, Cholangiocyte organoids can repair bile ducts after transplantation in the human liver. *Science (1979)*. **371**, 839–846 (2021).

117. F. Sampaziotis, A. W. Justin, O. C. Tysoe, S. Sawiak, E. M. Godfrey, S. S. Upponi, R. L. Gieseck, M. C. de Brito, N. L. Berntsen, M. J. Gómez-Vázquez, D. Ortmann, L. Yiangou, A. Ross, J. Bargehr, A. Bertero, M. C. F. Zonneveld, M. T. Pedersen, M. Pawlowski, L. Valestrand, P. Madrigal, N. Georgakopoulos, N. Pirmadjid, G. M. Skeldon, J. Casey, W. Shu, P. M. Materek, K. E. Snijders, S. E. Brown, C. A. Rimland, I. Simonic, S. E. Davies, K. B. Jensen, M. Zilbauer, W. T. H. Gelson, G. J. Alexander, S. Sinha, N. R. F. Hannan, T. A. Wynn, T. H. Karlsen, E. Melum, A. E. Markaki, K. Saeb-Parsy, L. Vallier, Reconstruction of the mouse extrahepatic biliary tree using primary human extrahepatic cholangiocyte organoids. *Nature Medicine*. **23**, 954 (2017).

118. F. Sampaziotis, M. Cardoso de Brito, P. Madrigal, A. Bertero, K. Saeb-Parsy, F. A. C Soares, E. Schrumpf, E. Melum, T. H. Karlsen, J. Andrew Bradley, W. T. H Gelson, S. Davies, A. Baker, A. Kaser, G. J. Alexander, N. R. F Hannan, L. Vallier, Cholangiocytes derived from human induced pluripotent stem cells for disease modeling and drug validation. *Nature Biotechnology*. **33** (2015), doi:10.1038/nbt.3275.

119. W. C. Peng, C. Y. Logan, M. Fish, T. Anbarchian, F. Aguisanda, A. Álvarez-Varela, P. Wu, Y. Jin, J. Zhu, B. Li, M. Grompe, B. Wang, R. Nusse, Inflammatory Cytokine TNFα Promotes the Long-Term Expansion of Primary Hepatocytes in 3D Culture. *Cell*. **175**, 1607-1619.e15 (2018).

120. E. Palma, E. J. Doornebal, S. Chokshi, Precision-cut liver slices: a versatile tool to advance liver research. *Hepatology International*. **13**, 51–57 (2019).

121. S. v Murphy, A. Atala, 3D bioprinting of tissues and organs (2014), doi:10.1038/nbt.2958.

122. A. C. Daly, M. E. Prendergast, A. J. Hughes, J. A. Burdick, Bioprinting for the Biologist. *Cell*. **184**, 18–32 (2021).

123. B. Grigoryan, S. J. Paulsen, D. C. Corbett, D. W. Sazer, C. L. Fortin, A. J. Zaita, P. T. Greenfield, N. J. Calafat, J. P. Gounley, A. H. Ta, F. Johansson, A. Randles, J. E. Rosenkrantz, J. D. Louis-Rosenberg, P. A. Galie, K. R. Stevens, J. S. Miller, Multivascular networks and functional intravascular topologies within biocompatible hydrogels. *Science (1979)*. **364**, 458–464 (2019).

124. L. G. Brunel, S. M. Hull, S. C. Heilshorn, Engineered assistive materials for 3D bioprinting: support baths and sacrificial inks. *Biofabrication*. **14**, 032001 (2022).

125. J. S. Miller, K. R. Stevens, M. T. Yang, B. M. Baker, D.-H. T. Nguyen, D. M. Cohen, E. Toro, A. A. Chen, P. A. Galie, X. Yu, R. Chaturvedi, S. N. Bhatia, C. S. Chen, Rapid casting of patterned vascular networks for perfusable engineered three-dimensional tissues. *Nature Materials*. **11**, 768–774 (2012).

126. I. S. Kinstlinger, S. H. Saxton, G. A. Calderon, K. Vasquez Ruiz, D. R. Yalacki, P. R. Deme, J. E. Rosenkrantz, J. D. Louis-Rosenberg, F. Johansson, K. D. Janson, D. W. Sazer, S. S. Panchavati, K.-D. Bissig, K. R. Stevens, J. S. Miller, Generation of model

tissues with dendritic vascular networks via sacrificial laser-sintered carbohydrate templates. *Nature Biomedical Engineering*. **4**, 916–932 (2020).

127. C. G. Groth, B. Arborgh, C. Björkén, B. Sundberg, G. Lundgren, Correction of hyperbilirubinemia in the glucuronyltransferase-deficient rat by intraportal hepatocyte transplantation - PubMed. *Transplant Proceedings*. **9**, 313–316 (1977).

128. Y. Yoshida, Y. Tokusashi, G. H. Lee, K. Ogawa, Intrahepatic transplantation of normal hepatocytes prevents Wilson's disease in Long-Evans cinnamon rats. *Gastroenterology*. **111**, 1654–1660 (1996).

129. J. M. L. de Vree, R. Ottenhoff, P. J. Bosma, A. J. Smith, J. Aten, R. P. J. Oude Elferink, Correction of liver disease by hepatocyte transplantation in a mouse model of progressive familial intrahepatic cholestasis. *Gastroenterology*. **119**, 1720–1730 (2000).

130. B. M. Bilir, D. Guinette, F. Karrer, D. A. Kumpe, J. Krysl, J. Stephens, L. McGavran, A. Ostrowska, J. Durham, Hepatocyte transplantation in acute liver failure. *Liver Transpl*. **6**, 32–40 (2000).

131. C. M. Habibullah, I. H. Syed, A. Qamar, Z. Taher-Uz, Human fetal hepatocyte transplantation in patients with fulminant hepatic failure. *Transplantation*. **58**, 951–952 (1994).

132. A. Schneider, M. Attaran, P. N. Meier, C. Strassburg, M. P. Manns, M. Ott, M. Barthold, L. Arseniev, T. Becker, B. Panning, Hepatocyte transplantation in an acute liver failure due to mushroom poisoning. *Transplantation*. **82**, 1115–1116 (2006).

133. A. A. Khan, A. Habeeb, N. Parveen, B. Naseem, R. P. Babu, A. K. Capoor, C. M. Habibullah, Peritoneal transplantation of human fetal hepatocytes for the treatment of acute fatty liver of pregnancy: a case report. *Tropical Gastroenterology : Official Journal of the Digestive Diseases Foundation*. **25**, 141–143 (2004).

134. G. Ambrosino, S. Varotto, S. C. Strom, G. Guariso, E. Franchin, D. Miotto, L. Caenazzo, S. Basso, P. Carraro, M. L. Valente, D. D'Amico, L. Zancan, L. D'Antiga, Isolated hepatocyte transplantation for Crigler-Najjar syndrome type 1. *Cell Transplantation*. **14**, 151–157 (2005).

135. I. J. Fox, J. R. Chowdhury, S. S. Kaufman, T. C. Goertzen, N. R. Chowdhury, P. I. Warkentin, K. Dorko, B. v. Sauter, S. C. Strom, Treatment of the Crigler–Najjar Syndrome Type I with Hepatocyte Transplantation. *New England Journal of Medicine*. **338**, 1422–1427 (1998).

136. M. Muraca, G. Gerunda, D. Neri, M. T. Vilei, A. Granato, P. Feltracco, M. Meroni, G. Giron, A. B. Burlina, Hepatocyte transplantation as a treatment for glycogen storage disease type 1a. *Lancet*. **359**, 317–318 (2002).

137. M. Grossman, D. J. Rader, D. W. M. Muller, D. M. Kolansky, K. Kozarsky, B. J. Clark, E. A. Stein, P. J. Lupien, H. B. Brewer, S. E. Raper, J. M. Wilson, A pilot study of ex vivo gene therapy for homozygous familial hypercholesterolaemia. *Nature Medicine*. **1**, 1148–1154 (1995).

138. P. A. Lysy, M. Najimi, X. Stéphenne, A. Bourgois, F. Smets, E. M. Sokal, Liver cell transplantation for Crigler-Najjar syndrome type I: Update and perspectives. *World Journal of Gastroenterology*. **14**, 3464–3470 (2008).

139. K. W. Lee, J. H. Lee, W. S. Sung, J. K. Sung, W. J. Jae, D. H. Lee, J. W. Kim, H. Y. Park, S. Y. Lee, H. L. Hwan, W. P. Jin, S. Y. Kim, H. H. Yoon, D. H. Jung, H. C. Yon, S. K. Lee, Hepatocyte transplantation for glycogen storage disease type Ib. *Cell Transplantation*. **16**, 629–637 (2007).

140. A. Dhawan, R. R. Mitry, R. D. Hughes, S. Lehec, C. Terry, S. Bansal, R. Arya, J. J. Wade, A. Verma, N. D. Heaton, M. Rela, G. Mieli-Vergani, Hepatocyte transplantation for inherited factor VII deficiency. *Transplantation*. **78**, 1812–1814 (2004).

141. J. Puppi, N. Tan, R. R. Mitry, R. D. Hughes, S. Lehec, G. Mieli-Vergani, J. Karani, M. P. Champion, N. Heaton, R. Mohamed, A. Dhawan, Hepatocyte transplantation followed by auxiliary liver transplantation - A novel treatment for ornithine transcarbamylase deficiency. *American Journal of Transplantation*. **8**, 452–457 (2008).

142. R. R. Mitry, A. Dhawan, R. D. Hughes, S. Bansal, S. Lehec, C. Terry, N. D. Heaton, J. B. Karani, G. Mieli-Vergani, M. Rela, One liver, three recipients: Segment IV from split-liver procedures as a source of hepatocytes for cell transplantation. *Transplantation*. **77**, 1614–1616 (2004).

143. J. Meyburg, A. M. Das, F. Hoerster, M. Lindner, H. Kriegbaum, G. Engelmann, J. Schmidt, M. Ott, A. Pettenazzo, T. Luecke, H. Bertram, G. F. Hoffmann, A. Burlina, One liver for four children: First clinical series of liver cell transplantation for severe neonatal urea cycle defects. *Transplantation*. **87**, 636–641 (2009).

144. K. A. Soltys, K. Setoyama, E. N. Tafaleng, A. Soto Gutiérrez, J. Fong, K. Fukumitsu, T. Nishikawa, M. Nagaya, R. Sada, K. Haberman, R. Gramignoli, K. Dorko, V. Tahan, A. Dreyzin, K. Baskin, J. J. Crowley, M. A. Quader, M. Deutsch, C. Ashokkumar, B. L. Shneider, R. H. Squires, S. Ranganathan, M. Reyes-Mugica, S. F. Dobrowolski, G. Mazariegos, R. Elango, D. B. Stolz, S. C. Strom, G. Vockley, J. Roy-Chowdhury, M. Cascalho, C. Guha, R. Sindhi, J. L. Platt, I. J. Fox, Host conditioning and rejection monitoring in hepatocyte transplantation in humans. *Journal of Hepatology*. **66**, 987–1000 (2017).

145. X. Stéphenne, F. G. Debray, F. Smets, N. Jazouli, G. Sana, T. Tondreau, R. Menten, P. Goffette, F. Boemer, R. Schoos, S. W. Gersting, M. Najimi, A. C. Muntau, P. Goyens, E. M. Sokal, Hepatocyte transplantation using the domino concept in a child with tetrabiopterin nonresponsive phenylketonuria. *Cell Transplant*. **21**, 2765–2770 (2012).

146. X. Stéphenne, M. Najimi, C. Sibille, M. C. Nassogne, F. Smets, E. M. Sokal, Sustained Engraftment and Tissue Enzyme Activity After Liver Cell Transplantation for Argininosuccinate Lyase Deficiency. *Gastroenterology*. **130**, 1317–1323 (2006).

147. B. B. Beck, S. Habbig, K. Dittrich, D. Stippel, I. Kaul, F. Koerber, H. Goebel, E. C. Salido, M. Kemper, J. Meyburg, B. Hoppe, Liver cell transplantation in severe infantile

oxalosisa potential bridging procedure to orthotopic liver transplantation? *Nephrology Dialysis Transplantation*. **27**, 2984–2989 (2012).

148. E. M. Sokal, F. Smets, A. Bourgois, L. van Maldergem, J. P. Buts, R. Reding, J. B. Otte, V. Evrard, D. Latinne, M. F. Vincent, A. Moser, H. E. Soriano, Hepatocyte transplantation in a 4-year-old girl with peroxisomal biogenesis disease: Technique, safety, and metabolic follow-up. *Transplantation*. **76**, 735–738 (2003).

149. S. C. Strom, R. A. Fisher, W. S. Rubinstein, U. A. Barranger, R. B. Towbin, M. Charron, L. Mieles, L. A. Pisarov, K. Dorko, M. T. Thompson, J. Reyes, Transplantation of human hepatocytes. *Transplantation Proceedings*. **29**, 2103–2106 (1997).

150. S. P. Horslen, T. C. McCowan, T. C. Goertzen, P. I. Warkentin, H. B. Cai, S. C. Strom, I. J. Fox, Isolated hepatocyte transplantation in an infant with a severe urea cycle disorder. *Pediatrics*. **111**, 1262–1267 (2003).

151. X. Stéphenne, M. Najimi, F. Smets, R. Reding, J. de Ville De Goyet, E. M. Sokal, Cryopreserved liver cell transplantation controls ornithine transcarbamylase deficient patient while awaiting liver transplantation. *American Journal of Transplantation*. **5**, 2058–2061 (2005).

152. R. Gramignoli, V. Tahan, K. Dorko, R. Venkataramanan, I. J. Fox, E. C. S. Ellis, M. Vosough, S. C. Strom, Rapid and sensitive assessment of human hepatocyte functions. *Cell Transplant*. **23**, 1545–1556 (2014).

153. E. Billerbeck, M. C. Mommersteeg, A. Shlomai, J. W. Xiao, L. Andrus, A. Bhatta, K. Vercauteren, E. Michailidis, M. Dorner, A. Krishnan, M. R. Charlton, L. Chiriboga, C. M. Rice, Y. P. de Jong, Humanized mice efficiently engrafted with fetal hepatoblasts and syngeneic immune cells develop human monocytes and NK cells. *Journal of Hepatology*. **65**, 334–343 (2016).

154. D. Haridass, Q. Yuan, P. D. Becker, T. Cantz, M. Iken, M. Rothe, N. Narain, M. Bock, M. Nörder, N. Legrand, H. Wedemeyer, K. Weijer, H. Spits, M. P. Manns, J. Cai, H. Deng, J. P. di Santo, C. A. Guzman, M. Ott, Repopulation Efficiencies of Adult Hepatocytes, Fetal Liver Progenitor Cells, and Embryonic Stem Cell-Derived Hepatic Cells in Albumin-Promoter-Enhancer Urokinase-Type Plasminogen Activator Mice. *The American Journal of Pathology*. **175**, 1483–1492 (2009).

155. R. L. Jirtle, C. Biles, G. Michalopoulos, Morphologic and Histochemical Analysis of Hepatocytes Transplanted Into Syngeneic Hosts.

156. J. Komori, L. Boone, A. Deward, T. Hoppo, E. Lagasse, The mouse lymph node as an ectopic transplantation site for multiple tissues. *Nature Biotechnology 2012 30:10*. **30**, 976–983 (2012).

157. A. Soto-Gutiérrez, N. Kobayashi, J. D. Rivas-Carrillo, N. Navarro-Álvarez, D. Zhao, T. Okitsu, H. Noguchi, H. Basma, Y. Tabata, Y. Chen, K. Tanaka, M. Narushima, A. Miki, T. Ueda, H. S. Jun, J. W. Yoon, J. Lebkowski, N. Tanaka, I. J. Fox, Reversal of mouse hepatic failure using an implanted liver-assist device containing ES cell–derived hepatocytes. *Nature Biotechnology 2006 24:11*. **24**, 1412–1419 (2006).

158. K. Takeishi, A. Collin de l'Hortet, Y. Wang, K. Handa, J. Guzman-Lepe, K. Matsubara, K. Morita, S. Jang, N. Haep, R. M. Florentino, F. Yuan, K. Fukumitsu, K. Tobita, W. Sun, J. Franks, E. R. Delgado, E. M. Shapiro, N. A. Fraunhoffer, A. W. Duncan, H. Yagi, T. Mashimo, I. J. Fox, A. Soto-Gutierrez, Assembly and Function of a Bioengineered Human Liver for Transplantation Generated Solely from Induced Pluripotent Stem Cells. *Cell Reports*. **31**, 107711 (2020).

159. N. Shiojiri, S. Inujima, K. Ishikawa, K. Terada, M. Mori, Cell Lineage Analysis during Liver Development Using the spfash-Heterozygous Mouse. *Laboratory Investigation 2001 81:1*. **81**, 17–25 (2001).

160. L. Yang, W. H. Wang, W. L. Qiu, Z. Guo, E. Bi, C. R. Xu, A single-cell transcriptomic analysis reveals precise pathways and regulatory mechanisms underlying hepatoblast differentiation. *Hepatology*. **66**, 1387–1401 (2017).

161. M. Tanaka, M. Okabe, K. Suzuki, Y. Kamiya, Y. Tsukahara, S. Saito, A. Miyajima, Mouse hepatoblasts at distinct developmental stages are characterized by expression of EpCAM and DLK1: Drastic change of EpCAM expression during liver development. *Mechanisms of Development*. **126**, 665–676 (2009).

162. M. Oertel, R. Rosencrantz, Y. Q. Chen, P. N. Thota, J. S. Sandhu, M. D. Dabeva, A. L. Pacchia, M. E. Adelson, J. P. Dougherty, D. A. Shafritz, Repopulation of rat liver by fetal hepatoblasts and adult hepatocytes transduced ex vivo with lentiviral vectors. *Hepatology*. **37**, 994–1005 (2003).

163. J. D. Baranski, R. R. Chaturvedi, K. R. Stevens, J. Eyckmans, B. Carvalho, R. D. Solorzano, M. T. Yang, J. S. Miller, S. N. Bhatia, C. S. Chen, Geometric control of vascular networks to enhance engineered tissue integration and function. *PNAS*. **110**, 7586–7591 (2013).

164. E. M. Wilson, J. Bial, B. Tarlow, G. Bial, B. Jensen, D. L. Greiner, M. A. Brehm, M. Grompe, Extensive double humanization of both liver and hematopoiesis in FRGN mice. *Stem Cell Research*. **13**, 404–412 (2014).

165. H. Azuma, N. Paulk, A. Ranade, C. Dorrell, M. Al-Dhalimy, E. Ellis, S. Strom, M. A. Kay, M. Finegold, M. Grompe, Robust expansion of human hepatocytes in Fah−/−/Rag2−/−/Il2rg−/− mice. *Nature Biotechnology*. **25**, 903–910 (2007).

166. B. C. Yan, C. Gong, J. Song, T. Krausz, M. Tretiakova, E. Hyjek, H. Al-Ahmadie, V. Alves, S.-Y. Xiao, R. A. Anders, J. A. Hart, J. Hart, Arginase-1: A New Immunohistochemical Marker of Hepatocytes and Hepatocellular Neoplasms. *Am J Surg Pathol*. **34** (2010) (available at www.ajsp.com%7C1147).

167. J. R. Schaub, K. A. Huppert, S. N. T. Kurial, B. Y. Hsu, A. E. Cast, B. Donnelly, R. A. Karns, F. Chen, M. Rezvani, H. Y. Luu, A. N. Mattis, A.-L. Rougemont, P. Rosenthal, S. S. Huppert, H. Willenbring, De novo formation of the biliary system by TGFβ-mediated hepatocyte transdifferentiation. *Nature*, 1 (2018).

168. I. M. Arias, H. J. Alter, J. L. Boyer, D. E. Cohen, D. A. Shafritz, S. S. Thorgeirsson, A. W. Wolkoff, Eds., *The Liver: Biology and Pathobiology* (John Wiley & Sons, ed. 6, 2020;

https://books.google.com/books?hl=en&lr=&id=cADMDwAAQBAJ&oi=fnd&pg=PP2&dq=liver+physiology+&ots=servUbTAjn&sig=tYZ-tv7PEEneq0xWomSBxcNEMPw#v=onepage&q=liver%20physiology&f=false).

169. K. A. Homan, N. Gupta, K. T. Kroll, D. B. Kolesky, M. Skylar-Scott, T. Miyoshi, D. Mau, M. T. Valerius, T. Ferrante, J. v. Bonventre, J. A. Lewis, R. Morizane, Flow-enhanced vascularization and maturation of kidney organoids in vitro. *Nature Methods*, 1 (2019).

170. M. Hofer, M. P. Lutolf, Engineering organoids. *Nature Reviews Materials 2021 6:5*. **6**, 402–420 (2021).

171. M. Li, J. C. Izpisua Belmonte, Organoids — Preclinical Models of Human Disease. *New England Journal of Medicine*. **380**, 569–579 (2019).

172. L. Cordero-Espinoza, A. M. Dowbaj, T. N. Kohler, B. Strauss, O. Sarlidou, G. Belenguer, C. Pacini, N. P. Martins, R. Dobie, J. R. Wilson-Kanamori, R. Butler, N. Prior, P. Serup, F. Jug, N. C. Henderson, F. Hollfelder, M. Huch, Dynamic cell contacts between periportal mesenchyme and ductal epithelium act as a rheostat for liver cell proliferation. *Cell Stem Cell*. **28**, 1907-1921.e8 (2021).

173. P. S. Barhouse, M. J. Andrade, Q. Smith, Home Away From Home: Bioengineering Advancements to Mimic the Developmental and Adult Stem Cell Niche. *Frontiers in Chemical Engineering*. **0**, 16 (2022).

174. A. Miyajima, M. Tanaka, T. Itoh, Stem/Progenitor Cells in Liver Development, Homeostasis, Regeneration, and Reprogramming. *Cell Stem Cell*. **14**, 561–574 (2014).

175. N. Kelley-Loughnane, G. E. Sabla, C. Ley-Ebert, B. J. Aronow, J. A. Bezerra, Independent and overlapping transcriptional activation during liver development and regeneration in mice. *Hepatology*. **35**, 525–534 (2002).

176. W. Li, R. N. Germain, M. Y. Gerner, Multiplex, quantitative cellular analysis in large tissue volumes with clearing-enhanced 3D microscopy (Ce3D). *Proc Natl Acad Sci U S A*. **114**, E7321–E7330 (2017).

177. R. R. Mitry, R. D. Hughes, M. M. Aw, C. Terry, G. Mieli-Vergani, R. Girlanda, P. Muiesan, M. Rela, N. D. Heaton, A. Dhawan, Human hepatocyte isolation and relationship of cell viability to early graft function. *Cell Transplantation*. **12**, 69–74 (2003).

178. T. Shimada, H. Yamazaki, M. Mimura, Y. Inui, F. P. Guengerich, Interindividual variations in human liver cytochrome P-450 enzymes involved in the oxidation of drugs, carcinogens and toxic chemicals: studies with liver microsomes of 30 Japanese and 30 Caucasians. *Journal of Pharmacology and Experimental Therapeutics*. **270** (1994).

179. X. Yuan, D. Waterworth, J. R. B. Perry, N. Lim, K. Song, J. C. Chambers, W. Zhang, P. Vollenweider, H. Stirnadel, T. Johnson, S. Bergmann, N. D. Beckmann, Y. Li, L. Ferrucci, D. Melzer, D. Hernandez, A. Singleton, J. Scott, P. Elliott, G. Waeber, L. Cardon, T. M. Frayling, J. S. Kooner, V. Mooser, Population-Based Genome-wide

Association Studies Reveal Six Loci Influencing Plasma Levels of Liver Enzymes. *American Journal of Human Genetics*. **83**, 520–528 (2008).

180. A. Rogue, C. Lambert, C. Spire, N. Claude, A. Guillouzo, Interindividual variability in gene expression profiles in human hepatocytes and comparison with HepaRG cells. *Drug Metab Dispos*. **40**, 151–158 (2012).

181. G. G. M. Pinkse, M. P. Voorhoeve, M. Noteborn, O. T. Terpstra, J. A. Bruijn, E. de Heer, Hepatocyte survival depends on β1-integrin-mediated attachment of hepatocytes to hepatic extracellular matrix. *Liver International*. **24**, 218–226 (2004).

182. J. S. Lee, W. O. Ward, G. Knapp, H. Ren, B. Vallanat, B. Abbott, K. Ho, S. J. Karp, J. C. Corton, Transcriptional ontogeny of the developing liver. *BMC Genomics*. **13**, 1–15 (2012).

183. M. Zabulica, R. C. Srinivasan, M. Vosough, C. Hammarstedt, T. Wu, R. Gramignoli, E. Ellis, K. Kannisto, A. Collin De L'Hortet, K. Takeishi, A. Soto-Gutierrez, S. C. Strom, Guide to the Assessment of Mature Liver Gene Expression in Stem Cell-Derived Hepatocytes. *Stem Cells and Development*. **28**, 907–919 (2019).

184. U. M. Zanger, M. Schwab, Cytochrome P450 enzymes in drug metabolism: Regulation of gene expression, enzyme activities, and impact of genetic variation. *Pharmacology & Therapeutics*. **138**, 103–141 (2013).

185. M. Sonnier, T. Cresteil, Delayed ontogenesis of CYP1A2 in the human liver. *European Journal of Biochemistry*. **251**, 893–898 (1998).

186. J. C. Stevens, New perspectives on the impact of cytochrome P450 3A expression for pediatric pharmacology. *Drug Discovery Today*. **11**, 440–445 (2006).

187. G. Song, X. Sun, R. N. Hines, D. G. McCarver, B. G. Lake, T. G. Osimitz, M. R. Creek, H. J. Clewell, M. Yoon, Determination of Human Hepatic CYP2C8 and CYP1A2 Age-Dependent Expression to Support Human Health Risk Assessment for Early Ages. *Drug Metab Dispos*. **45**, 468–475 (2017).

188. S. N. Hart, Y. Cui, C. D. Klaassen, X.-B. Zhong, Three Patterns of Cytochrome P450 Gene Expression during Liver Maturation in Mice (2009), doi:10.1124/dmd.108.023812.

189. C. Martinez-Jimenez, R. Jover, M. Teresa Donato, J. Castell, M. Jose Gomez-Lechon, Transcriptional Regulation and Expression of CYP3A4 in Hepatocytes. *Current Drug Metabolism*. **8**, 185–194 (2007).

190. J. H. Lin, CYP induction-mediated drug interactions: In vitro assessment and clinical implications. *Pharmaceutical Research*. **23**, 1089–1116 (2006).

191. K. E. Thummel, D. D. Shen, T. D. Podoll, K. L. Kunze, W. F. Trager, P. S. Hartwell, V. A. Raisys, C. L. Marsh, J. P. McVicar, D. M. Barr, J. D. Perkins, R. L. Carithers, Use of midazolam as a human cytochrome P450 3A probe: I. In vitro-in vivo correlations in liver transplant patients. *Journal of Pharmacology and Experimental Therapeutics*. **271**, 549–556 (1994).

192. H. Yamazaki, A. Okayama, N. Imai, F. P. Guengerich, M. Shimizu, Inter-individual variation of cytochrome P4502J2 expression and catalytic activities in liver microsomes from Japanese and Caucasian populations. *Xenobiotica*. **36**, 1201–1209 (2006).

193. C. Xu, C. Y. T. Li, A. N. T. Kong, Induction of phase I, II and III drug metabolism/transport by xenobiotics. *Archives of Pharmacal Research 2005 28:3*. **28**, 249–268 (2005).

194. O. A. Almazroo, M. K. Miah, R. Venkataramanan, Drug Metabolism in the Liver. *Clinics in Liver Disease*. **21**, 1–20 (2017).

195. J. J. Santiago, A. L. Dangerfield, S. G. Rattan, K. L. Bathe, R. H. Cunnington, J. E. Raizman, K. M. Bedosky, D. H. Freed, E. Kardami, I. M. C. Dixon, Cardiac fibroblast to myofibroblast differentiation in vivo and in vitro: Expression of focal adhesion components in neonatal and adult rat ventricular myofibroblasts. *Developmental Dynamics*. **239**, 1573–1584 (2010).

196. J. Solon, I. Levental, K. Sengupta, P. C. Georges, P. A. Janmey, Fibroblast Adaptation and Stiffness Matching to Soft Elastic Substrates. *Biophysical Journal*. **93**, 4453–4461 (2007).

197. K. J. Livak, T. D. Schmittgen, Analysis of relative gene expression data using real-time quantitative PCR and the 2-ΔΔCT method. *Methods*. **25**, 402–408 (2001).

198. P. Ramachandran, R. Dobie, J. R. Wilson-Kanamori, E. F. Dora, B. E. P. Henderson, N. T. Luu, J. R. Portman, K. P. Matchett, M. Brice, J. A. Marwick, R. S. Taylor, M. Efremova, R. Vento-Tormo, N. O. Carragher, T. J. Kendall, J. A. Fallowfield, E. M. Harrison, D. J. Mole, S. J. Wigmore, P. N. Newsome, C. J. Weston, J. P. Iredale, F. Tacke, J. W. Pollard, C. P. Ponting, J. C. Marioni, S. A. Teichmann, N. C. Henderson, Resolving the fibrotic niche of human liver cirrhosis at single-cell level. *Nature 2019 575:7783*. **575**, 512–518 (2019).

199. T. S. Andrews, J. Atif, J. C. Liu, C. T. Perciani, X. Z. Ma, C. Thoeni, M. Slyper, G. Eraslan, A. Segerstolpe, J. Manuel, S. Chung, E. Winter, I. Cirlan, N. Khuu, S. Fischer, O. Rozenblatt-Rosen, A. Regev, I. D. McGilvray, G. D. Bader, S. A. MacParland, Single-Cell, Single-Nucleus, and Spatial RNA Sequencing of the Human Liver Identifies Cholangiocyte and Mesenchymal Heterogeneity. *Hepatology Communications*. **0**, 2021 (2021).

200. V. L. Payen, A. Lavergne, N. Alevra Sarika, M. Colonval, L. Karim, M. Deckers, M. Najimi, W. Coppieters, B. Charloteaux, E. M. Sokal, A. el Taghdouini, Single-cell RNA sequencing of human liver reveals hepatic stellate cell heterogeneity. *JHEP Reports*. **3** (2021), doi:10.1016/J.JHEPR.2021.100278/ATTACHMENT/EF40E473-EA5B-485E-BD36-3FB38C450866/MMC10.PDF.

201. S. A. MacParland, J. C. Liu, X. Z. Ma, B. T. Innes, A. M. Bartczak, B. K. Gage, J. Manuel, N. Khuu, J. Echeverri, I. Linares, R. Gupta, M. L. Cheng, L. Y. Liu, D. Camat, S. W. Chung, R. K. Seliga, Z. Shao, E. Lee, S. Ogawa, M. Ogawa, M. D. Wilson, J. E. Fish, M. Selzner, A. Ghanekar, D. Grant, P. Greig, G. Sapisochin, N. Selzner, N. Winegarden, O. Adeyi, G. Keller, G. D. Bader, I. D. McGilvray, Single cell RNA sequencing of human

liver reveals distinct intrahepatic macrophage populations. *Nature Communications 2018 9:1*. **9**, 1–21 (2018).

202. J. M. Segal, D. Kent, D. J. Wesche, S. S. Ng, M. Serra, B. Oulès, G. Kar, G. Emerton, S. J. I. Blackford, S. Darmanis, R. Miquel, T. V. Luong, R. Yamamoto, A. Bonham, W. Jassem, N. Heaton, A. Vigilante, A. King, R. Sancho, S. Teichmann, S. R. Quake, H. Nakauchi, S. T. Rashid, Single cell analysis of human foetal liver captures the transcriptional profile of hepatobiliary hybrid progenitors. *Nature Communications 2019 10:1*. **10**, 1–14 (2019).

203. J. C. Hsu, R. Bravo, R. Taub, Interactions among LRF-1, JunB, c-Jun, and c-Fos define a regulatory program in the G1 phase of liver regeneration. *Mol Cell Biol*. **12**, 4654–4665 (1992).

204. R. Taub, Liver regeneration 4: transcriptional control of liver regeneration - PubMed. *FASEB J.* **10**, 413–427 (1996).

205. G. X. Y. Zheng, J. M. Terry, P. Belgrader, P. Ryvkin, Z. W. Bent, R. Wilson, S. B. Ziraldo, T. D. Wheeler, G. P. McDermott, J. Zhu, M. T. Gregory, J. Shuga, L. Montesclaros, J. G. Underwood, D. A. Masquelier, S. Y. Nishimura, M. Schnall-Levin, P. W. Wyatt, C. M. Hindson, R. Bharadwaj, A. Wong, K. D. Ness, L. W. Beppu, H. J. Deeg, C. McFarland, K. R. Loeb, W. J. Valente, N. G. Ericson, E. A. Stevens, J. P. Radich, T. S. Mikkelsen, B. J. Hindson, J. H. Bielas, Massively parallel digital transcriptional profiling of single cells. *Nature Communications 2017 8:1*. **8**, 1–12 (2017).

206. T. Stuart, A. Butler, P. Hoffman, C. Hafemeister, E. Papalexi, W. M. Mauck, Y. Hao, M. Stoeckius, P. Smibert, R. Satija, Comprehensive Integration of Single-Cell Data. *Cell*. **177**, 1888-1902.e21 (2019).

207. G. K. Michalopoulos, Z. Khan, Liver Stem Cells: Experimental Findings and Implications for Human Liver Disease. *Gastroenterology*. **149**, 876–882 (2015).

208. A. X. Chen, A. Chhabra, H. H. G. Song, H. E. Fleming, C. S. Chen, S. N. Bhatia, Controlled Apoptosis of Stromal Cells to Engineer Human Microlivers. *Advanced Functional Materials*. **30**, 1910442 (2020).

209. A. M. Merlot, D. S. Kalinowski, D. R. Richardson, Unraveling the mysteries of serum albumin-more than just a serum protein. *Frontiers in Physiology*. **5 AUG**, 299 (2014).

210. J. Zaias, M. Mineau, C. Cray, D. Yoon, N. H. Altman, Reference Values for Serum Proteins of Common Laboratory Rodent Strains. *J Am Assoc Lab Anim Sci*. **48**, 387 (2009).

211. J. Rouwkema, B. F. J. M. Koopman, C. A. V. Blitterswijk, W. J. A. Dhert, J. Malda, Supply of Nutrients to Cells in Engineered Tissues. *http://dx.doi.org/10.5661/bger-26-163*. **26**, 163–178 (2013).

212. H. H. G. Song, R. T. Rumma, C. K. Ozaki, E. R. Edelman, C. S. Chen, Vascular tissue engineering: progress, challenges, and clinical promise. *Cell Stem Cell*. **22**, 340 (2018).

213. D. Therriault, S. R. White, J. A. Lewis, Chaotic mixing in three-dimensional microvascular networks fabricated by direct-write assembly. *Nature Materials 2003 2:4*. **2**, 265–271 (2003).

214. C. Xiang, Y. Du, G. Meng, L. S. Yi, S. Sun, N. Song, X. Zhang, Y. Xiao, J. JieWan, Z. Yi, Y. Liu, B. Xie, M. Wu, J. Shu, D. Sun, J. Jia, Z. Liang, D. Sun, Y. Huang, Y. Shi, J. Xu, F. Lu, C. Li, K. Xiang, Z. Yuan, S. Lu, H. Deng, Long-term functional maintenance of primary human hepatocytes in vitro. *Science (1979)*. **364**, 399–402 (2019).

215. S. N. Bhatia, U. J. Balis, M. L. Yarmush, M. Toner, Effect of cell–cell interactions in preservation of cellular phenotype: cocultivation of hepatocytes and nonparenchymal cells. *The FASEB Journal*. **13**, 1883–1900 (1999).

216. S. N. Bhatia, G. H. Underhill, K. S. Zaret, I. J. Fox, Cell and tissue engineering for liver disease. *Science Translational Medicine*. **6**, 245sr2-245sr2 (2014).

217. S. Rafii, J. M. Butler, B.-S. Ding, Angiocrine functions of organ-specific endothelial cells. *Nature*. **529**, 316–325 (2016).

218. P. O. Seglen, Preparation of isolated rat liver cells. *Methods Cell Biol*. **13**, 29–83 (1976).

219. W. E. Naugler, B. D. Tarlow, L. M. Fedorov, M. Taylor, C. Pelz, B. Li, J. Darnell, M. Grompe, Fibroblast Growth Factor Signaling Controls Liver Size in Mice With Humanized Livers. *Gastroenterology*. **149**, 728 (2015).

220. S. M. Czerniecki, N. M. Cruz, J. L. Harder, R. Menon, J. Annis, E. A. Otto, R. E. Gulieva, L. v. Islas, Y. K. Kim, L. M. Tran, T. J. Martins, J. W. Pippin, H. Fu, M. Kretzler, S. J. Shankland, J. Himmelfarb, R. T. Moon, N. Paragas, B. S. Freedman, High-Throughput Screening Enhances Kidney Organoid Differentiation from Human Pluripotent Stem Cells and Enables Automated Multidimensional Phenotyping. *Cell Stem Cell*. **22**, 929-940.e4 (2018).

221. S. Hou, H. Tiriac, B. P. Sridharan, L. Scampavia, F. Madoux, J. Seldin, G. R. Souza, D. Watson, D. Tuveson, T. P. Spicer, Advanced Development of Primary Pancreatic Organoid Tumor Models for High-Throughput Phenotypic Drug Screening. *SLAS Discovery*. **23**, 574–584 (2018).

222. H. Renner, M. Grabos, K. J. Becker, T. E. Kagermeier, J. Wu, M. Otto, S. Peischard, D. Zeuschner, Y. Tsytsyura, P. Disse, J. Klingauf, S. A. Leidel, G. Seebohm, H. R. Schöler, J. M. Bruder, A fully automated high-throughput workflow for 3d-based chemical screening in human midbrain organoids. *Elife*. **9**, 1–39 (2020).

223. M. C. Regier, J. J. Tokar, J. W. Warrick, L. Pabon, E. Berthier, D. J. Beebe, K. R. Stevens, User-defined morphogen patterning for directing human cell fate stratification. *Scientific Reports 2019 9:1*. **9**, 1–12 (2019).

224. K. M. Loh, R. van Amerongen, R. Nusse, Generating Cellular Diversity and Spatial Form: Wnt Signaling and the Evolution of Multicellular Animals. *Dev Cell*. **38**, 643–655 (2016).

225. E. Bier, E. M. de Robertis, EMBRYO DEVELOPMENT. BMP gradients: A paradigm for morphogen-mediated developmental patterning. *Science (1979)*. **348** (2015), doi:10.1126/SCIENCE.AAA5838.

226. K. A. Houck, G. K. Michalopoulos, Altered responses of regenerating hepatocytes to norepinephrine and transforming growth factor type β. *Journal of Cellular Physiology*. **141**, 503–509 (1989).

227. A. Kaimori, J. Potter, J. Y. Kaimori, C. Wang, E. Mezey, A. Koteish, Transforming Growth Factor-β1 Induces an Epithelial-to-Mesenchymal Transition State in Mouse Hepatocytes in Vitro*. *Journal of Biological Chemistry*. **282**, 22089–22101 (2007).

228. F. A. Oberhammer, M. Pavelka, S. Sharma, R. Tiefenbacher, A. F. Purchio, W. Bursch, R. Schulte-Hermann, Induction of apoptosis in cultured hepatocytes and in regressing liver by transforming growth factor β1. *Proc Natl Acad Sci U S A*. **89**, 5408–5412 (1992).